



Centrum voor Wiskunde en Informatica

**REPORTRAPPORT**

Multiresolution Signal Decomposition Schemes. Part 2: Morphological  
Wavelets

H.J.A.M. Heijmans, J. Goutsias

Probability, Networks and Algorithms (PNA)

**PNA-R9905 June 30, 1999**

Report PNA-R9905  
ISSN 1386-3711

CWI  
P.O. Box 94079  
1090 GB Amsterdam  
The Netherlands

CWI is the National Research Institute for Mathematics and Computer Science. CWI is part of the Stichting Mathematisch Centrum (SMC), the Dutch foundation for promotion of mathematics and computer science and their applications.

SMC is sponsored by the Netherlands Organization for Scientific Research (NWO). CWI is a member of ERCIM, the European Research Consortium for Informatics and Mathematics.

Copyright © Stichting Mathematisch Centrum  
P.O. Box 94079, 1090 GB Amsterdam (NL)  
Kruislaan 413, 1098 SJ Amsterdam (NL)  
Telephone +31 20 592 9333  
Telefax +31 20 592 4199

# Multiresolution Signal Decomposition Schemes.

## Part 2: Morphological Wavelets

Henk J.A.M. Heijmans

*CWI*

*P.O. Box 94079, 1090 GB Amsterdam, The Netherlands*

John Goutsias

*Center for Imaging Science*

*and Department of Electrical and Computer Engineering*

*The Johns Hopkins University, Baltimore, MD 21218, USA*

### ABSTRACT

In its original form, the wavelet transform is a linear tool. However, it has been increasingly recognized that nonlinear extensions are possible. A major impulse to the development of nonlinear wavelet transforms has been given by the introduction of the lifting scheme by Sweldens. The aim of this report, which is a sequel to a previous report devoted exclusively to the pyramid transform, is to present an axiomatic framework encompassing most existing linear and nonlinear wavelet decompositions. Furthermore, it introduces some, thus far unknown, wavelets based on mathematical morphology, such as the morphological Haar wavelet, both in one and two dimensions. A general and flexible approach for the construction of nonlinear (morphological) wavelets is provided by the lifting scheme. This paper discusses one example in considerable detail, the max-lifting scheme, which has the intriguing property that it preserves local maxima in a signal over a range of scales, depending on how local or global these maxima are.

*1991 Mathematics Subject Classification:* 68U10, 94A12

*Keywords and Phrases:* Analysis and synthesis operators, Biorthogonal linear wavelets, Coupled and uncoupled wavelet decompositions, Lifting scheme, Mathematical morphology, Max-lifting, Median operator, Morphological Haar wavelet, Multiresolution signal processing and analysis, Nonlinear wavelet transforms, Pyramid transforms, Quantization, Quincunx sampling, S-transform.

*Note:* Work by the first author carried out under project PNA4.3 "Morphological Image Processing." This work was supported in part by NATO Collaborative Research Grant CRG.971503. Henk Heijmans was also supported by INTAS under grant 96-785. John Goutsias was also supported by the Office of Naval Research (U.S.A.), Mathematical, Computer, and Information Sciences Division, under ONR Grant N00014-90-1345, and the National Science Foundation, under NSF Award #9729576.

## 1. Introduction

Today, it is generally accepted that multiresolution approaches are extremely important in many signal and image processing applications. This is largely due to the fact that signals (and images in particular) often contain physically relevant features at many different scales or resolutions. For a proper understanding of such signals, multiresolution (or multiscale) techniques are indispensable. But there exist other good reasons why taking recourse to multiresolution approaches. A major one is that multiresolution algorithms may offer some attractive computational advantages.

In a previous report [26], to be referred to here as Part 1, we have presented an axiomatic framework for pyramid decompositions of signals which encompasses several existing approaches; in particular, linear pyramids (such as the Laplacian pyramid proposed by Burt and Adelson [6]), and morphological tools such as the skeleton and the granulometry [30, 37]. A short overview of this framework is provided in Subsection 2.2.

Wavelet analysis is a relatively new tool developed over the past ten or fifteen years. During this period, it has attracted the interest of scientists from various disciplines, in particular mathematics, physics, computer science, and electrical engineering. Nowadays, it has reached a certain level of maturity, as is clearly reflected by the existence of numerous textbooks, journals, and conferences on this topic. A very interesting account on the emergence and development of wavelet theory can be found in the monograph *The World According to Wavelets* by Barbara Burke Hubbard [5].

Wavelet analysis is known as a *linear* tool. However, it is starting to be recognized that nonlinear extensions are possible [8, 10, 11, 12, 13, 15, 18, 20, 21, 22, 23, 25, 26, 27, 28, 29, 31, 32, 40]. The *lifting scheme*, recently introduced by Sweldens [45, 46, 47] (see also [4] for a predecessor of this scheme, known as a “ladder network”), has provided a useful tool for constructing nonlinear wavelet transforms. The enormous flexibility and freedom that the lifting scheme offers has challenged researchers to develop various nonlinear wavelet transforms [8, 10, 11, 12, 13, 18, 20, 21, 22, 23, 27, 28, 29, 31, 33]. We briefly discuss some of these works in the concluding section of this report, and point out their relationship to our study.

The aim of this report is twofold. First, we present an axiomatic framework to wavelet-type multiresolution signal decomposition that encompasses all known linear and nonlinear wavelet decomposition schemes. Second, we introduce a family of nonlinear wavelets based on morphological operators. The simplest nontrivial example of a morphological wavelet is the so-called morphological Haar wavelet. As we said before, the lifting scheme opens a way to construct more general wavelet decompositions. In this paper, we restrict ourselves to constructions based on morphological operators. Particular attention is paid to the max-lifting scheme, which has the interesting property that it preserves local maxima of a signal over several scales.

This report is organized as follows. In Section 2, we give a brief reminder of basic concepts of mathematical morphology and of the pyramid transform introduced in Part 1. In Section 3, we recall some known results about the linear wavelet transform and the concept of multiresolution analysis. Then, in Section 4, we present a general definition of a wavelet transform, which we refer to as the *coupled wavelet decomposition scheme*. A special case is the *uncoupled wavelet decomposition scheme*, a class which the linear biorthogonal wavelets as well as the S-transform belong to. Section 5 is devoted entirely to a simple nontrivial uncoupled wavelet decomposition scheme based on morphological operators, the so-called *morphological Haar wavelet*. We discuss the one-dimensional as well as the non-separable two-dimensional case. In Section 6, we discuss the lifting scheme within the axiomatic context of this report. In particular, it is shown that two nonlinear lifting steps generally lead to a coupled wavelet decomposition scheme. A number of examples, based on morphological operators, are discussed. Another important example of the lifting scheme is discussed in some detail in Section 7. This is referred to as the *max-lifting*

*scheme*, the most striking property of which is that it preserves local maxima of a signal over several scales, depending on how local or global these maxima are. Finally, in Section 8, we put our results in a broader perspective, by discussing some related work recently found in the literature.

## 2. Preliminaries

### 2.1. Some morphological concepts

We first recall some concepts from mathematical morphology that we use in the sequel. The main concept is that of an adjunction. We refer to [30] for a comprehensive discussion.

**2.1. Definition.** Consider two partially ordered sets (posets)  $\mathcal{L}, \mathcal{M}$  and two operators  $\varepsilon: \mathcal{L} \rightarrow \mathcal{M}$  and  $\delta: \mathcal{M} \rightarrow \mathcal{L}$ . The pair  $(\varepsilon, \delta)$  defines an adjunction between  $\mathcal{L}$  and  $\mathcal{M}$  if

$$\delta(y) \leq x \iff y \leq \varepsilon(x), \quad x \in \mathcal{L}, y \in \mathcal{M}.$$

It is easy to show that, in an adjunction, both operators  $\varepsilon$  and  $\delta$  are increasing; i.e.,  $x_1 \leq x_2$  implies that  $\varepsilon(x_1) \leq \varepsilon(x_2)$  (the same for  $\delta$ ). Recall that a poset  $\mathcal{L}$  is called a *lattice* if every finite subset in  $\mathcal{L}$  has a supremum (least upper bound) and an infimum (greatest lower bound). The set  $\mathcal{L}$  is called a *complete lattice* if *every* (finite or infinite) subset of  $\mathcal{L}$  has an infimum and a supremum. If  $\mathcal{K} \subseteq \mathcal{L}$ , then we denote the supremum and infimum of  $\mathcal{K}$  by  $\bigvee \mathcal{K}$  and  $\bigwedge \mathcal{K}$ , respectively. Instead of  $\bigvee \{x_1, x_2, \dots, x_n\}$  we write  $x_1 \vee x_2 \vee \dots \vee x_n$  (same for the infimum). If  $(\varepsilon, \delta)$  is an adjunction between two lattices  $\mathcal{L}$  and  $\mathcal{M}$ , then

$$\varepsilon(x_1 \wedge x_2 \wedge \dots \wedge x_n) = \varepsilon(x_1) \wedge \varepsilon(x_2) \wedge \dots \wedge \varepsilon(x_n), \quad x_1, x_2, \dots, x_n \in \mathcal{L}$$

and, dually,

$$\delta(y_1 \vee y_2 \vee \dots \vee y_n) = \delta(y_1) \vee \delta(y_2) \vee \dots \vee \delta(y_n), \quad y_1, y_2, \dots, y_n \in \mathcal{M}.$$

In a complete lattice, this relationship also holds for infinite infima and suprema, respectively. Operators  $\varepsilon$  and  $\delta$ , with the properties stated above, are called *erosion* and *dilation*, respectively. In the following,  $\text{id}$  denotes the identity operator. The next result can be easily proved.

**2.2. Proposition.** *Let  $(\varepsilon, \delta)$  be an adjunction between two posets  $\mathcal{L}$  and  $\mathcal{M}$ ; then:*

$$\begin{aligned} \varepsilon\delta\varepsilon &= \varepsilon & \text{and} & & \delta\varepsilon\delta &= \delta \\ \varepsilon\delta &\geq \text{id} & \text{and} & & \delta\varepsilon &\leq \text{id}. \end{aligned}$$

**2.3. Definition.** Let  $\psi$  be an operator from a poset  $\mathcal{L}$  into itself.

- (a)  $\psi$  is *idempotent*, if  $\psi^2 = \psi$ .
- (b) If  $\psi$  is increasing and idempotent, then  $\psi$  is called a (*morphological*) *filter*.
- (c) A filter  $\psi$  which satisfies  $\psi \leq \text{id}$  ( $\psi$  is anti-extensive) is called an *opening*.
- (d) A filter  $\psi$  which satisfies  $\psi \geq \text{id}$  ( $\psi$  is extensive) is called a *closing*.

Finally, we have the following result.

**2.4. Proposition.** *Let  $(\varepsilon, \delta)$  be an adjunction between two posets  $\mathcal{L}$  and  $\mathcal{M}$ . Then,  $\varepsilon\delta$  is a closing on  $\mathcal{M}$  and  $\delta\varepsilon$  is an opening on  $\mathcal{L}$ .*

## 2.2. A brief reminder on the pyramid transform

In Part 1, we have presented a comprehensive discussion on the pyramid transform. In this section, we briefly recall the main ideas of that work.

Consider a family  $V_j$  of signal spaces. Here,  $j$  may range over a finite or an infinite index set. Assume that we have two families of operators, a family  $\psi_j^\uparrow$  of *analysis operators* mapping  $V_j$  into  $V_{j+1}$ , and a family  $\psi_j^\downarrow$  of *synthesis operators* mapping  $V_{j+1}$  back into  $V_j$ . Here, the upward arrow indicates that the corresponding operator maps a signal to the higher level, whereas the downward arrow indicates that the operator maps a signal to a lower level. Refer to Figure 1 for an illustration. The analysis operator  $\psi_j^\uparrow$  is chosen to reduce information from a signal  $x_j \in V_j$ , yielding a *scaled signal*  $x_{j+1} = \psi_j^\uparrow(x_j)$  in  $V_{j+1}$ . The synthesis operator  $\psi_j^\downarrow$  maps the scaled signal  $x_{j+1}$  back to  $\hat{x}_j = \psi_j^\downarrow(x_{j+1})$  in  $V_j$ , in such a way that  $\psi_j^\downarrow\psi_j^\uparrow(x_j)$  is “close” to  $x_j$ . By composing analysis operators, we can travel from any level  $i$  to any higher level  $j$ . This gives an operator

$$\psi_{i,j}^\uparrow = \psi_{j-1}^\uparrow \psi_{j-2}^\uparrow \cdots \psi_i^\uparrow, \quad j > i,$$

which maps an element in  $V_i$  to an element in  $V_j$ . On the other hand, by composing synthesis operators, we can travel from any level  $j$  to any lower level  $i$ . This gives an operator

$$\psi_{j,i}^\downarrow = \psi_i^\downarrow \psi_{i+1}^\downarrow \cdots \psi_{j-1}^\downarrow, \quad j > i,$$

which takes us from level  $j$  back to level  $i$ .

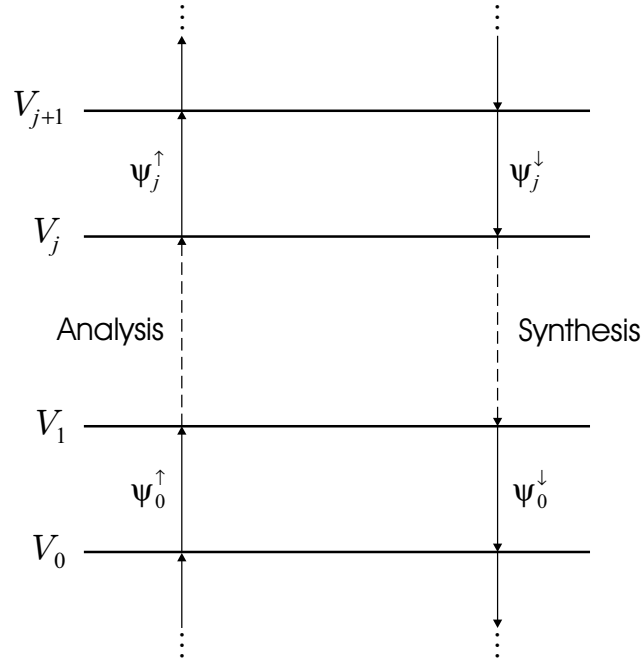


**Fig. 1.** The pyramid decomposition scheme.

Since the analysis operators are designed to reduce the information content of a signal, they are not invertible in general. In particular,  $\psi_j^\downarrow\psi_j^\uparrow$  will not be the identity operator in general. On the other hand, we always avoid synthesis operators  $\psi_j^\downarrow$  that reduce information content. In other words,  $\psi_j^\downarrow$  is taken to be injective. In fact, both conditions are automatically satisfied if we make the following assumption, which we refer to as the *pyramid condition*.

**2.5. Pyramid Condition.** The analysis and synthesis operators  $\psi_j^\uparrow, \psi_j^\downarrow$  are said to satisfy the *pyramid condition* if  $\psi_j^\uparrow \psi_j^\downarrow = \text{id}$  on  $V_{j+1}$ .

It is easily seen that the pyramid condition implies that  $\psi_j^\uparrow \psi_j^\downarrow \psi_j^\uparrow = \psi_j^\uparrow$ ,  $\psi_j^\downarrow \psi_j^\uparrow \psi_j^\downarrow = \psi_j^\downarrow$ , and that  $\psi_j^\downarrow \psi_j^\uparrow$  is idempotent. Now, suppose that all previous conditions are satisfied, and that we have addition and subtraction operators  $\dot{+}, \dot{-}$  on  $V_j$ , such that

$$x_1 \dot{+} (x_2 \dot{-} x_1) = x_2, \quad \text{for } x_1, x_2 \in V_j$$

(note that, in Part 1, we have made an assumption which is slightly weaker). Given an input signal  $x_0 \in V_0$ , we consider the following recursive signal analysis scheme, called the *pyramid transform*:

$$x_0 \rightarrow \{x_1, y_0\} \rightarrow \{x_2, y_1, y_0\} \rightarrow \cdots \rightarrow \{x_{k+1}, y_k, y_{k-1}, \dots, y_0\} \rightarrow \cdots$$

where

$$\begin{cases} x_{j+1} = \psi_j^\uparrow(x_j) \in V_{j+1}, & j \geq 0 \\ y_j = x_j \dot{-} \psi_j^\downarrow(x_{j+1}). \end{cases}$$

The original signal  $x_0 \in V_0$  can be *exactly* reconstructed from  $x_{k+1}$  and  $y_0, y_1, \dots, y_k$  by means of the backward recursion

$$x_j = \psi_j^\downarrow(x_{j+1}) \dot{+} y_j, \quad j = k, k-1, \dots, 0.$$

Refer to Figure 2 for an illustration.

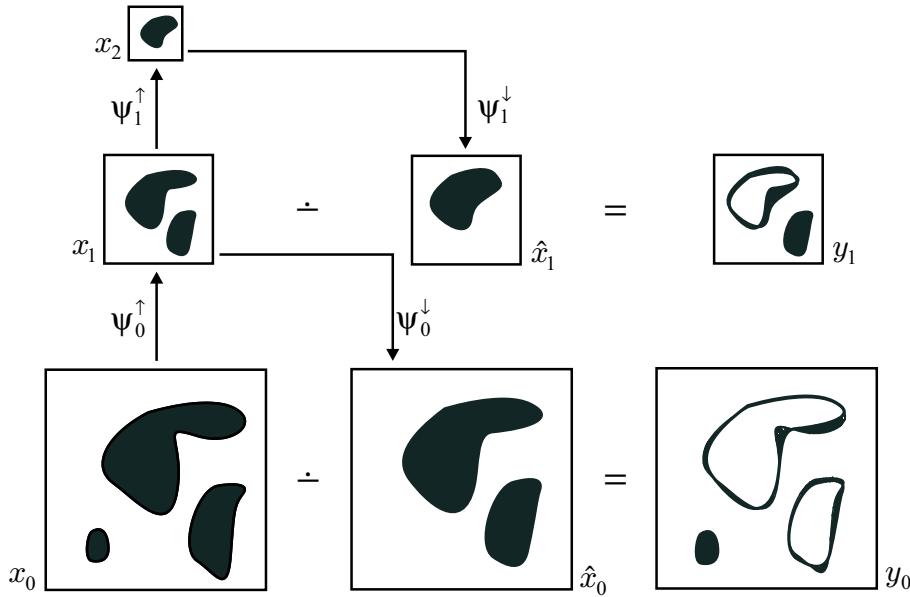


**Fig. 2.** An illustration of the pyramid transform.

Before we conclude this section, we point out here the relationship between our framework and the *nonlinear (convex) multiresolution analysis* introduced by Combettes and Pesquet [15]. For simplicity, take  $j = 0$  (however, the observations below are valid for arbitrary  $j$ ). Define

$$\pi_i = \psi_{i,0}^\downarrow \psi_{0,i}^\uparrow, \quad \text{for } i > 0$$

and

$$V_0^{(i)} = \text{Ran}(\pi_i).$$

In Part 1, we have shown that

$$\pi_i \pi_k = \pi_k \pi_i = \pi_i, \quad \text{for } i \geq k, \quad (2.1)$$

which yields that the sets  $V_0^{(i)}$  are nested, in the sense that

$$V_0^{(i+1)} \subseteq V_0^{(i)} \subseteq V_0, \quad i > 0.$$

Following Combettes and Pesquet [15], we call such a family of nested spaces  $V_0^{(i)}$ , with corresponding projections  $\pi_i$  satisfying (2.1), a *nonlinear multiresolution analysis*.

In [15], Combettes and Pesquet introduce the concept of a convex multiresolution analysis. This consists of a family  $C_j$  of closed convex subsets of a Hilbert space, satisfying some conditions, one of them being

$$C_{j+1} \subseteq C_j, \quad \text{for } j \in \mathbb{Z}, \quad (2.2)$$

and another one being

$$P_{j+1}P_j = P_{j+1}, \quad \text{for } j \in \mathbb{Z}, \quad (2.3)$$

where  $P_j$  is the projection on  $C_j$ . It is easy to fit this case to our pyramid framework. Put  $V_j = C_j$ ,  $\psi_j^\uparrow = P_{j+1}$  and  $\psi_j^\downarrow = P_j$ . Condition (2.2) trivially implies the required pyramid condition  $P_{j+1}P_j = \text{id}$  on  $C_{j+1}$  (notice that we do not need condition (2.3) for this to be true). On the other hand, if we omit condition (2.2), then the pyramid condition amounts to

$$P_{j+1}P_jP_{j+1} = P_{j+1}, \quad \text{for } j \in \mathbb{Z},$$

which is weaker than (2.3).

### 3. Linear Wavelet Transform and Multiresolution Analysis

In this section, we briefly recall the basic theory of linear biorthogonal wavelets. For a comprehensive discussion, the reader is referred to existing textbooks [16, 35, 49].

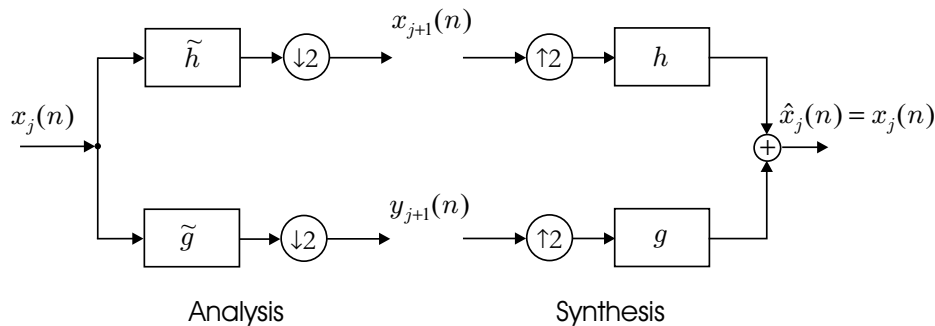


**Fig. 3.** A two-channel linear filter bank:  $\tilde{h}$ ,  $h$  are lowpass filters, whereas  $\tilde{g}$ ,  $g$  are highpass filters.

Consider the two-channel *linear filter bank* depicted in Figure 3. For simplicity, we assume that all filters have real coefficients. This filter bank is called a *perfect reconstruction filter bank* if the output  $\hat{x}_j(n)$  equals the input  $x_j(n)$ . Denoting by  $F(z)$  the  $z$ -transform of a filter's impulse response  $f(n)$ , it can be shown that perfect reconstruction is achieved if

$$\tilde{H}(z)H(z) + \tilde{G}(z)G(z) = 2 \quad (3.1)$$

$$\tilde{H}(-z)H(z) + \tilde{G}(-z)G(z) = 0. \quad (3.2)$$

If all filters are assumed to be FIR (finite impulse response), then there exists a  $k \in \mathbb{Z}$  such that

$$H(z) = z^{2k+1}\tilde{G}(-z) \quad \text{and} \quad G(z) = -z^{2k+1}\tilde{H}(-z); \quad (3.3)$$

see [49].  $\mathbb{Z}$  here denotes the set of integers. In this case, the following properties hold:

$$\tilde{H}(z)H(z) + \tilde{H}(-z)H(-z) = 2 \quad (3.4)$$

$$\tilde{H}(z)G(z) + \tilde{H}(-z)G(-z) = 0 \quad (3.5)$$

$$\tilde{G}(z)G(z) + \tilde{G}(-z)G(-z) = 2 \quad (3.6)$$

$$\tilde{G}(z)H(z) + \tilde{G}(-z)H(-z) = 0. \quad (3.7)$$

Notice that these properties imply that we have perfect reconstruction in the reverse synthesis/analysis scheme depicted in Figure 4; i.e.,  $x'_{j+1} = x_{j+1}$  and  $y'_{j+1} = y_{j+1}$ .

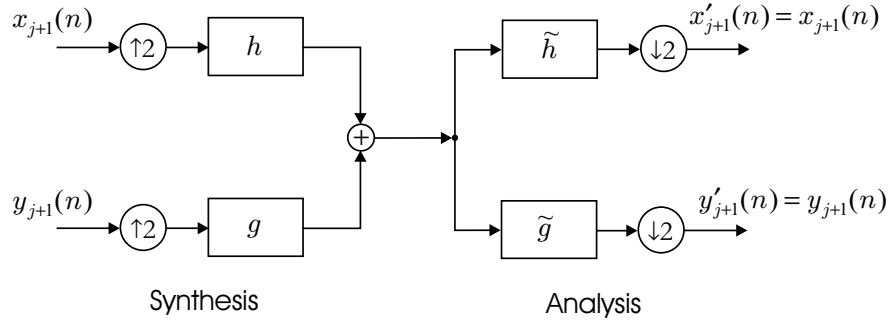


**Fig. 4.** The reverse linear synthesis/analysis scheme.

The aforementioned perfect reconstruction filter bank corresponds to a *biorthogonal multiresolution analysis*, generated by two *scaling functions*  $\tilde{\mathbf{v}}, \mathbf{v}$  and two *wavelet functions*  $\tilde{\mathbf{w}}, \mathbf{w}$  in  $L^2(\mathbb{R})$ ; i.e., the space of all finite energy functions on the real line  $\mathbb{R}$ . The scaling functions satisfy the *dilation equations*

$$\tilde{\mathbf{v}}(t) = \sqrt{2} \sum_{n=-\infty}^{\infty} \tilde{h}(n)\tilde{\mathbf{v}}(2t - n) \quad \text{and} \quad \mathbf{v}(t) = \sqrt{2} \sum_{n=-\infty}^{\infty} h(n)\mathbf{v}(2t - n), \quad (3.8)$$

whereas the wavelet functions are given by

$$\tilde{\mathbf{w}}(t) = \sqrt{2} \sum_{n=-\infty}^{\infty} \tilde{g}(n)\tilde{\mathbf{v}}(2t - n) \quad \text{and} \quad \mathbf{w}(t) = \sqrt{2} \sum_{n=-\infty}^{\infty} g(n)\mathbf{v}(2t - n). \quad (3.9)$$

Note that we use the following convention: functions defined on  $\mathbb{R}$  are printed in boldface to distinguish them from functions defined on  $\mathbb{Z}$ . Let us define by  $\mathbf{v}_{j,n}(t)$  the signal

$$\mathbf{v}_{j,n}(t) = 2^{-j/2}\mathbf{v}(2^{-j}t - n), \quad j, n \in \mathbb{Z} \quad (3.10)$$

(same for  $\tilde{\mathbf{v}}_{j,n}, \mathbf{w}_{j,n}, \tilde{\mathbf{w}}_{j,n}$ ). Let  $V_j$  be the linear subspace of  $L^2(\mathbb{R})$  spanned by the family  $\{\mathbf{v}_{j,n} \mid n \in \mathbb{Z}\}$ ; the subspaces  $\tilde{V}_j, W_j, \tilde{W}_j$  are defined analogously. These spaces constitute a *biorthogonal multiresolution analysis*, in the sense that  $\{V_j\}_{j \in \mathbb{Z}}$  and  $\{\tilde{V}_j\}_{j \in \mathbb{Z}}$  are two multiresolution approximations of  $L^2(\mathbb{R})$ , and

$$V_{j+1} \oplus W_{j+1} = V_j \quad \text{and} \quad \tilde{V}_{j+1} \oplus \tilde{W}_{j+1} = \tilde{V}_j \quad (3.11)$$

$$V_j \perp \tilde{W}_j \quad \text{and} \quad \tilde{V}_j \perp W_j, \quad (3.12)$$

where  $V \oplus W$  denotes the *direct sum* of spaces  $V$  and  $W$ , whereas  $V \perp W$  denotes that space  $V$  is *orthogonal* to space  $W$ . Moreover,

$$\langle \mathbf{v}_{j,m}, \tilde{\mathbf{v}}_{j,n} \rangle = \langle \mathbf{w}_{j,m}, \tilde{\mathbf{w}}_{j,n} \rangle = \delta(m-n), \quad j, m, n \in \mathbb{Z},$$

where  $\langle \cdot, \cdot \rangle$  denotes the *inner product* on  $L^2(\mathbb{R})$ , and  $\delta(n)$  is the *Dirac-delta sequence*. Recall that a sequence  $\{V_j\}_{j \in \mathbb{Z}}$  of closed subspaces of  $L^2(\mathbb{R})$  is called a *multiresolution approximation* of  $L^2(\mathbb{R})$  if there exists a function  $\mathbf{u} \in V_0$ , with a nonvanishing integral, such that  $\{\mathbf{u}(t-n)\}_{n \in \mathbb{Z}}$  is a *Riesz basis* of  $V_0$ , and

$$\mathbf{x}(t) \in V_j \iff \mathbf{x}(t-2^j k) \in V_j, \quad j, k \in \mathbb{Z}$$

$$V_{j+1} \subseteq V_j, \quad j \in \mathbb{Z}$$

$$\mathbf{x}(t) \in V_j \iff \mathbf{x}(t/2) \in V_{j+1}, \quad j \in \mathbb{Z}$$

$$\lim_{j \rightarrow \infty} V_j = \bigcap_{j=-\infty}^{\infty} V_j = \{\mathbf{0}\}$$

$$\overline{\lim_{j \rightarrow -\infty} V_j} = \overline{\bigcup_{j=-\infty}^{\infty} V_j} = L^2(\mathbb{R}),$$

where  $\bar{A}$  denotes the *closure* of a set  $A$ , and  $\mathbf{0}$  denotes the signal which is identically zero [35, 36].

Consider now a signal  $\mathbf{x}_j \in V_j$ ; then  $\mathbf{x}_j$  can be written as a linear combination of  $\mathbf{v}_{j,n}$ ,  $n \in \mathbb{Z}$ ; i.e.,

$$\mathbf{x}_j = \sum_{n=-\infty}^{\infty} x_j(n) \mathbf{v}_{j,n} \quad \text{with} \quad x_j(n) = \langle \mathbf{x}_j, \tilde{\mathbf{v}}_{j,n} \rangle. \quad (3.13)$$

Since  $V_{j+1} \oplus W_{j+1} = V_j$ , we may also write

$$\mathbf{x}_j = \sum_{n=-\infty}^{\infty} x_{j+1}(n) \mathbf{v}_{j+1,n} + \sum_{n=-\infty}^{\infty} y_{j+1}(n) \mathbf{w}_{j+1,n},$$

where  $x_{j+1}(n) = \langle \mathbf{x}_j, \tilde{\mathbf{v}}_{j+1,n} \rangle$  and  $y_{j+1}(n) = \langle \mathbf{x}_j, \tilde{\mathbf{w}}_{j+1,n} \rangle$ . The transformation that maps the continuous signal  $\mathbf{x}_j$  onto the discrete signals  $x_{j+1}(n)$ ,  $y_{j+1}(n)$ , is referred to as the *biorthogonal (linear) wavelet transform* of  $\mathbf{x}_j$ . Using the facts that (see (3.8)–(3.10))

$$\tilde{\mathbf{v}}_{j+1,n} = \sum_{k=-\infty}^{\infty} \tilde{h}(k) \tilde{\mathbf{v}}_{j,2n+k} \quad \text{and} \quad \tilde{\mathbf{w}}_{j+1,n} = \sum_{k=-\infty}^{\infty} \tilde{g}(k) \tilde{\mathbf{v}}_{j,2n+k},$$

we easily find that

$$x_{j+1}(n) = \sum_{k=-\infty}^{\infty} \tilde{h}(k-2n) x_j(k) \quad \text{and} \quad y_{j+1}(n) = \sum_{k=-\infty}^{\infty} \tilde{g}(k-2n) x_j(k).$$

A similar computation shows that the inverse transformation is given by

$$x_j(n) = \sum_{k=-\infty}^{\infty} h(n-2k) x_{j+1}(k) + \sum_{k=-\infty}^{\infty} g(n-2k) y_{j+1}(k).$$

These expressions are in conformity with the perfect reconstruction filter bank scheme depicted in Figure 3.

## 4. General Wavelet Decomposition Schemes

In this section, we present a formal definition of a general wavelet decomposition scheme. This scheme encompasses linear wavelet decompositions as a special case, but allows also a broad class of nonlinear wavelet decomposition schemes. We start in Subsection 4.1 with the definition of the so-called coupled wavelet decomposition scheme which comprises two analysis operators, one for the signal and one for the detail, and one synthesis operator. The uncoupled wavelet decomposition scheme introduced in Subsection 4.2 is a special case of the coupled wavelet decomposition, in the sense that the synthesis operator is the sum of two synthesis operators, the signal and the detail synthesis operators. The linear wavelet decomposition belongs to this second class; in this case the signal and detail analysis (resp. synthesis) operators correspond to lowpass and highpass analysis (resp. synthesis) operators.

### 4.1. Coupled wavelet decomposition

The coupled wavelet decomposition extends the pyramid scheme discussed in Part 1; see also Subsection 2.2. Assume that there exist sets  $V_j$  and  $W_j$ . We refer to  $V_j$  as the *signal space at level  $j$*  and to  $W_j$  as the *detail space at level  $j$* . Signal analysis consists of decomposing a signal in the direction of increasing  $j$  by means of *signal analysis operators*  $\psi_j^\uparrow: V_j \rightarrow V_{j+1}$  and *detail analysis operators*  $\omega_j^\uparrow: V_j \rightarrow W_{j+1}$ . On the other hand, *signal synthesis* proceeds in the direction of decreasing  $j$ , by means of *synthesis operators*  $\Psi_j^\downarrow: V_{j+1} \times W_{j+1} \rightarrow V_j$ . This is illustrated in Figure 5.

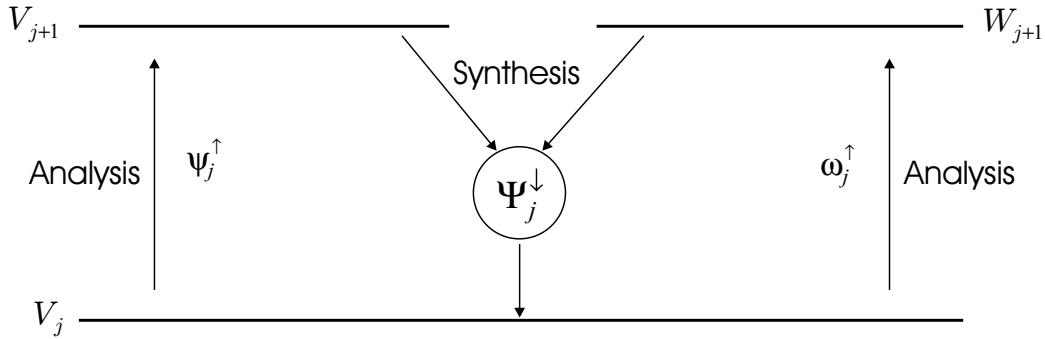


**Fig. 5.** One stage of the coupled wavelet decomposition scheme.

The previous decomposition scheme is required to yield a complete signal representation, in the sense that the mappings  $(\psi_j^\uparrow, \omega_j^\uparrow): V_j \rightarrow V_{j+1} \times W_{j+1}$  and  $\Psi_j^\downarrow: V_{j+1} \times W_{j+1} \rightarrow V_j$  are inverses of each other. This leads to the following conditions:

$$\Psi_j^\downarrow(\psi_j^\uparrow(x), \omega_j^\uparrow(x)) = x, \quad \text{if } x \in V_j, \quad (4.1)$$

which is called the *perfect reconstruction condition*, and

$$\begin{cases} \psi_j^\uparrow(\Psi_j^\downarrow(x, y)) = x, & \text{if } x \in V_{j+1}, \quad y \in W_{j+1} \\ \omega_j^\uparrow(\Psi_j^\downarrow(x, y)) = y, & \text{if } x \in V_{j+1}, \quad y \in W_{j+1}. \end{cases} \quad (4.2)$$

The two conditions in (4.2) guarantee that the decomposition is non-redundant. Condition (4.1) implies that the mapping  $\Psi_j^\uparrow: V_j \rightarrow V_{j+1} \times W_{j+1}$ , given by

$$\Psi_j^\uparrow(x) = (\psi_j^\uparrow(x), \omega_j^\uparrow(x)),$$

is *injective* (i.e., one-to-one) and that  $\Psi_j^\downarrow$  is *surjective* (i.e., onto). On the other hand, (4.2) implies that  $\Psi_j^\uparrow$  is surjective and that  $\Psi_j^\downarrow$  is injective. Furthermore, if (4.1) holds and if  $\Psi_j^\uparrow$  is surjective (or  $\Psi_j^\downarrow$  is injective) then (4.2) holds as well. Also, if (4.2) holds and if  $\Psi_j^\downarrow$  is surjective (or  $\Psi_j^\uparrow$  is injective), then (4.1) holds as well.

Now, given an input signal  $x_0 \in V_0$ , consider the following recursive analysis scheme:

$$x_0 \rightarrow \{x_1, y_1\} \rightarrow \{x_2, y_2, y_1\} \rightarrow \cdots \rightarrow \{x_k, y_k, y_{k-1}, \dots, y_1\} \rightarrow \cdots \quad (4.3)$$

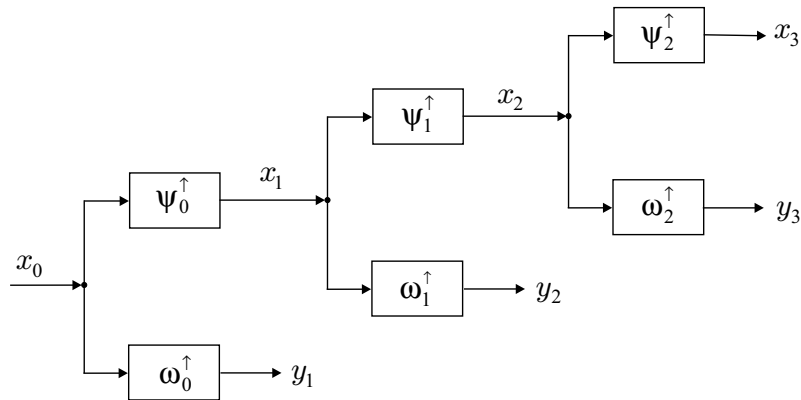
where

$$\begin{cases} x_{j+1} = \psi_j^\uparrow(x_j) \in V_{j+1}, & j \geq 0 \\ y_{j+1} = \omega_j^\uparrow(x_j) \in W_{j+1}, & j \geq 0. \end{cases} \quad (4.4)$$

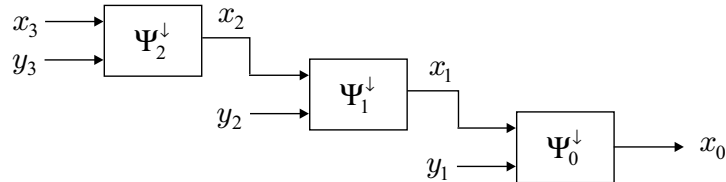
The original signal  $x_0$  can be *exactly* reconstructed from  $x_k$  and  $y_1, y_2, \dots, y_k$  by means of the following recursive synthesis scheme:

$$x_j = \Psi_j^\downarrow(x_{j+1}, y_{j+1}), \quad j = k-1, k-2, \dots, 0, \quad (4.5)$$

which shows that the decomposition (4.3), (4.4) is invertible. We refer to the signal representation scheme governed by (4.1), (4.2), and (4.3)–(4.5) as the *coupled wavelet decomposition scheme*. Block diagrams illustrating this scheme, for the case when  $k = 3$ , are depicted in Figure 6.



(a)



(b)

**Fig. 6.** A 3-level coupled wavelet decomposition scheme: (a) signal analysis, (b) signal synthesis.

The relationship between the coupled wavelet decomposition scheme and the pyramid scheme discussed in Part 1 can be easily established. Recall that the latter scheme is governed by the *pyramid condition*

$$\psi_j^\uparrow \psi_j^\downarrow = \text{id on } V_{j+1}. \quad (4.6)$$

Let the operators  $\psi_j^\uparrow, \omega_j^\uparrow, \Psi_j^\downarrow$  constitute a coupled wavelet decomposition. Fix an element  $y_j^0 \in W_j$ , for every  $j$ , and define  $\psi_j^\downarrow: V_{j+1} \rightarrow V_j$  as

$$\psi_j^\downarrow(x) = \Psi_j^\downarrow(x, y_{j+1}^0), \quad x \in V_{j+1}.$$

Now, the first identity in (4.2) gives  $\psi_j^\uparrow(\psi_j^\downarrow(x)) = x, x \in V_{j+1}$ . In other words, the pair  $(\psi_j^\uparrow, \psi_j^\downarrow)$  satisfies the pyramid condition (4.6).

## 4.2. Uncoupled wavelet decomposition

Of particular interest is the case when there exists a binary operation  $\dot{+}$  on  $V_j$ , which we call *addition* (notice that  $\dot{+}$  may also depend on  $j$ ), and operators  $\psi_j^\downarrow: V_{j+1} \rightarrow V_j$  and  $\omega_j^\downarrow: W_{j+1} \rightarrow V_j$  such that

$$\Psi_j^\downarrow(x, y) = \psi_j^\downarrow(x) \dot{+} \omega_j^\downarrow(y), \quad x \in V_{j+1}, y \in W_{j+1}. \quad (4.7)$$

We refer to  $\psi_j^\downarrow, \omega_j^\downarrow$  as the *signal synthesis* and the *detail synthesis operators*, respectively. Conditions (4.1), (4.2) become

$$\psi_j^\downarrow \psi_j^\uparrow(x) \dot{+} \omega_j^\downarrow \omega_j^\uparrow(x) = x, \quad \text{if } x \in V_j \quad (4.8)$$

$$\psi_j^\uparrow(\psi_j^\downarrow(x) \dot{+} \omega_j^\downarrow(y)) = x, \quad \text{if } x \in V_{j+1}, y \in W_{j+1} \quad (4.9)$$

$$\omega_j^\uparrow(\psi_j^\downarrow(x) \dot{+} \omega_j^\downarrow(y)) = y, \quad \text{if } x \in V_{j+1}, y \in W_{j+1}. \quad (4.10)$$

We refer to the signal representation scheme governed by (4.3)–(4.5), (4.7)–(4.10) as the *uncoupled wavelet decomposition scheme*. One stage of this scheme is illustrated in Figure 7.

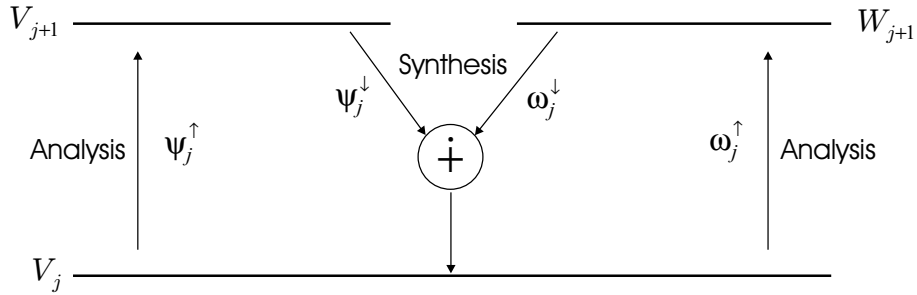


**Fig. 7.** One stage of the uncoupled wavelet decomposition scheme.

Given an input signal  $x_0 \in V_0$  and the corresponding recursive analysis scheme given in (4.3), (4.4),  $x_0$  can be perfectly reconstructed from  $x_k$  and  $y_1, y_2, \dots, y_k$  by means of the following recursive synthesis scheme:

$$x_j = \psi_j^\downarrow(x_{j+1}) \dot{+} \omega_j^\downarrow(y_{j+1}), \quad j = k-1, k-2, \dots, 0.$$

Therefore, signal  $x_j$  at level  $j$  is reconstructed from information that is only available at level  $j+1$ . First, signal  $x_{j+1}$  is mapped down to level  $j$  by means of the signal synthesis operator  $\psi_j^\downarrow$

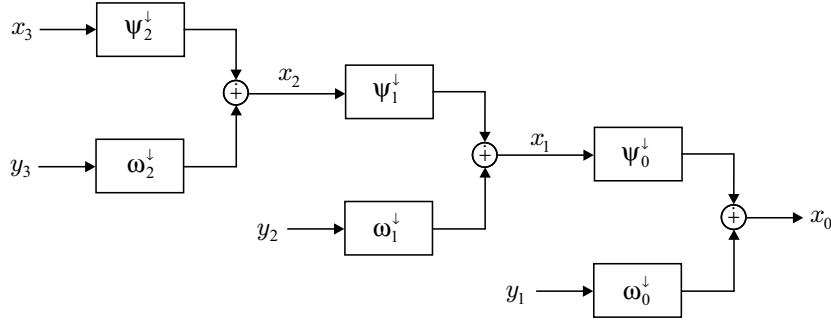


**Fig. 8.** The signal synthesis part of a 3-level uncoupled wavelet decomposition scheme.

so as to obtain an approximation  $\hat{x}_j = \psi_j^\downarrow(x_{j+1})$  of  $x_j$ ; then, the detail signal  $y_{j+1}$  is mapped down to level  $j$  by means of the detail synthesis operator  $\omega_j^\downarrow$  so as to obtain the detail signal  $e_j = \omega_j^\downarrow(y_{j+1})$  at level  $j$ ; finally, the results are combined by means of the addition operator  $\dot{+}$ .

Equation (4.7) concerns only the structure of the synthesis part. A block diagram illustrating this part, for the case when  $k = 3$ , is depicted in Figure 8. The analysis part is the same as in Figure 6(a).

In the examples provided below, we consider only one step in the decomposition; i.e., we only consider decompositions between  $V_0$  and  $V_1, W_1$ . For simplicity, we delete the subindices  $j = 0$  in the corresponding analysis and synthesis operators.

**4.1. Example (lazy wavelet).** The simplest example of an uncoupled wavelet decomposition is the transform that splits a one-dimensional discrete signal  $x(n)$  into its odd and even samples. Let  $V_0 = V_1 = W_1 = \ell^2(\mathbb{Z})$ ; i.e., the space of all finite energy sequences on  $\mathbb{Z}$ . Then, the analysis operators are given by

$$\psi^\uparrow(x)(n) = x(2n) \quad (4.11)$$

$$\omega^\uparrow(x)(n) = x(2n + 1), \quad (4.12)$$

whereas the synthesis operators are given by

$$\psi^\downarrow(x)(2n) = x(n) \quad \text{and} \quad \psi^\downarrow(x)(2n + 1) = 0 \quad (4.13)$$

$$\omega^\downarrow(y)(2n) = 0 \quad \text{and} \quad \omega^\downarrow(y)(2n + 1) = y(n). \quad (4.14)$$

It is obvious that conditions (4.8)–(4.10) are trivially satisfied, with  $\dot{+}$  being the standard addition. The lazy wavelet, better known in the signal processing community as the *polyphase transform of order 2* [49], is not of great interest by itself; the reason why it is treated here is because it is often used as a starting point for the lifting scheme to be discussed in Section 6. ■

**4.2. Example (Haar wavelet).** The simplest non-trivial linear uncoupled wavelet decomposition is the so-called *Haar wavelet* [16, 35]. As in the previous example, choose  $V_0 = V_1 = W_1 = \ell^2(\mathbb{Z})$ . Define the analysis operators

$$\psi^\uparrow(x)(n) = \frac{1}{\sqrt{2}}(x(2n) + x(2n + 1)) \quad (4.15)$$

$$\omega^\uparrow(x)(n) = \frac{1}{\sqrt{2}}(x(2n) - x(2n + 1)), \quad (4.16)$$

and the synthesis operators

$$\psi^\downarrow(x)(2n) = \psi^\downarrow(x)(2n+1) = \frac{1}{\sqrt{2}} x(n) \quad (4.17)$$

$$\omega^\downarrow(y)(2n) = \frac{1}{\sqrt{2}} y(n) \quad \text{and} \quad \omega^\downarrow(y)(2n+1) = -\frac{1}{\sqrt{2}} y(n). \quad (4.18)$$

Again, it is easy to show that conditions (4.8)–(4.10) are all satisfied, provided that  $\dot{+}$  is taken to be the standard addition.  $\blacksquare$

**4.3. Example (quantization).** In the previous two (linear) examples, the signal  $\psi^\uparrow(x)$  contains half the number of samples of the original signal  $x$ . We now present a simple nonlinear example where the number of samples of  $x$  and  $\psi^\uparrow(x)$  are the same, but where  $\psi^\uparrow$  reduces the number of bits needed to represent a signal by one.

Let  $V_0 = \mathcal{T}_N^{\mathbb{Z}}$ ,  $V_1 = \mathcal{T}_{N-1}^{\mathbb{Z}}$ , and  $W_1 = \{0, 1\}^{\mathbb{Z}}$ , where  $\mathcal{T}_k = \{0, 1, \dots, 2^k - 1\}$ . Define the analysis operators

$$\begin{aligned} \psi^\uparrow(x)(n) &= \lfloor x(n)/2 \rfloor \\ \omega^\uparrow(x)(n) &= x(n) - 2\lfloor x(n)/2 \rfloor, \end{aligned}$$

where  $\lfloor \cdot \rfloor$  denotes the floor function (i.e., for  $t \in \mathbb{R}$ ,  $\lfloor t \rfloor$  is the largest integer  $\leq t$ ), and the synthesis operators

$$\begin{aligned} \psi^\downarrow(x)(n) &= 2x(n) \\ \omega^\downarrow(y)(n) &= y(n). \end{aligned}$$

Observe that the pair  $(\psi^\uparrow, \psi^\downarrow)$  defines an adjunction. The reader may readily verify that conditions (4.8)–(4.10) are satisfied, with  $\dot{+}$  being the standard addition. The signal analysis operator  $\psi^\uparrow$  discards one bit of information in  $x(n)$ . In fact, this bit is stored in the detail signal  $\omega^\uparrow(x)(n)$ , thus enabling perfect reconstruction.  $\blacksquare$

**4.4. Example (S-transform).** The S-transform can be considered as a nonlinear modification of the Haar wavelet with the additional property that it maps integer-valued signals onto integer-valued signals, but without abandoning the property of perfect reconstruction. In this case, the analysis operators are given by

$$\begin{aligned} \psi^\uparrow(x)(n) &= \left\lfloor \frac{x(2n) + x(2n+1)}{2} \right\rfloor \\ \omega^\uparrow(x)(n) &= x(2n+1) - x(2n). \end{aligned}$$

The corresponding synthesis operators are given by

$$\begin{aligned} \psi^\downarrow(x)(2n) &= \psi^\downarrow(x)(2n+1) = x(n) \\ \omega^\downarrow(y)(2n) &= -\left\lfloor \frac{y(n)}{2} \right\rfloor \quad \text{and} \quad \omega^\downarrow(y)(2n+1) = \left\lfloor \frac{y(n)+1}{2} \right\rfloor. \end{aligned}$$

Refer to Figure 9 for an illustration.

The specific character of these operators guarantee that integer signals are mapped onto integer signals, and we may choose  $V_0 = V_1 = W_1 = \mathbb{Z}^{\mathbb{Z}}$ , i.e., all doubly infinite integer-valued sequences. It is easy to show that conditions (4.8)–(4.10) are all satisfied here as well, provided that  $\dot{+}$  is taken to be the standard addition.

The S-transform, where “S” stands for “sequential,” has been known in the literature for several years, and has been successfully used in medical imaging for lossless compression [41]. During the years, several modifications and generalizations have been proposed; e.g., see [43]. In Section 6, we consider the S-transform in the context of lifting and present a simple modification to this scheme.  $\blacksquare$

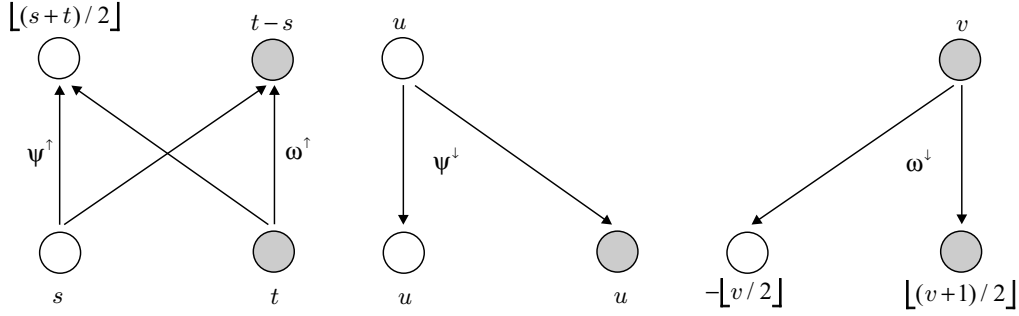


**Fig. 9.** An illustration of the S-transform. The white and gray nodes correspond to the even and odd samples, respectively.

### 4.3. Linear biorthogonal wavelets

The linear biorthogonal wavelet transform, discussed in Section 3, fits well into the framework of uncoupled wavelet decompositions. We consider this case from two different perspectives.

First, let us choose  $V_j$  and  $W_j$  as in Section 3, and let  $\psi_j^\uparrow, \omega_j^\uparrow$  be the *projections* of  $V_j$  onto  $V_{j+1}$  and  $W_{j+1}$ , respectively, corresponding with the decomposition

$$V_j = V_{j+1} \oplus W_{j+1}.$$

In this case, every  $\mathbf{x} \in V_j$  satisfies

$$\mathbf{x} = \psi_j^\uparrow(\mathbf{x}) + \omega_j^\uparrow(\mathbf{x}).$$

Now, if we choose for  $\psi_j^\downarrow$  and  $\omega_j^\downarrow$  the identity operator (observe that  $V_{j+1}$  and  $W_{j+1}$  are subspaces of  $V_j$ ), then the conditions (4.8)–(4.10) are trivially satisfied, provided that  $\dot{+}$  is taken to be the standard addition.

A different, but equivalent, perspective can be obtained by representing  $V_j, W_j$  in terms of the bases  $\{\mathbf{v}_{j,n} \mid n \in \mathbb{Z}\}$  and  $\{\mathbf{w}_{j,n} \mid n \in \mathbb{Z}\}$ , respectively. With every signal  $x \in \ell^2(\mathbb{Z})$  we can associate a unique element  $\mathbf{x}_j \in V_j$  by putting

$$\mathbf{x}_j = \sum_{n=-\infty}^{\infty} x_j(n) \mathbf{v}_{j,n};$$

see (3.13). Decomposing  $\mathbf{x}_j$  as  $\mathbf{x}_{j+1} + \mathbf{y}_{j+1}$ , with  $\mathbf{x}_{j+1} \in V_{j+1}$  and  $\mathbf{y}_{j+1} \in W_{j+1}$ , and writing

$$\mathbf{x}_{j+1} = \sum_{n=-\infty}^{\infty} x_{j+1}(n) \mathbf{v}_{j+1,n}, \quad \mathbf{y}_{j+1} = \sum_{n=-\infty}^{\infty} y_{j+1}(n) \mathbf{w}_{j+1,n},$$

we obtain the analysis and synthesis operators (which are now operators mapping  $\ell^2(\mathbb{Z})$  into itself):

$$\psi_j^\uparrow(x)(n) = \sum_{k=-\infty}^{\infty} \tilde{h}(k-2n)x(k) \quad (4.19)$$

$$\omega_j^\uparrow(x)(n) = \sum_{k=-\infty}^{\infty} \tilde{g}(k-2n)x(k) \quad (4.20)$$

$$\psi_j^\downarrow(x)(n) = \sum_{k=-\infty}^{\infty} h(n-2k)x(k) \quad (4.21)$$

$$\omega_j^\downarrow(y)(n) = \sum_{k=-\infty}^{\infty} g(n-2k)y(k). \quad (4.22)$$

If the  $z$ -transforms of the filters involved are related by means of (3.3), then all conditions in (4.8)–(4.10) are satisfied (with  $V_j$  and  $W_j$  replaced by  $\ell^2(\mathbb{Z})$ ). In fact, the perfect reconstruction condition (4.8) is equivalent to (3.1), (3.2), condition (4.9) is equivalent to (3.4), (3.5), and condition (4.10) is equivalent to (3.6), (3.7).

In Part 1, Section 4, we have seen that, in the linear case, the pyramid condition  $\psi^\uparrow\psi^\downarrow = \text{id}$ , with  $\psi^\uparrow$  and  $\psi^\downarrow$  given by (4.19) and (4.21), respectively, amounts to the condition

$$\sum_{k=-\infty}^{\infty} \tilde{h}(2n-k)h(k) = \delta(n).$$

Multiplying both sides of this equation with  $z^{-2n}$  and summing over  $n$  yields:

$$\begin{aligned} 1 &= \sum_{n=-\infty}^{\infty} \sum_{k=-\infty}^{\infty} \tilde{h}(2n-k)h(k)z^{-2n} \\ &= \sum_{k=-\infty}^{\infty} h(2k)z^{-2k} \sum_{n=-\infty}^{\infty} \tilde{h}(2n-2k)z^{-2n+2k} \\ &\quad + \sum_{k=-\infty}^{\infty} h(2k+1)z^{-2k-1} \sum_{n=-\infty}^{\infty} \tilde{h}(2n-2k-1)z^{-2n+2k+1}, \end{aligned}$$

which gives

$$H_e(z)\tilde{H}_e(z) + H_o(z)\tilde{H}_o(z) = 1. \quad (4.23)$$

Here,  $H_e(z)$  is the *even* part of  $H(z)$  (i.e.,  $H_e(z) = \frac{1}{2}(H(z) + H(-z))$ ) and  $H_o(z)$  is the *odd* part of  $H(z)$  (i.e.,  $H_o(z) = \frac{1}{2}(H(z) - H(-z))$ ). It is easy to verify that (4.23) is equivalent to

$$\tilde{H}(z)H(z) + \tilde{H}(-z)H(-z) = 2,$$

which coincides with (3.4). Defining  $G(z)$  and  $\tilde{G}(z)$  by means of equation (3.3), it is easy to verify that conditions (3.1)–(3.7) are all satisfied. Thus, we have shown the following result (see also [42]).

**4.5. Proposition.** *Consider the signal analysis and synthesis operators*

$$\psi^\uparrow(x)(n) = \sum_{k=-\infty}^{\infty} \tilde{h}(k-2n)x(k) \quad (4.24)$$

$$\psi^\downarrow(x)(n) = \sum_{k=-\infty}^{\infty} h(n-2k)x(k) \quad (4.25)$$

such that the pyramid condition  $\psi^\uparrow\psi^\downarrow = \text{id}$  is satisfied; i.e.,

$$\sum_{k=-\infty}^{\infty} \tilde{h}(2n-k)h(k) = \delta(n), \quad n \in \mathbb{Z}.$$

Then, there exist detail analysis and synthesis operators

$$\begin{aligned} \omega^\uparrow(x)(n) &= \sum_{k=-\infty}^{\infty} \tilde{g}(k-2n)x(k) \\ \omega^\downarrow(y)(n) &= \sum_{k=-\infty}^{\infty} g(n-2k)y(k) \end{aligned}$$

such that this system defines a linear biorthogonal wavelet decomposition.

Basically, this result says that, in the linear case, any pyramid that satisfies the pyramid condition can be extended to a wavelet decomposition. Choosing  $k = 0$  in (3.3), we get

$$g(n) = (-1)^n \tilde{h}(n+1) \quad \text{and} \quad \tilde{g}(n) = (-1)^n h(n-1). \quad (4.26)$$

**4.6. Example (Burt-Adelson wavelet).** Consider the Burt-Adelson pyramid discussed in Example 4.2 of Part 1. The signal analysis and synthesis operators are given by

$$\psi^\uparrow(x)(n) = \frac{1}{8}(-x(2n-2) + 2x(2n-1) + 6x(2n) + 2x(2n+1) - x(2n+2)) \quad (4.27)$$

$$\psi^\downarrow(x)(2n) = x(n) \quad \text{and} \quad \psi^\downarrow(x)(2n+1) = \frac{1}{2}(x(n) + x(n+1)). \quad (4.28)$$

From (4.24), (4.25), (4.27), and (4.28), we have that

$$\begin{cases} \tilde{h}(0) = 3/4, & \tilde{h}(-1) = \tilde{h}(1) = 1/4, & \tilde{h}(-2) = \tilde{h}(2) = -1/8, & \tilde{h}(n) = 0, & \text{otherwise} \\ h(0) = 1, & h(-1) = h(1) = 1/2, & h(n) = 0, & \text{otherwise.} \end{cases} \quad (4.29)$$

Using (4.26) and (4.29), we find

$$\begin{cases} g(-3) = g(1) = 1/8, & g(-2) = g(0) = 1/4, & g(-1) = -3/4, & g(n) = 0, & \text{otherwise} \\ \tilde{g}(0) = 1/2, & \tilde{g}(1) = -1, & \tilde{g}(2) = 1/2, & \tilde{g}(n) = 0, & \text{otherwise.} \end{cases}$$

This leads to the following detail analysis and synthesis operators:

$$\begin{aligned} \omega^\uparrow(x)(n) &= \frac{1}{2}x(2n) - x(2n+1) + \frac{1}{2}x(2n+2) \\ \omega^\downarrow(y)(2n) &= \frac{1}{4}y(n) + \frac{1}{4}y(n+1) \\ \omega^\downarrow(y)(2n+1) &= \frac{1}{8}y(n) - \frac{3}{4}y(n+1) + \frac{1}{8}y(n+2). \end{aligned}$$

One can easily check that, indeed, the conditions (4.8)–(4.10) concerning the uncoupled wavelet decomposition scheme are all satisfied. We may call the resulting linear signal decomposition scheme the *Burt-Adelson wavelet decomposition*. However, it is not difficult to see that this example produces the four discrete analysis and synthesis filters associated with a spline biorthogonal wavelet of order (2, 2) [16, Chapter 8] (see also [14]). ■

#### 4.4. Nonlinear biorthogonal-like multiresolution analysis

The linear biorthogonal multiresolution analysis, discussed in Section 3, can be conceptually extended to the more general framework of the uncoupled wavelet decomposition scheme. Indeed, consider  $V_j^{(j+1)} = \text{Ran}(\hat{\psi}_j)$  and  $W_j^{(j+1)} = \text{Ran}(\hat{\omega}_j)$ , where  $\hat{\psi}_j = \psi_j^\downarrow \psi_j^\uparrow$  and  $\hat{\omega}_j = \omega_j^\downarrow \omega_j^\uparrow$  (recall our discussion and notation in Subsection 2.2). From (4.8), we get that every signal  $x \in V_j$  has a unique decomposition  $x = x' \dot{+} y'$ , where  $x' \in V_j^{(j+1)}$  and  $y' \in W_j^{(j+1)}$ , namely  $x = \hat{\psi}_j(x) \dot{+} \hat{\omega}_j(x)$ . Thus, we may write, in analogy with (3.11),

$$V_j = V_j^{(j+1)} \oplus W_j^{(j+1)}.$$

Let us assume that there exists an  $0_v \in V_j$  (which depends on  $j$  in general) such that  $x \dot{+} 0_v = 0_v \dot{+} x = x$ , for every  $x \in V_j$ , and  $\psi_j^\downarrow(0_v) = 0_v$ . If there exists an  $0_w \in W_j$  (which also depends on  $j$  in general) such that  $\omega_j^\downarrow(0_w) = 0_w$ , then (4.9) and (4.10) imply that

$$\psi_j^\uparrow \psi_j^\downarrow(x) = x, \quad \text{for } x \in V_{j+1} \quad (4.30)$$

$$\omega_j^\uparrow \omega_j^\downarrow(y) = y, \quad \text{for } y \in W_{j+1} \quad (4.31)$$

$$\psi_j^\uparrow \omega_j^\downarrow(y) = 0_v, \quad \text{for } y \in W_{j+1} \quad (4.32)$$

$$\omega_j^\uparrow \psi_j^\downarrow(x) = 0_w, \quad \text{for } x \in V_{j+1}. \quad (4.33)$$

This implies that  $\hat{\psi}_j$  and  $\hat{\omega}_j$  are idempotent operators on  $V_j$  (also called *projections*). Furthermore (4.32), (4.33) imply that

$$\hat{\psi}_j \hat{\omega}_j = \hat{\omega}_j \hat{\psi}_j = \underline{0},$$

where  $\underline{0}$  is the operator on  $V_j$  which is identically  $0_v$ . The projections  $\hat{\psi}_j$  and  $\hat{\omega}_j$  are *complementary* in the sense that

$$\hat{\psi}_j \dot{+} \hat{\omega}_j = \text{id},$$

where  $(\hat{\psi}_j \dot{+} \hat{\omega}_j)(x) = \hat{\psi}_j(x) \dot{+} \hat{\omega}_j(x)$ , for  $x \in V_j$ .

## 5. Morphological Haar Wavelet

### 5.1. The one-dimensional case

In this section, we discuss a morphological variant of the Haar wavelet in one dimension. The major difference with the classical linear Haar wavelet, discussed in Example 4.2, is that the linear signal analysis filter of the latter is replaced by an erosion (or dilation); i.e., by taking the minimum (or maximum) over two samples. Let  $V_0 = V_1 = W_1 = \mathbb{R}^{\mathbb{Z}}$  be the lattice of doubly infinite real-valued sequences. Define the analysis and synthesis operators as (compare with (4.15)–(4.18)):

$$\psi^\uparrow(x)(n) = x(2n) \wedge x(2n+1) \quad (5.1)$$

$$\omega^\uparrow(x)(n) = x(2n) - x(2n+1) \quad (5.2)$$

$$\psi^\downarrow(x)(2n) = \psi^\downarrow(x)(2n+1) = x(n) \quad (5.3)$$

$$\omega^\downarrow(y)(2n) = y(n) \vee 0 \quad \text{and} \quad \omega^\downarrow(y)(2n+1) = -(y(n) \wedge 0). \quad (5.4)$$

In Part 1, we have seen that the operators  $\psi^\uparrow, \psi^\downarrow$  satisfy the pyramid condition (4.6). The corresponding pyramid was called the morphological Haar pyramid (see Example 5.5 in Part 1). It can also be shown that (5.1)–(5.4) satisfy conditions (4.8)–(4.10), provided that  $\dot{+}$  is taken to be the standard addition. Therefore, the morphological Haar wavelet is another example of an uncoupled wavelet decomposition scheme.

Figure 10 illustrates the computations associated with the analysis and synthesis operators of a 3-stage morphological Haar wavelet decomposition scheme. The gray nodes indicate the detail signal.

Figure 11 depicts an example of the linear Haar wavelet decomposition scheme, given by (4.15), (4.16), whereas Figure 12 depicts an example of the morphological Haar wavelet decomposition scheme, given by (5.1), (5.2). In these figures, as well as other figures in this report, we have normalized the vertical axis of plots depicting detail signals in such a way that (almost) the entire range is used. To be precise, the vertical axis of the plot of a detail signal

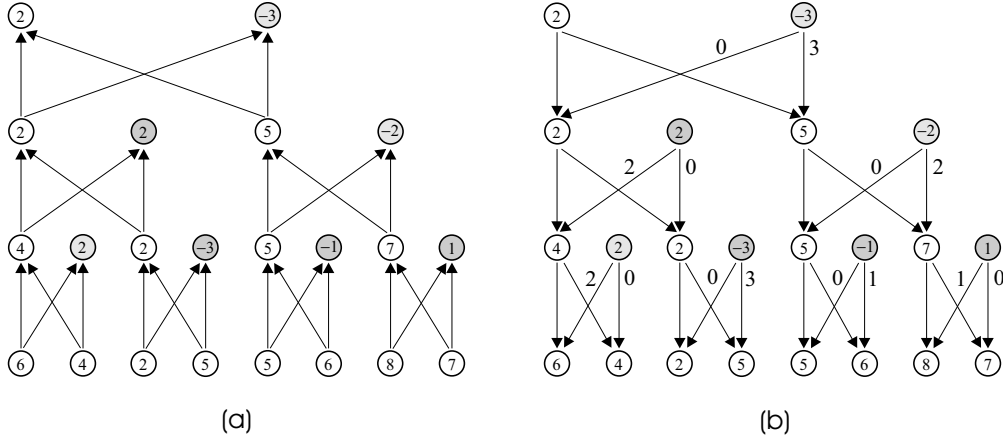


**Fig. 10.** Computations associated with a 3-stage morphological Haar wavelet decomposition scheme: (a) signal analysis, (b) signal synthesis. The gray nodes indicate the detail signal.

$y$  runs from  $y_{min} - \epsilon$  to  $y_{max} + \epsilon$ , where  $y_{min}, y_{max}$  are the minimum and maximum values of  $y$ , respectively, and  $\epsilon = 0.1 \times \max(|y_{min}|, |y_{max}|)$ . For two dimensional detail images, we use a similar convention: pixels where the detail signal matches its minimum (resp. maximum) value are displayed in black (resp. white).

Notice that the signal analysis operator in the morphological case guarantees that the range of values of the scaled signals  $\{x_j, j \geq 1\}$  is the same as the range of values of the original signal  $x_0$ . It furthermore guarantees that, if the original signal  $x_0$  is discrete-valued, the scaled signals  $\{x_j, j \geq 1\}$  will be discrete-valued as well, a highly desirable property in lossless coding applications [7]. Moreover, the morphological Haar wavelet decomposition scheme does a better job in preserving the shape of the three main features (the three dips) in  $x_0$  as compared to the linear case. This is expected, since the signal analysis filters in the linear Haar wavelet decomposition scheme are linear lowpass filters, and as such smooth-out edges. The signal analysis filters in the morphological Haar case are nonlinear, and as such preserve edge information.

In (5.1), we have chosen to use minimum. It is obvious that we can also take maximum instead; i.e., we can set

$$\psi^\uparrow(x)(n) = x(2n) \vee x(2n + 1),$$

and leave  $\omega^\uparrow$  unchanged. In this case, the corresponding signal synthesis operator  $\psi^\downarrow$  is the same as in (5.3), but the detail synthesis operator becomes

$$\omega^\downarrow(y)(2n) = y(n) \wedge 0 \quad \text{and} \quad \omega^\downarrow(y)(2n + 1) = -(y(n) \vee 0).$$

Notice that, when we use minimum in the signal analysis operator,  $(\psi^\uparrow, \psi^\downarrow)$  is an adjunction, whereas when we use maximum,  $(\psi^\downarrow, \psi^\uparrow)$  is an adjunction.

It is not difficult to define a binary version of the wavelet decomposition scheme (5.1)–(5.4). Indeed, let  $V_0 = V_1 = W_1 = \{0, 1\}^{\mathbb{Z}}$  be the Boolean lattice of doubly infinite sequences of 0’s and 1’s. We choose the “exclusive OR” operation, denoted by  $\Delta$ , as the binary operation  $\dot{+}$  on  $V_0$ . Then, we define analysis and synthesis operators (cf. (5.1)–(5.4)) as follows:

$$\psi^\uparrow(x)(n) = x(2n) \tag{5.5}$$

$$\omega^\uparrow(x)(n) = x(2n) \Delta x(2n + 1) \tag{5.6}$$

$$\psi^\downarrow(x)(2n) = \psi^\downarrow(x)(2n + 1) = x(n) \tag{5.7}$$

$$\omega^\downarrow(y)(2n) = 0 \quad \text{and} \quad \omega^\downarrow(y)(2n + 1) = y(n). \tag{5.8}$$

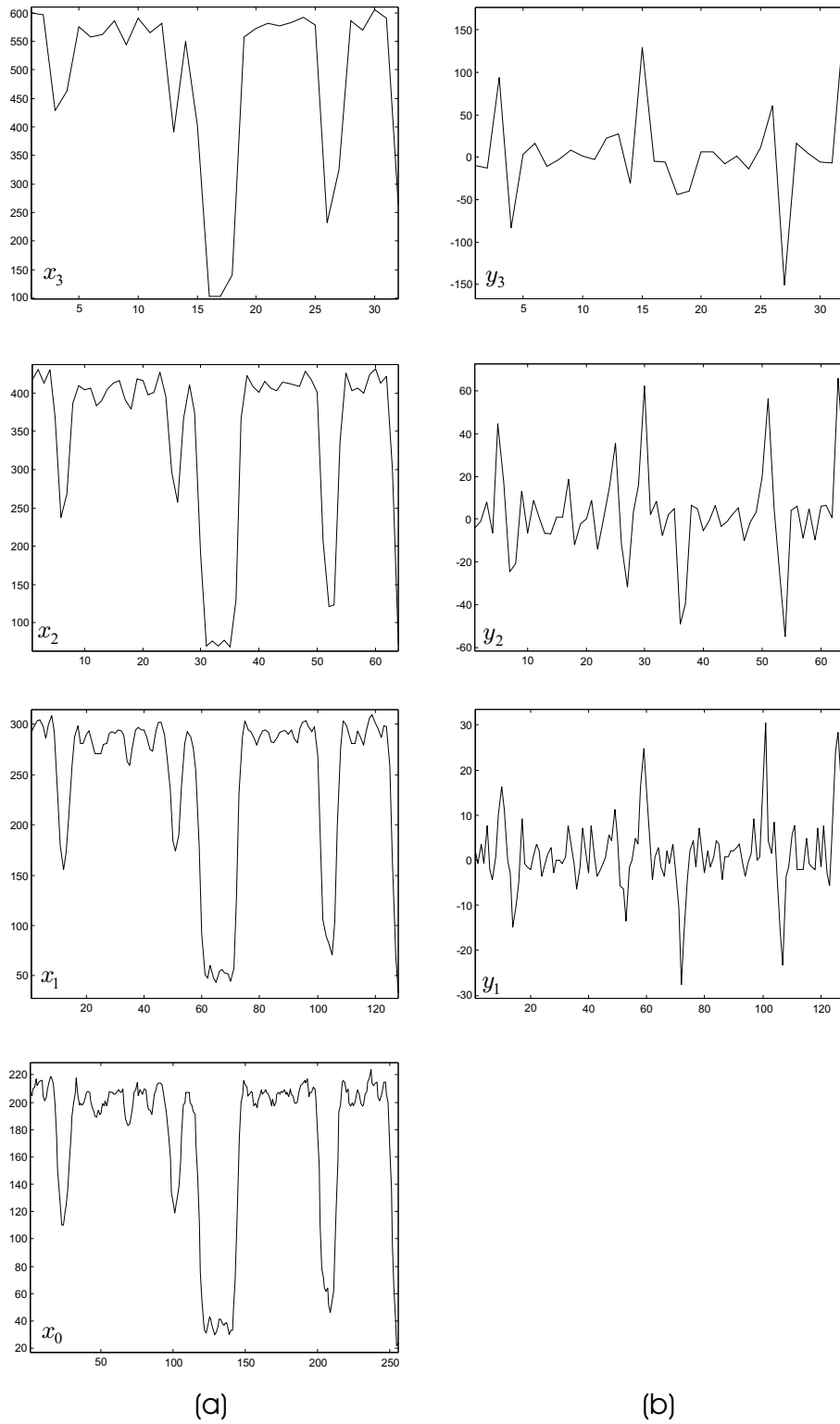


**Fig. 11.** Multiresolution signal decomposition based on the linear Haar wavelet transform: (a) A signal  $x_0$  and its scaled signal decomposition  $\{x_1, x_2, x_3\}$  obtained by means of the analysis operator  $\psi^\uparrow$  in (4.15). (b) The detail signals  $\{y_1, y_2, y_3\}$  obtained from  $\{x_0, x_1, x_2\}$  by means of the analysis operator  $\omega^\uparrow$  in (4.16).

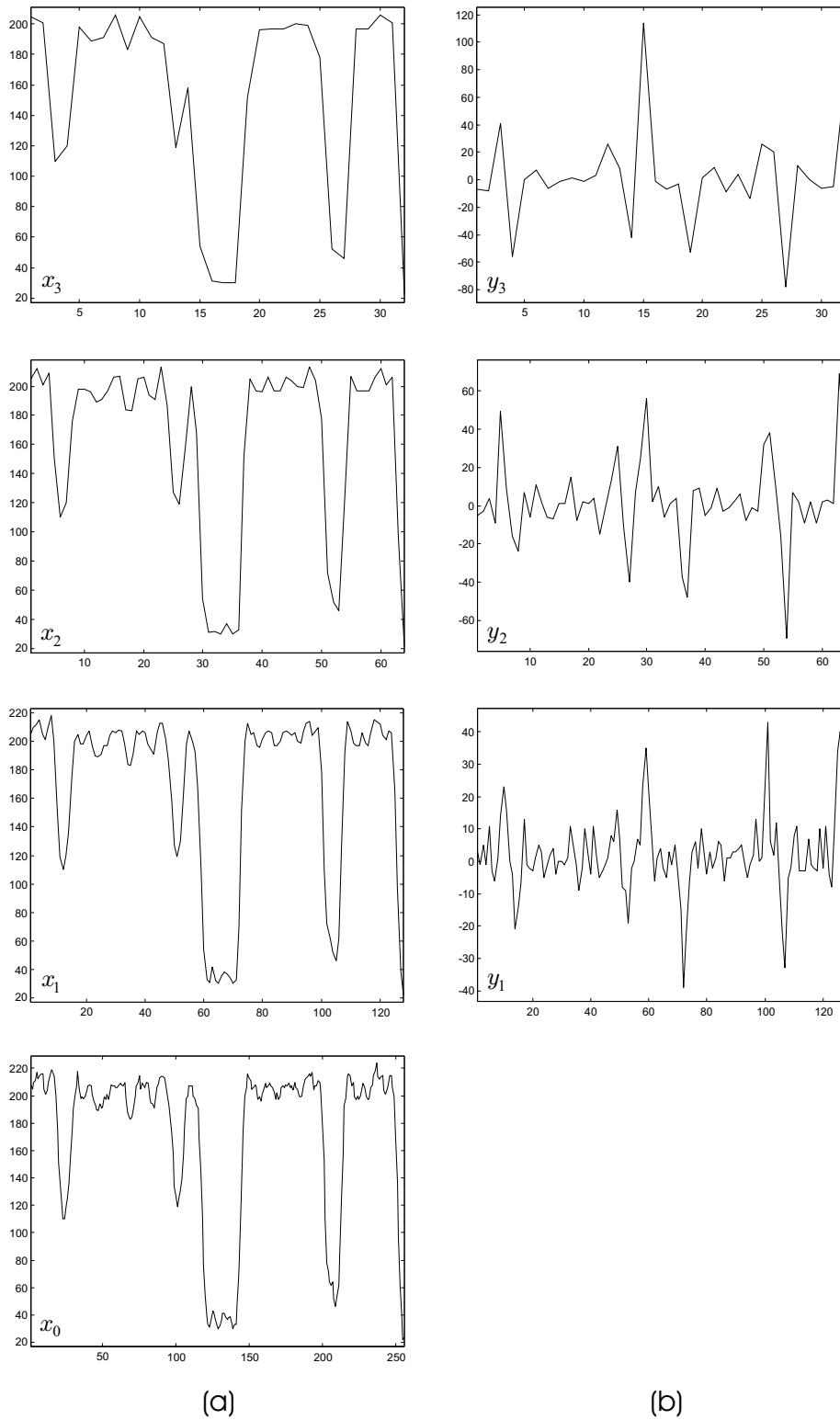


**Fig. 12.** Multiresolution signal decomposition based on the morphological Haar wavelet transform: (a) A signal  $x_0$  and its scaled signal decomposition  $\{x_1, x_2, x_3\}$  obtained by means of the analysis operator  $\psi^\uparrow$  in (5.1). (b) The detail signals  $\{y_1, y_2, y_3\}$  obtained from  $\{x_0, x_1, x_2\}$  by means of the analysis operator  $\omega^\uparrow$  in (5.2).

It is easy to verify that this defines an uncoupled wavelet decomposition scheme. Notice that the detail signal  $\omega^\uparrow(x)$  contains 1's only at a transition (from 0 to 1 or vice versa) in signal  $x$  that occurs at an even point. The decomposition is *self-dual*, in the sense that

$$\psi^\uparrow(\bar{x}) = \overline{\psi^\uparrow(x)} \quad \text{and} \quad \omega^\uparrow(\bar{x}) = \omega^\uparrow(x),$$

where  $\bar{x}(n) = 1 - x(n)$ . An example is illustrated in Figure 13. Such a binary scheme can be extended, without any serious effort, to finite-valued signals with values in  $\{0, 1, \dots, N - 1\}$ ,  $N < \infty$ , and with  $\Delta$  being replaced by “addition modulo  $N$ .”

## 5.2. The two-dimensional case

We can extend the morphological Haar wavelet decomposition scheme to two and higher dimensions by using a separable filter bank (e.g., by sequentially applying the one-dimensional decomposition on the columns and rows of a two-dimensional image) [35, 49]. However, we can also define a non-separable two-dimensional version of the morphological Haar wavelet.

Indeed, let  $V_0$  and  $V_1$  consist of all functions from  $\mathbb{Z}^2$  into  $\mathbb{R}$  and let  $W_1$  consist of all functions from  $\mathbb{Z}^2$  into  $\mathbb{R}^3$ . We introduce the following notation. By  $\mathbf{n}, 2\mathbf{n}$  we denote the points  $(m, n), (2m, 2n) \in \mathbb{Z}^2$ , respectively, and by  $2\mathbf{n}_+, 2\mathbf{n}^+, 2\mathbf{n}_+^\dagger$  we denote the points  $(2m + 1, 2n), (2m, 2n + 1), (2m + 1, 2n + 1)$ , respectively. Define

$$\psi^\uparrow(x)(\mathbf{n}) = x(2\mathbf{n}) \wedge x(2\mathbf{n}_+) \wedge x(2\mathbf{n}^+) \wedge x(2\mathbf{n}_+^\dagger) \quad (5.9)$$

$$\omega^\uparrow(x)(\mathbf{n}) = (\omega_v(x)(\mathbf{n}), \omega_h(x)(\mathbf{n}), \omega_d(x)(\mathbf{n})), \quad (5.10)$$

where  $\omega_v, \omega_h, \omega_d$  represent the vertical, horizontal, and diagonal detail signals, given by:

$$\omega_v(x)(\mathbf{n}) = \frac{1}{2}(x(2\mathbf{n}) - x(2\mathbf{n}^+) + x(2\mathbf{n}_+) - x(2\mathbf{n}_+^\dagger)) \quad (5.11)$$

$$\omega_h(x)(\mathbf{n}) = \frac{1}{2}(x(2\mathbf{n}) - x(2\mathbf{n}_+) + x(2\mathbf{n}^+) - x(2\mathbf{n}_+^\dagger)) \quad (5.12)$$

$$\omega_d(x)(\mathbf{n}) = \frac{1}{2}(x(2\mathbf{n}) - x(2\mathbf{n}_+) - x(2\mathbf{n}^+) + x(2\mathbf{n}_+^\dagger)). \quad (5.13)$$

The synthesis operators are now given by

$$\psi^\downarrow(x)(2\mathbf{n}) = \psi^\downarrow(x)(2\mathbf{n}_+) = \psi^\downarrow(x)(2\mathbf{n}^+) = \psi^\downarrow(x)(2\mathbf{n}_+^\dagger) = x(\mathbf{n}), \quad (5.14)$$

and

$$\begin{aligned} \omega^\downarrow(y)(2\mathbf{n}) &= (y_v(\mathbf{n}) + y_h(\mathbf{n})) \vee (y_v(\mathbf{n}) + y_d(\mathbf{n})) \vee (y_h(\mathbf{n}) + y_d(\mathbf{n})) \vee 0 \\ \omega^\downarrow(y)(2\mathbf{n}_+) &= (y_v(\mathbf{n}) - y_h(\mathbf{n})) \vee (y_v(\mathbf{n}) - y_d(\mathbf{n})) \vee (-y_h(\mathbf{n}) - y_d(\mathbf{n})) \vee 0 \\ \omega^\downarrow(y)(2\mathbf{n}^+) &= (y_h(\mathbf{n}) - y_v(\mathbf{n})) \vee (-y_v(\mathbf{n}) - y_d(\mathbf{n})) \vee (y_h(\mathbf{n}) - y_d(\mathbf{n})) \vee 0 \\ \omega^\downarrow(y)(2\mathbf{n}_+^\dagger) &= (-y_v(\mathbf{n}) - y_h(\mathbf{n})) \vee (y_d(\mathbf{n}) - y_v(\mathbf{n})) \vee (y_d(\mathbf{n}) - y_h(\mathbf{n})) \vee 0, \end{aligned}$$

where we write  $y \in W_1$  as  $y = (y_v, y_h, y_d)$ . It is not difficult to show that conditions (4.8)–(4.10) are all satisfied, provided that  $\dot{+}$  is taken to be the standard addition. Therefore, this is a two-dimensional example of an uncoupled wavelet decomposition scheme.

The analysis operators  $\psi^\uparrow$  and  $\omega^\uparrow$  in (5.9), (5.10) map a quadruple of signal values, as the ones depicted in the left hand-side of Figure 14, to the quadruple at the right hand-side; here  $x_1 = \psi^\uparrow(x)$  and  $y_v = \omega_v(x)$  (the same for  $y_h, y_d$ ). An example, illustrating one step of this decomposition is depicted in Figure 15.

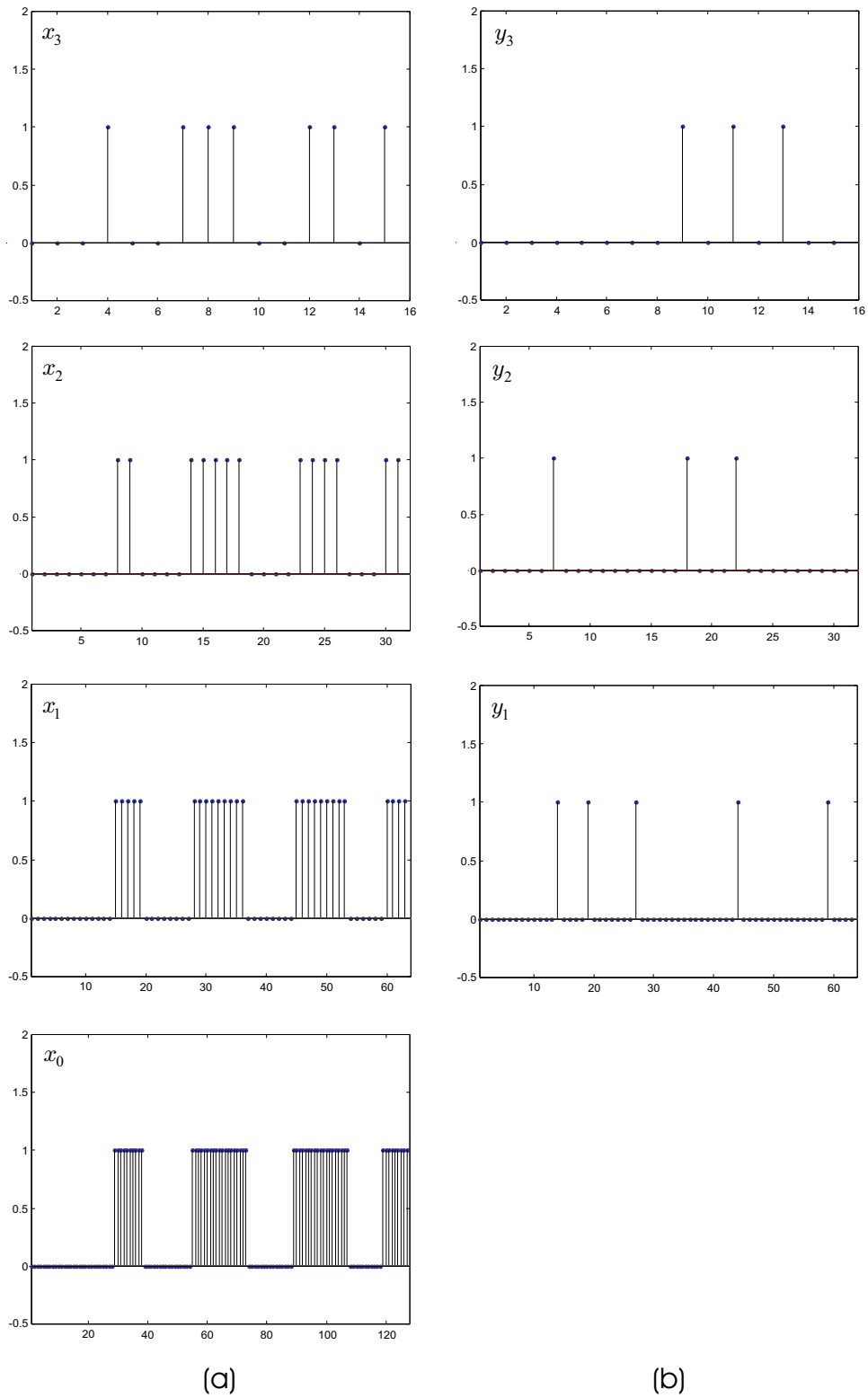


**Fig. 13.** Multiresolution signal decomposition based on the binary morphological Haar wavelet transform: (a) A binary signal  $x_0$  and its scaled signal decomposition  $\{x_1, x_2, x_3\}$  obtained by means of the analysis operator  $\psi^\uparrow$  in (5.5). (b) The detail signals  $\{y_1, y_2, y_3\}$  obtained from  $\{x_0, x_1, x_2\}$  by means of the analysis operator  $\omega^\uparrow$  in (5.6).

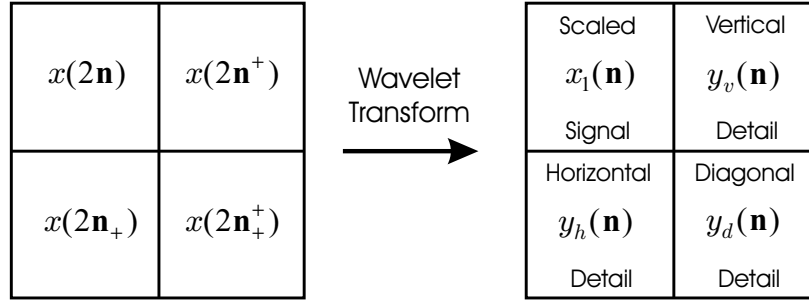


**Fig. 14.** The two-dimensional Haar wavelet transforms an input signal  $x$  to a scaled signal  $x_1$  and the vertical, horizontal, and diagonal detail signals  $y_v, y_h, y_d$ , respectively.

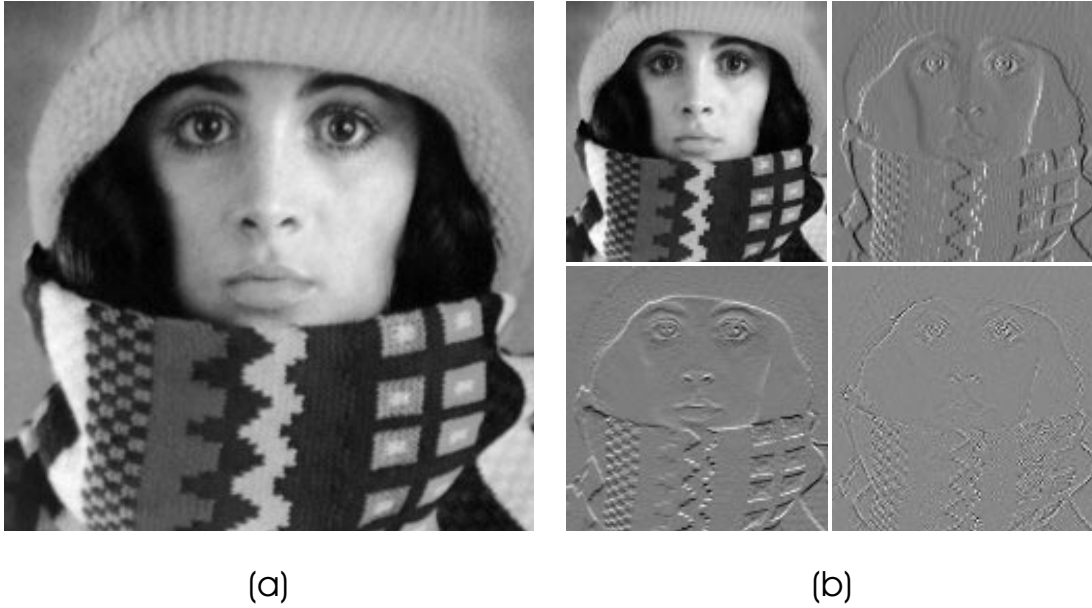


**Fig. 15.** Multiresolution image decomposition based on the two-dimensional morphological Haar wavelet transform: (a) An image  $x$ , and (b) its decomposition into the scaled image  $\psi^\uparrow(x)$ , given by (5.9), and the detail images  $\omega_v(x)$ ,  $\omega_h(x)$  and  $\omega_d(x)$ , given by (5.11)–(5.13).

As in the one-dimensional case, the minimum in the expression for  $\psi^\uparrow$  can be replaced by a maximum. Moreover, as we explain below, it can also be replaced by any (extension of a) *positive Boolean function* without destroying the condition of perfect reconstruction. Recall that every Boolean function  $b$  can be written as a sum-of-products, where the sum represents the “OR” or “maximum” and where the product represents the “AND” or “minimum.” If the Boolean function is positive, then this sum-of-products can be written without complemented variables. Such a positive Boolean function can be easily extended from  $\{0, 1\}$  to  $\mathbb{R}$  by replacing the sum by maximum and the product by minimum [30, Section 11.4].

Suppose now that  $b$  is a positive Boolean function of four variables and let  $\psi^\uparrow$  be given by

$$\psi^\uparrow(x)(\mathbf{n}) = b(x(2\mathbf{n}), x(2\mathbf{n}_+), x(2\mathbf{n}^+), x(2\mathbf{n}_+^+)),$$

and take  $\omega^\uparrow$  to be the same as in (5.10). The value of  $b(u_1, u_2, u_3, u_4)$  equals one of its four arguments; which one depends on the ranking of these four elements, and can be deduced from

(the signs of)  $u_1 - u_2, u_1 - u_3, u_1 - u_4$ . Knowing the value of  $b(u_1, u_2, u_3, u_4)$ , along with the three differences  $u_1 - u_2, u_1 - u_3, u_1 - u_4$ , we are able to compute  $u_1, u_2, u_3, u_4$ . This observation can be used to recover the original signal  $x$  from  $\psi^\uparrow(x)$  and  $\omega^\uparrow(x)$ . Namely, using (5.11)–(5.13), it is easy to show that

$$\begin{aligned} x(2\mathbf{n}) - x(2\mathbf{n}_+) &= \omega_h(x)(\mathbf{n}) + \omega_d(x)(\mathbf{n}) \\ x(2\mathbf{n}) - x(2\mathbf{n}^+) &= \omega_v(x)(\mathbf{n}) + \omega_d(x)(\mathbf{n}) \\ x(2\mathbf{n}) - x(2\mathbf{n}_+^\dagger) &= \omega_v(x)(\mathbf{n}) + \omega_h(x)(\mathbf{n}). \end{aligned}$$

This leads to the signal synthesis operator (5.14) and to detail synthesis operators that are similar to the ones used by the two-dimensional version of the morphological Haar wavelet decomposition scheme discussed above. The particular form of the detail synthesis operators depends on the choice for the Boolean function  $b$ . Clearly, the resulting wavelet decomposition will be uncoupled.

We can take  $b$  to be the  $k$ 'th order statistic of  $u_1, u_2, u_3, u_4$ ; i.e., the  $k$ 'th value of the sequence of length 4 obtained by arranging  $u_1, u_2, u_3, u_4$  in decreasing order. Observe that, in this case and for  $k = 4$ , we obtain the morphological Haar wavelet (and for  $k = 1$  its dual). In the following, and for the sake of illustration, we present a two-dimensional binary example that is built by taking  $b$  to be the *median* of the sequence  $u_1, u_1, u_2, u_3, u_4$ .

Consider an input signal  $x$ , with  $x(2\mathbf{n}) = a$ ,  $x(2\mathbf{n}_+) = b$ ,  $x(2\mathbf{n}^+) = c$ , and  $x(2\mathbf{n}_+^\dagger) = d$ . The signal analysis operator is given by

$$\psi^\uparrow(x)(\mathbf{n}) = \text{median}(x(2\mathbf{n}), x(2\mathbf{n}), x(2\mathbf{n}_+), x(2\mathbf{n}^+), x(2\mathbf{n}_+^\dagger)). \quad (5.15)$$

Take  $\omega^\uparrow$  as in (5.10), where

$$\omega_v(x)(\mathbf{n}) = x(2\mathbf{n}) \triangle x(2\mathbf{n}^+) \quad (5.16)$$

$$\omega_h(x)(\mathbf{n}) = x(2\mathbf{n}) \triangle x(2\mathbf{n}_+) \quad (5.17)$$

$$\omega_d(x)(\mathbf{n}) = x(2\mathbf{n}) \triangle x(2\mathbf{n}_+^\dagger). \quad (5.18)$$

Referring to Figure 14, the coefficients in the matrix  $\begin{bmatrix} a & c \\ b & d \end{bmatrix}$  are mapped to  $\begin{bmatrix} t & v \\ u & w \end{bmatrix}$ , where  $t = \text{median}(a, a, b, c, d)$ ,  $u = a \triangle b$ ,  $v = a \triangle c$ , and  $w = a \triangle d$ . It is not difficult to verify that

$$a = t \triangle (u \wedge v \wedge w),$$

where  $t = \text{median}(a, a, b, c, d)$ ,  $u = a \triangle b$ ,  $v = a \triangle c$ , and  $w = a \triangle d$ . To understand this, we distinguish two cases: (i)  $u \wedge v \wedge w = 0$ : this means that at least one of the values  $u, v, w$  equals 0, which implies that at least one of the values  $b, c, d$  equals  $a$ . This yields that  $t = a$ , which is in agreement with  $a = t \triangle 0$ . (ii)  $u \wedge v \wedge w = 1$ : then  $u = v = w = 1$ , hence  $b = c = d = \bar{a}$ . This yields that  $t = \bar{a}$ . Again, this is in agreement with  $a = t \triangle 1$ .

Having  $a$  recovered from  $t, u, v, w$ , we can recover  $b$  from  $b = (a \triangle b) \triangle a = u \triangle t \triangle (u \wedge v \wedge w)$ . Similarly, we can find  $c$  and  $d$ . This leads to synthesis operators, given by (5.14) and

$$\begin{aligned} \omega^\downarrow(y)(2\mathbf{n}) &= y_v(\mathbf{n}) \wedge y_h(\mathbf{n}) \wedge y_d(\mathbf{n}) \\ \omega^\downarrow(y)(2\mathbf{n}_+) &= y_h(\mathbf{n}) \triangle (y_v(\mathbf{n}) \wedge y_h(\mathbf{n}) \wedge y_d(\mathbf{n})) \\ \omega^\downarrow(y)(2\mathbf{n}^+) &= y_v(\mathbf{n}) \triangle (y_v(\mathbf{n}) \wedge y_h(\mathbf{n}) \wedge y_d(\mathbf{n})) \\ \omega^\downarrow(y)(2\mathbf{n}_+^\dagger) &= y_d(\mathbf{n}) \triangle (y_v(\mathbf{n}) \wedge y_h(\mathbf{n}) \wedge y_d(\mathbf{n})). \end{aligned}$$

It is again not difficult to show that conditions (4.8)–(4.10) are all satisfied, provided that  $\dot{+}$  is taken to be the “exclusive OR” operator. An example, illustrating one step of this decomposition, is depicted in Figure 16.

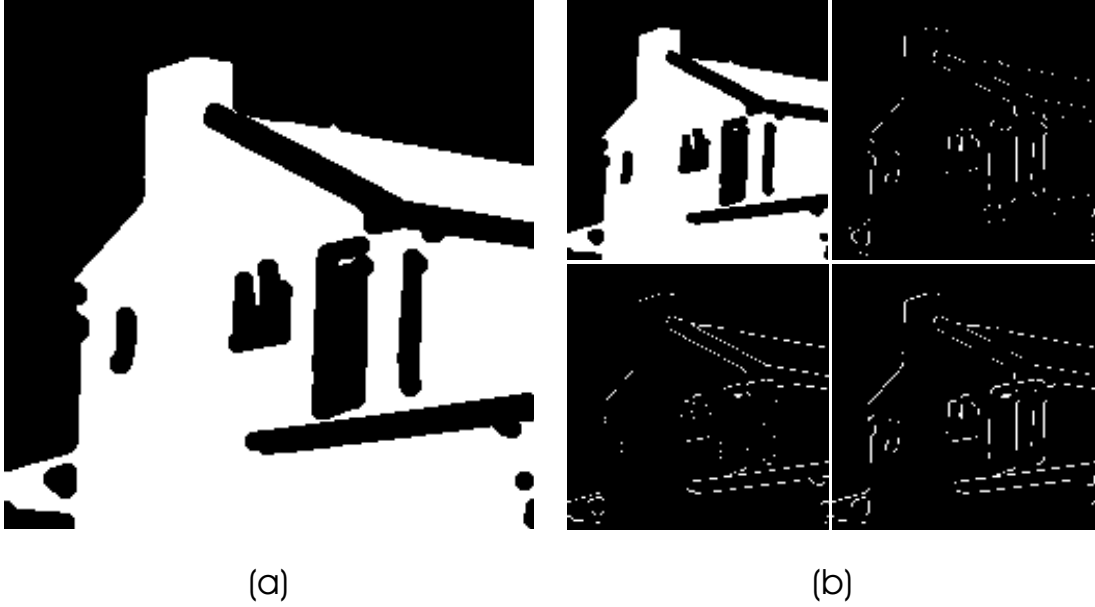


**Fig. 16.** Multiresolution binary image decomposition based on the two-dimensional median wavelet transform: (a) A binary image  $x$ , and (b) its decomposition into the scaled image  $\psi^\uparrow(x)$ , given by (5.15), and the detail images  $\omega_v(x)$ ,  $\omega_h(x)$  and  $\omega_d(x)$ , given by (5.16)–(5.18).

### 5.3. Invariance properties

The morphological Haar wavelet has some specific invariance properties, besides of being translation invariant in the spatial domain. As we will see in Section 6 and Section 7, such invariance properties (see below for a concrete definition) are typical in wavelet decompositions based on morphological operators.

Consider a wavelet decomposition scheme between  $V_0$  and  $V_1 \times W_1$  given by the analysis operators  $\psi^\uparrow, \omega^\uparrow$  and the synthesis operator  $\Psi^\downarrow$ . For simplicity, we restrict ourselves here to signals with values in  $\mathbb{R}$ , that is, elements of  $V_0, V_1, W_1$  are functions with values in  $\mathbb{R}$ . For a function  $f: E \rightarrow \mathbb{R}$  and a constant  $c \in \mathbb{R}$  we define the functions  $f + c$  and  $c \cdot f$  by

$$(f + c)(p) = f(p) + c, \quad (c \cdot f)(p) = cf(p), \quad p \in E.$$

**5.1. Definition.** The decomposition with analysis operators  $\psi^\uparrow, \omega^\uparrow$  is said to be *gray-shift invariant* if

$$\psi^\uparrow(x + c) = \psi^\uparrow(x) + c \quad \text{and} \quad \omega^\uparrow(x + c) = \omega^\uparrow(x), \quad x \in V_0, \quad c \in \mathbb{R}. \quad (5.19)$$

The decomposition is called *gray-multiplication invariant* if

$$\psi^\uparrow(c \cdot x) = c \cdot \psi^\uparrow(x) \quad \text{and} \quad \omega^\uparrow(c \cdot x) = c \cdot \omega^\uparrow(x), \quad x \in V_0, \quad c > 0.$$

It is easy to verify that the synthesis operator  $\Psi^\downarrow$  of a coupled wavelet decomposition scheme which is gray-shift (resp. gray-multiplication) invariant, satisfies

$$\Psi^\downarrow(x + c, y) = \Psi^\downarrow(x, y) + c, \quad x \in V_1, \quad y \in W_1, \quad c \in \mathbb{R} \quad (5.20)$$

(resp.  $\Psi^\downarrow(c \cdot x, c \cdot y) = c \cdot \Psi^\downarrow(x, y)$ ,  $x \in V_1, y \in W_1, c > 0$ ). Indeed, from (4.2) and (5.19), we have that

$$\psi^\uparrow(\Psi^\downarrow(x + c, y)) = x + c = \psi^\uparrow(\Psi^\downarrow(x, y)) + c = \psi^\uparrow(\Psi^\downarrow(x, y) + c).$$

On the other hand

$$\omega^\uparrow(\Psi^\downarrow(x+c, y)) = y = \omega^\uparrow(\Psi^\downarrow(x, y)) = \omega^\uparrow(\Psi^\downarrow(x, y) + c).$$

Since the mapping  $(\psi^\uparrow, \omega^\uparrow): V_0 \rightarrow V_1 \times W_1$  is injective, we have that  $\Psi^\downarrow(x+c, y) = \Psi^\downarrow(x, y) + c$ .

Suppose now that we have an uncoupled wavelet decomposition scheme with synthesis operators  $\psi^\downarrow$  and  $\omega^\downarrow$ , and assume for simplicity that  $\dot{+}$  is the standard addition. In the gray-shift invariant case, and from (5.20), we find

$$\psi^\downarrow(x+c) = \psi^\downarrow(x) + c, \quad x \in V_1, \quad c \in \mathbb{R},$$

whereas in the gray-multiplication invariant case we find

$$\psi^\downarrow(c \cdot x) = c \cdot \psi^\downarrow(x) \quad \text{and} \quad \omega^\downarrow(c \cdot y) = c \cdot \omega^\downarrow(y), \quad x \in V_1, \quad y \in W_1, \quad c > 0.$$

It is easy to verify that the morphological Haar wavelet decomposition given by (5.1)–(5.4), as well as the two-dimensional variant of Subsection 5.2, satisfies both of these invariance properties.

## 6. The Lifting Scheme

A useful and very general technique for constructing new wavelet decompositions from existing ones has been recently proposed by Sweldens [45, 46, 47], and is known as the *lifting scheme*. Lifting amounts to modifying the analysis and synthesis operators in such a way that the properties of the modified scheme are “better” than those of the original one. Here, “better” can be interpreted in different ways. For example, in the linear case, it may mean that the number of vanishing moments is larger.

Lifting can be used to construct wavelet decompositions for signals that are defined on arbitrary domains, or to construct nonlinear wavelet decompositions, which is of interest to us. Two types of lifting schemes can be distinguished:

- *Prediction Lifting*. This modifies the detail analysis operator  $\omega^\uparrow$  and the signal synthesis operator  $\Psi^\downarrow$  in the coupled case, or the signal synthesis operator  $\psi^\downarrow$  in the uncoupled case.
- *Update Lifting*. This modifies the signal analysis operator  $\psi^\uparrow$  and the signal synthesis operator  $\Psi^\downarrow$  in the coupled case, or the detail synthesis operator  $\omega^\downarrow$  in the uncoupled case.

We treat these two cases separately. In both cases, the lifting operator may differ from level to level. However, for simplicity of presentation, we restrict ourselves to operators between levels 0 and 1.

### 6.1. Prediction lifting

Consider one level of a coupled wavelet decomposition scheme, governed by the analysis operators  $\psi^\uparrow: V_0 \rightarrow V_1$ ,  $\omega^\uparrow: V_0 \rightarrow W_1$  and the synthesis operator  $\Psi^\downarrow: V_1 \times W_1 \rightarrow V_0$ , such that the conditions (4.1), (4.2) are satisfied. In many applications, such as data compression, it is desirable to develop wavelet schemes that produce small detail signals  $y_1 = \omega^\uparrow(x_0)$ . Starting from a scheme like above, we might try to decrease the detail signal  $y_1$  by utilizing signal information contained in  $x_1 = \psi^\uparrow(x_0)$ . This may be accomplished by means of a *prediction operator*  $\pi: V_1 \rightarrow W_1$  and a difference operator  $\hat{-}$  on  $W_1$  and by setting

$$y'_1 = y_1 \hat{-} \pi(x_1), \tag{6.1}$$

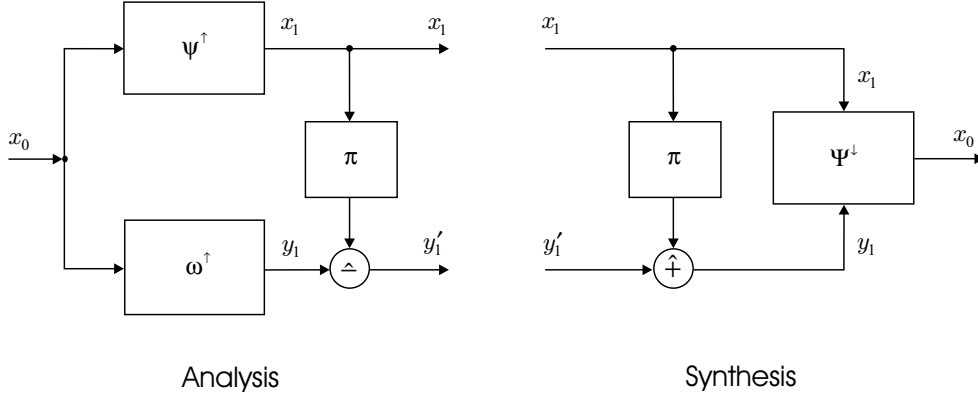


**Fig. 17.** The analysis and synthesis steps of a prediction lifting scheme.

as the new detail signal. This leads to the analysis step depicted in Figure 17.

Assume now that there exists an addition operator  $\hat{+}$  on  $W_1$  such that

$$(y_1 \hat{+} y_2) \hat{-} y_2 = (y_1 \hat{-} y_2) \hat{+} y_2 = y_1, \quad y_1, y_2 \in W_1. \quad (6.2)$$

It is evident that the original signal  $x_0$  can be reconstructed from  $x_1$  and  $y_1'$ , since

$$x_0 = \Psi^\downarrow(x_1, y_1) = \Psi^\downarrow(x_1, y_1' \hat{+} \pi(x_1)).$$

This leads to the synthesis step depicted in Figure 17. Thus, we arrive at the *prediction lifting scheme* with analysis and synthesis operators given by:

$$\psi_p^\uparrow(x) = \psi^\uparrow(x), \quad x \in V_0 \quad (6.3)$$

$$\omega_p^\uparrow(x) = \omega^\uparrow(x) \hat{-} \pi\psi^\uparrow(x), \quad x \in V_0 \quad (6.4)$$

$$\Psi_p^\downarrow(x, y) = \Psi^\downarrow(x, y \hat{+} \pi(x)), \quad x \in V_1, y \in W_1. \quad (6.5)$$

To show that this defines a coupled wavelet decomposition scheme, we must verify that  $\psi_p^\uparrow$ ,  $\omega_p^\uparrow$ , and  $\Psi_p^\downarrow$  satisfy conditions (4.1) and (4.2) as well. Indeed, let  $x \in V_0$ ; then

$$\begin{aligned} \Psi_p^\downarrow(\psi_p^\uparrow(x), \omega_p^\uparrow(x)) &= \Psi^\downarrow(\psi_p^\uparrow(x), \omega_p^\uparrow(x) \hat{+} \pi\psi_p^\uparrow(x)) \\ &= \Psi^\downarrow(\psi^\uparrow(x), (\omega^\uparrow(x) \hat{-} \pi\psi^\uparrow(x)) \hat{+} \pi\psi^\uparrow(x)) \\ &= \Psi^\downarrow(\psi^\uparrow(x), \omega^\uparrow(x)) = x, \end{aligned}$$

where we have used (4.1) for the original scheme, and (6.2), (6.3)–(6.5). Now, let  $x \in V_1, y \in W_1$ ; then

$$\psi_p^\uparrow(\Psi_p^\downarrow(x, y)) = \psi^\uparrow(\Psi^\downarrow(x, y \hat{+} \pi(x))) = x,$$

where we have used the first equation in (4.2) for the original scheme, and (6.3), (6.5). Finally, let  $x \in V_1, y \in W_1$ ; then

$$\begin{aligned} \omega_p^\uparrow(\Psi_p^\downarrow(x, y)) &= \omega^\uparrow(\Psi^\downarrow(x, y \hat{+} \pi(x))) \hat{-} \pi\psi^\uparrow(\Psi^\downarrow(x, y \hat{+} \pi(x))) \\ &= (y \hat{+} \pi(x)) \hat{-} \pi(x) = y, \end{aligned}$$

where we have used (4.2), (6.2), (6.4), (6.5).

The following result provides some additional properties for the case when the initial wavelet decomposition is uncoupled.

**6.1. Proposition.** Consider an uncoupled wavelet decomposition scheme between  $V_0$  and  $V_1, W_1$ , with synthesis operators  $\psi^\downarrow, \omega^\downarrow$ , a prediction operator  $\pi : V_1 \rightarrow W_1$ , and binary operations  $\hat{+}, \hat{-}$  on  $W_1$  such that (6.2) is satisfied. Furthermore, assume that:

- (i) the binary operator  $\dot{+}$  on  $V_0$  is associative and commutative;
- (ii)  $\omega^\downarrow : W_1 \rightarrow V_0$  is “linear,” in the sense that

$$\omega^\downarrow(y_1 \hat{+} y_2) = \omega^\downarrow(y_1) \dot{+} \omega^\downarrow(y_2), \quad y_1, y_2 \in W_1. \quad (6.6)$$

Then, the prediction-lifted wavelet decomposition, given by (6.3)–(6.5), is uncoupled (with respect to the same addition operator  $\dot{+}$ ) with synthesis operators

$$\begin{aligned} \psi_p^\downarrow(x) &= \psi^\downarrow(x) \dot{+} \omega^\downarrow \pi(x) \\ \omega_p^\downarrow(y) &= \omega^\downarrow(y). \end{aligned}$$

PROOF. Under the given assumptions, we can write

$$\begin{aligned} \Psi_p^\downarrow(x, y) &= \Psi^\downarrow(x, y \hat{+} \pi(x)) \\ &= \psi^\downarrow(x) \dot{+} \omega^\downarrow(y \hat{+} \pi(x)) \\ &= \psi^\downarrow(x) \dot{+} (\omega^\downarrow(y) \dot{+} \omega^\downarrow \pi(x)) \\ &= (\psi^\downarrow(x) \dot{+} \omega^\downarrow \pi(x)) \dot{+} \omega^\downarrow(y), \end{aligned}$$

which proves the result. ■

**6.2. Example (Lifting the lazy wavelet).** Consider the case of the lazy wavelet, discussed in Example 4.1. Set  $\hat{+}, \hat{-}$  to be the standard addition and  $\hat{-}$  to be the standard subtraction, and take  $\pi(x)(n) = x(n)$ . From (4.11), (4.12) and (6.3), (6.4), we obtain the analysis operators:

$$\psi_p^\uparrow(x)(n) = x(2n) \quad (6.7)$$

$$\omega_p^\uparrow(x)(n) = x(2n+1) - x(2n). \quad (6.8)$$

From Proposition 6.1 we deduce that the synthesis operators associated with the lifting scheme are given by

$$\begin{aligned} \psi_p^\downarrow(x)(2n) &= \psi_p^\downarrow(x)(2n+1) = x(n) \\ \omega_p^\downarrow(y)(2n) &= 0 \quad \text{and} \quad \omega_p^\downarrow(y)(2n+1) = y(n). \end{aligned}$$

This decomposition produces a “better” detail signal than the one produced by the lazy wavelet decomposition, in the sense that its most significant values appear only at locations of signal discontinuity. This is illustrated in Figure 18. ■

**6.3. Example (Lifting the morphological Haar wavelet).** Consider the morphological Haar wavelet discussed in Subsection 5.1. Recall that  $V_0 = V_1 = W_1 = \mathbb{R}^{\mathbb{Z}}$  and that  $\dot{+}$  is the standard addition. Let  $\hat{+}$  and  $\hat{-}$  on  $W_1$  be defined by

$$y_1 \hat{+} y_2 = \frac{1}{2}(y_1 + y_2) \quad \text{and} \quad y_1 \hat{-} y_2 = 2y_1 - y_2,$$

where  $+, -$  are the standard addition and subtraction. Obviously, the equalities in (6.2) are satisfied. Define the prediction operator  $\pi : V_1 \rightarrow W_1$  by

$$\pi(x)(n) = x(n) - x(n+1).$$

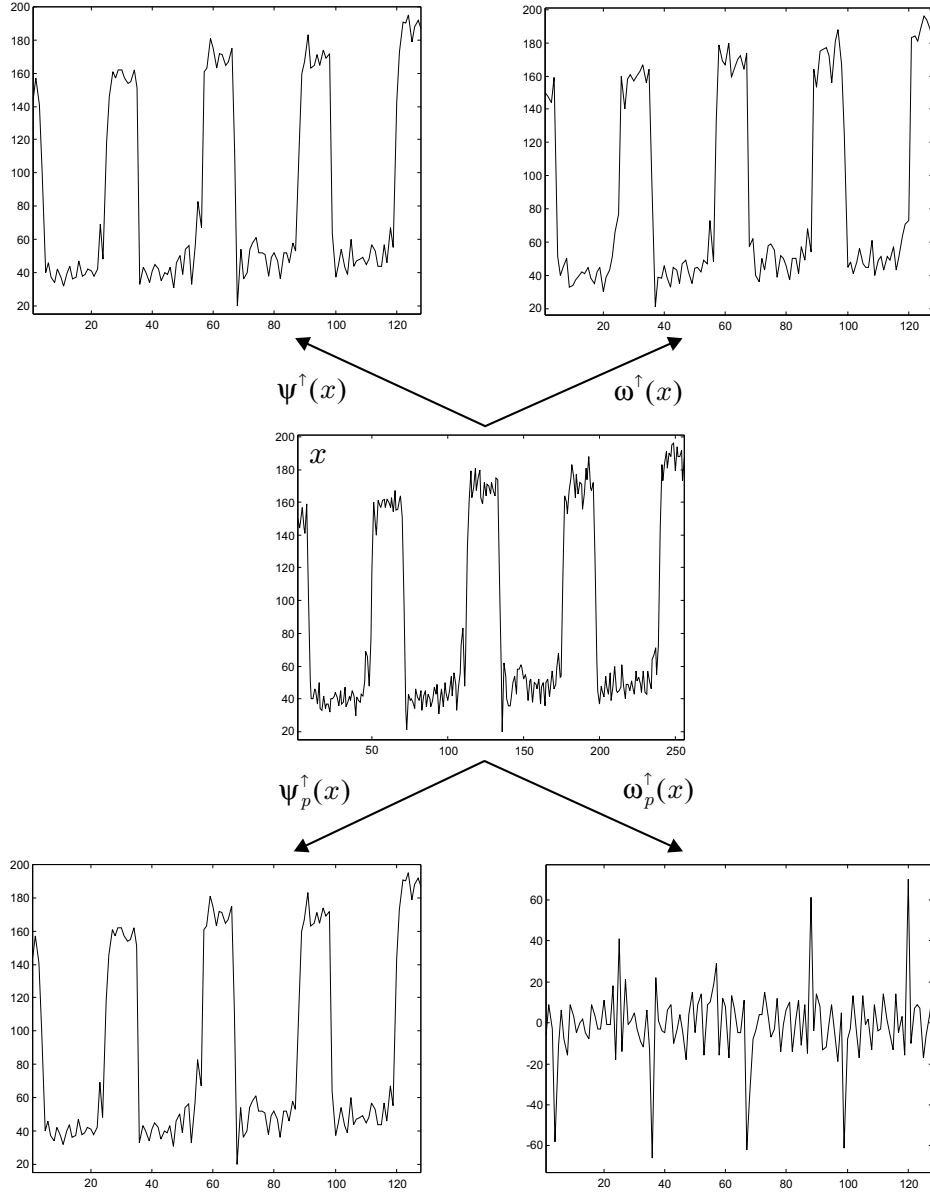


**Fig. 18.** The lazy wavelet decomposition scheme, with analysis operators  $\psi^\uparrow$ ,  $\omega^\uparrow$ , as compared to the wavelet decomposition scheme (6.7), (6.8) obtained after prediction lifting. The detail signal  $\omega_p^\uparrow(x)$  is “better” than the detail signal  $\omega^\uparrow(x)$ , in the sense that the most significant values of  $\omega_p^\uparrow(x)$  appear only at locations of signal discontinuity.

From (5.1)–(5.4) and (6.3)–(6.5), we obtain a coupled nonlinear wavelet decomposition scheme with analysis and synthesis operators given by:

$$\psi_p^\uparrow(x)(n) = x(2n) \wedge x(2n + 1) \quad (6.9)$$

$$\omega_p^\uparrow(x)(n) = 2(x(2n) - x(2n + 1)) - (x(2n) \wedge x(2n + 1)) + (x(2n + 2) \wedge x(2n + 3)) \quad (6.10)$$

$$\Psi_p^\downarrow(x, y)(2n) = x(n) + \left[ \frac{1}{2}(y(n) + x(n) - x(n + 1)) \vee 0 \right] \quad (6.11)$$

$$\Psi_p^\downarrow(x, y)(2n + 1) = x(n) - \left[ \frac{1}{2}(y(n) + x(n) - x(n + 1)) \wedge 0 \right]. \quad (6.12)$$

This scheme has two “vanishing moments” as opposed to the morphological Haar wavelet that

has only one. By one “vanishing moment” we mean that a constant input signal  $x(n) = b$  produces a zero detail signal, whereas by two “vanishing moments” we mean that a linear signal  $x(n) = an + b$  produces a zero detail signal. This is illustrated in Figure 19. Observe that the wavelet transform in (6.9), (6.10) maps integer-valued signals onto integer-valued signals. ■

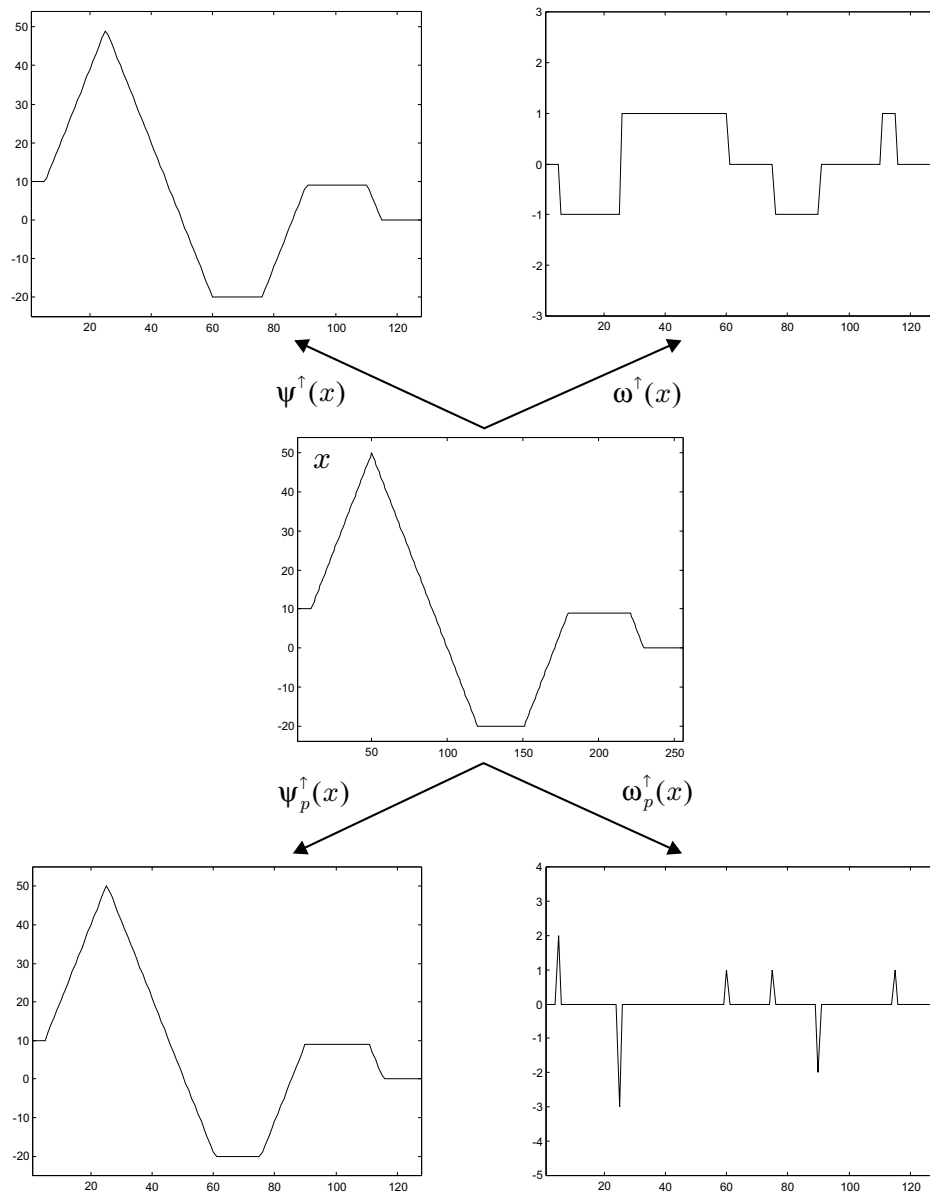


**Fig. 19.** The morphological Haar wavelet decomposition scheme, with analysis operators  $\psi^\uparrow$ ,  $\omega^\uparrow$ , as compared to the wavelet decomposition scheme (6.9), (6.10) obtained after prediction lifting. Notice that  $\omega^\uparrow(x)$  is zero at points where the input signal is constant, whereas  $\omega_p^\uparrow(x)$  is zero at points where the input signal is linear.

## 6.2. Update lifting

Instead of modifying the detail signal  $y_1$ , as we did in (6.1), we may choose to modify the scaled signal  $x_1$  using the information in  $y_1$ . We assume that there exist addition and subtraction

operators  $\dot{+}$ ,  $\dot{-}$  on  $V_1$  such that

$$(x_1 \dot{+} x_2) \dot{-} x_2 = (x_1 \dot{-} x_2) \dot{+} x_2 = x_1, \quad x_1, x_2 \in V_1. \quad (6.13)$$

We get a modified scaled signal by setting

$$x'_1 = x_1 \dot{-} \lambda(y_1). \quad (6.14)$$

Here,  $\lambda$  is an operator, mapping  $W_1$  into  $V_1$ , called the *update operator*. Although, in principle, every mapping  $\lambda$  can be allowed as an update operator, in practice we choose  $\lambda$  in such a way that the resulting scaled signal satisfies a certain constraint. In the linear case, it is often required that the resulting analysis filter  $x_0 \mapsto x'_1$  is a lowpass filter. Alternatively, we may require that this mapping preserves a given signal attribute (e.g., average or maximum). If the unmodified scaled signal  $x_1$  does not satisfy the constraint, we may choose  $\lambda$  in such a way that  $x'_1$ , given by (6.14), does satisfy this constraint. We refer to the work of Sweldens [45, 46, 47] and Daubechies and Sweldens [17] for more details.

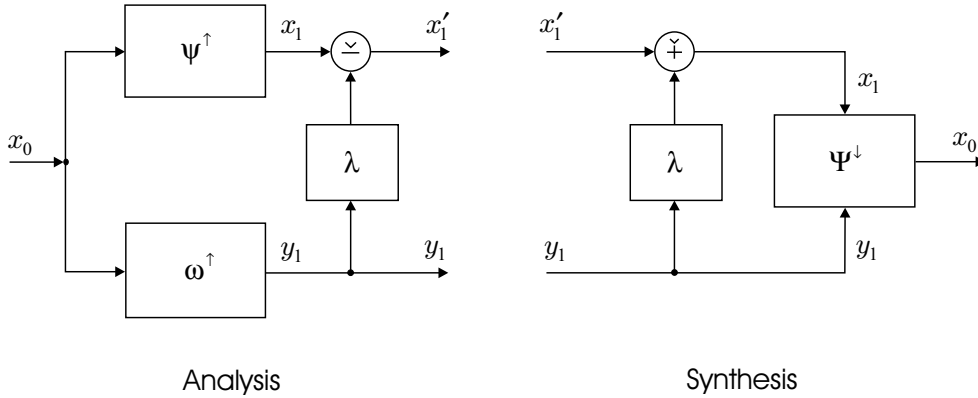


**Fig. 20.** The analysis and synthesis steps of an update lifting scheme.

The update step in (6.14) gives rise to the diagrams depicted in Figure 20. It is clear that the input signal  $x_0$  can be reconstructed from  $x'_1$  and  $y_1$ , since

$$x_0 = \Psi^\downarrow(x_1, y_1) = \Psi^\downarrow(x'_1 \dot{+} \lambda(y_1), y_1).$$

Thus, we arrive at the *update lifting scheme* with analysis and synthesis operators given by:

$$\psi_u^\uparrow(x) = \psi^\uparrow(x) \dot{-} \lambda\omega^\uparrow(x), \quad x \in V_0 \quad (6.15)$$

$$\omega_u^\uparrow(x) = \omega^\uparrow(x), \quad x \in V_0 \quad (6.16)$$

$$\Psi_u^\downarrow(x, y) = \Psi^\downarrow(x \dot{+} \lambda(y), y), \quad x \in V_1, y \in W_1. \quad (6.17)$$

In the same way as we did for the prediction lifting scheme, we can show that (6.15)–(6.17) defines a coupled wavelet decomposition scheme. Furthermore, the following analogue to Proposition 6.1 can be established.

**6.4. Proposition.** *Consider an uncoupled wavelet decomposition scheme between  $V_0$  and  $V_1, W_1$ , with synthesis operators  $\psi^\downarrow, \omega^\downarrow$ , an update operator  $\lambda : W_1 \rightarrow V_1$ , and binary operations  $\dot{+}, \dot{-}$  on  $V_1$  such that (6.13) is satisfied. Furthermore, assume that:*

- (i) the binary operator  $\dot{+}$  on  $V_0$  is associative and commutative;
- (ii)  $\psi^\downarrow : V_1 \rightarrow V_0$  is “linear,” in the sense that

$$\psi^\downarrow(v_1 \check{+} v_2) = \psi^\downarrow(v_1) \dot{+} \psi^\downarrow(v_2), \quad v_1, v_2 \in V_1. \quad (6.18)$$

Then, the update-lifted wavelet decomposition, given by (6.15)–(6.17), is uncoupled (with respect to the same addition operator  $\dot{+}$ ) with synthesis operators

$$\begin{aligned} \psi_u^\downarrow(x) &= \psi^\downarrow(x) \\ \omega_u^\downarrow(y) &= \omega^\downarrow(y) \dot{+} \psi^\downarrow \lambda(y). \end{aligned}$$

**6.5. Example.** Consider the case of the wavelet decomposition scheme, discussed in Example 6.2, obtained from lifting the lazy wavelet by means of linear prediction. Set  $\check{+}, \dot{+}$  to be the standard addition and  $\check{-}$  to be the standard subtraction, and take  $\lambda(y)(n) = -\lfloor y(n)/2 \rfloor$ . From (6.7), (6.8) and (6.15), (6.16), we obtain the analysis operators:

$$\psi_u^\uparrow(x)(n) = x(2n) + \left\lfloor \frac{x(2n+1) - x(2n)}{2} \right\rfloor \quad (6.19)$$

$$\omega_u^\uparrow(x)(n) = x(2n+1) - x(2n). \quad (6.20)$$

From Proposition 6.4 we derive that the resulting decomposition is uncoupled, with synthesis operators:

$$\psi_u^\downarrow(x)(2n) = \psi_u^\downarrow(x)(2n+1) = x(n) \quad (6.21)$$

$$\omega_u^\downarrow(y)(2n) = -\left\lfloor \frac{y(n)}{2} \right\rfloor \quad \text{and} \quad \omega_u^\downarrow(y)(2n+1) = y(n) - \left\lfloor \frac{y(n)}{2} \right\rfloor. \quad (6.22)$$

In the integer-valued case,

$$x(2n) + \left\lfloor \frac{x(2n+1) - x(2n)}{2} \right\rfloor = \left\lfloor \frac{x(2n) + x(2n+1)}{2} \right\rfloor \quad (6.23)$$

$$y(n) - \left\lfloor \frac{y(n)}{2} \right\rfloor = \left\lfloor \frac{y(n) + 1}{2} \right\rfloor; \quad (6.24)$$

therefore, the previous wavelet decomposition scheme is the S-transform considered in Example 4.4. ■

The previous example shows that, by update lifting the wavelet scheme obtained from lifting the lazy wavelet by means of linear prediction, and by restricting ourselves to integer-valued signals, we obtain a very useful wavelet decomposition scheme, known as the S-transform. Therefore, by combining a prediction lifting step followed with an update step we obtain a wavelet decomposition scheme that requires special consideration. This scheme, to be referred to as *prediction-update lifting*, is discussed next.

### 6.3. Prediction-update lifting

If the lifting scheme comprises a prediction step  $\pi$  followed by an update step  $\lambda$ , then the resulting decomposition is clearly given by

$$\begin{aligned} y'_1 &= y_1 \hat{-} \pi(x_1) \\ x'_1 &= x_1 \check{-} \lambda(y'_1). \end{aligned}$$

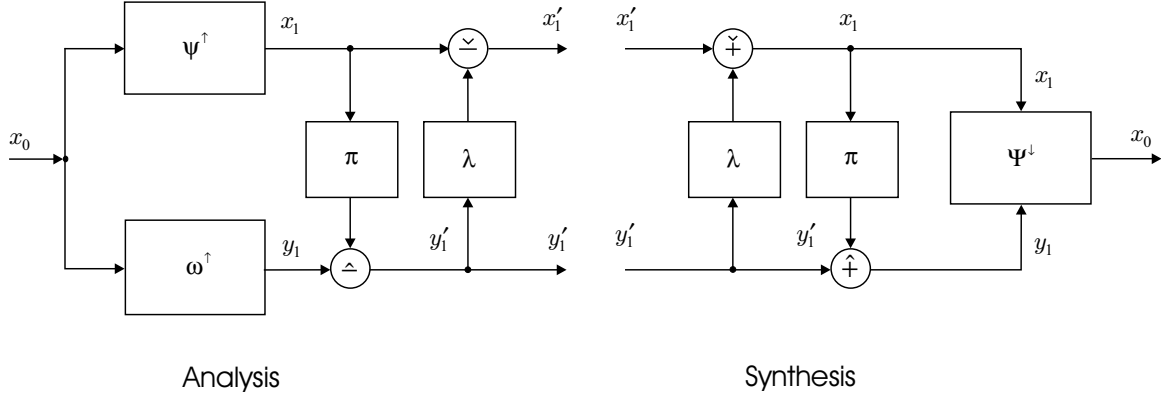


**Fig. 21.** The analysis and synthesis steps of a prediction-update lifting scheme.

Refer to Figure 21 for an illustration. The original signal  $x_0$  can be reconstructed from  $x'_1$  and  $y'_1$ , since

$$x_0 = \Psi^\downarrow(x_1, y_1) = \Psi^\downarrow(x'_1 \dot{+} \lambda(y'_1), y'_1 \hat{+} \pi(x'_1 \dot{-} \lambda(y'_1))).$$

This leads to the synthesis step depicted in Figure 21. Thus, we arrive at the *prediction-update lifting scheme* with analysis and synthesis operators given by

$$\psi_{pu}^\uparrow(x) = \psi^\uparrow(x) \dot{-} \lambda(\omega^\uparrow(x) \hat{-} \pi\psi^\uparrow(x)), \quad x \in V_0 \quad (6.25)$$

$$\omega_{pu}^\uparrow(x) = \omega^\uparrow(x) \hat{-} \pi\psi^\uparrow(x), \quad x \in V_0 \quad (6.26)$$

$$\Psi_{pu}^\downarrow(x, y) = \Psi^\downarrow(x \dot{+} \lambda(y), y \hat{+} \pi(x \dot{-} \lambda(y))), \quad x \in V_1, y \in W_1. \quad (6.27)$$

In general, prediction-update lifting gives rise to a coupled wavelet decomposition scheme, even when the original wavelet transform is uncoupled. Similar results hold for the dual case of a lifting scheme that comprises an update step  $\lambda$  followed by a prediction step  $\pi$ . This leads to the so-called *update-prediction lifting scheme*.

**6.6. Example.** In this example, we show how to arrive at the morphological Haar wavelet by a simple prediction-update lifting of the lazy wavelet. Let us take  $\hat{-}$ ,  $\dot{-}$  to be the standard subtraction, and  $\hat{+}$ ,  $\dot{+}$ ,  $\dot{+}$  to be the standard addition and set

$$\pi(x)(n) = x(n) \quad \text{and} \quad \lambda(y)(n) = -(0 \wedge y(n)). \quad (6.28)$$

Then, from (4.11), (4.12), (6.25), (6.26), and (6.28), we find

$$\psi_{pu}^\uparrow(x)(n) = x(2n) + (0 \wedge (x(2n+1) - x(2n))) = x(2n) \wedge x(2n+1) \quad (6.29)$$

$$\omega_{pu}^\uparrow(x)(n) = x(2n+1) - x(2n), \quad (6.30)$$

which, apart from a minus sign in (6.30), coincides with the morphological Haar wavelet introduced in Subsection 5.1. ■

**6.7. Example (Lifting based on the median operator).** Let us take  $\hat{-}$ ,  $\dot{-}$  to be the standard subtraction, and  $\hat{+}$ ,  $\dot{+}$ ,  $\dot{+}$  to be the standard addition. Consider the case of a prediction-update lifting scheme with initial signal decomposition given by means of the lazy wavelet, and prediction and update operators given by:

$$\pi(x)(n) = x(n) \quad (6.31)$$

$$\lambda(y)(n) = -\text{median}(0, y(n-1), y(n)). \quad (6.32)$$

From (4.11)–(4.14) and (6.25)–(6.32), we obtain an uncoupled wavelet decomposition scheme, with analysis and synthesis operators given by:

$$\psi_{pu}^\uparrow(x)(n) = x(2n) + \text{median}(0, x(2n-1) - x(2n-2), x(2n+1) - x(2n)) \quad (6.33)$$

$$\omega_{pu}^\uparrow(x)(n) = x(2n+1) - x(2n) \quad (6.34)$$

$$\psi_{pu}^\downarrow(x)(n) = x(n) \quad (6.35)$$

$$\omega_{pu}^\downarrow(y)(2n) = -\text{median}(0, y(n-1), y(n)) \quad (6.36)$$

$$\omega_{pu}^\downarrow(y)(2n+1) = y(n) - \text{median}(0, y(n-1), y(n)). \quad (6.37)$$

Notice that, the update operator adjusts the value of  $x(2n)$  based on the local structure of the input signal  $x(n)$ . If the difference  $x(2n-1) - x(2n-2)$  is negative (or positive) and the difference  $x(2n+1) - x(2n)$  is positive (or negative), then no adjustment is made. This happens, for example, when  $x(2n)$  is a local minimum (or maximum), as illustrated in Figure 22(a). If however both differences  $x(2n-1) - x(2n-2)$  and  $x(2n+1) - x(2n)$  are negative (or positive), then  $x(2n)$  is adjusted by adding the smallest (in absolute value) difference. For example, when  $x(n)$  (locally) oscillates between two values, as depicted in Figure 22(b), then (6.33) will bring  $x(2n)$  in line with  $x(2n-1)$ , thus getting a scaled signal  $\psi_{pu}^\uparrow(x)$  that approximates  $x$  “better” than the scaled signal  $\psi^\uparrow(x)$  before prediction-update lifting. Finally, notice that the resulting wavelet decomposition is gray-shift and gray-multiplication invariant (recall Definition 5.1). Concerning the last property, one may observe that it holds for positive as well as for negative constants  $c$ . Alternatively, we may choose

$$\pi(x)(n) = \frac{1}{2} (x(n) + x(n+1)), \quad (6.38)$$

and  $\lambda(y)$  as in (6.32). This choice leads to an uncoupled wavelet decomposition scheme that has two “vanishing moments.” In this case, the detail signal, resulting from an input signal  $x(n) = an + b$ , will be zero.

Finally, one can replace the previous linear prediction operator, with the nonlinear prediction operator:

$$\pi(x)(n) = \text{median}(x(n-1), x(n), x(n+1)). \quad (6.39)$$

This choice, together with (6.32) for the update operator, leads to a coupled wavelet decomposition scheme. Figure 23 depicts examples of such decompositions. Although the decompositions depicted in Figure 23(a) and Figure 23(c) are very similar, the decomposition depicted in Figure 23(b) needs more attention. In this case, the detail signal  $\omega_{pu}^\uparrow(x)$  is small at points where the input signal  $x$  is linear-like (e.g., at points  $0 \leq n \leq 18$  and  $60 \leq n \leq 80$ ). This is expected, since the resulting decomposition has two “vanishing moments,” as it was explained above. ■

**6.8. Example (Lifting binary wavelets).** Let us now consider the binary case, for which  $V_0 = V_1 = W_1 = \{0, 1\}^{\mathbb{Z}}$ . The previous example, based on the median operator, can be reformulated for binary signals as well. For this case, we take  $\hat{-}$ ,  $\check{-}$ ,  $\hat{+}$ ,  $\check{+}$ ,  $\dot{+}$  to be the “exclusive OR” operator  $\Delta$ . We can now proceed with a prediction-update lifting scheme, with initial signal decomposition given by means of the lazy wavelet and prediction and update operators given by:

$$\pi(x)(n) = x(n)$$

$$\lambda(y)(n) = \text{median}(0, y(n-1), y(n)) = y(n) \wedge y(n-1).$$

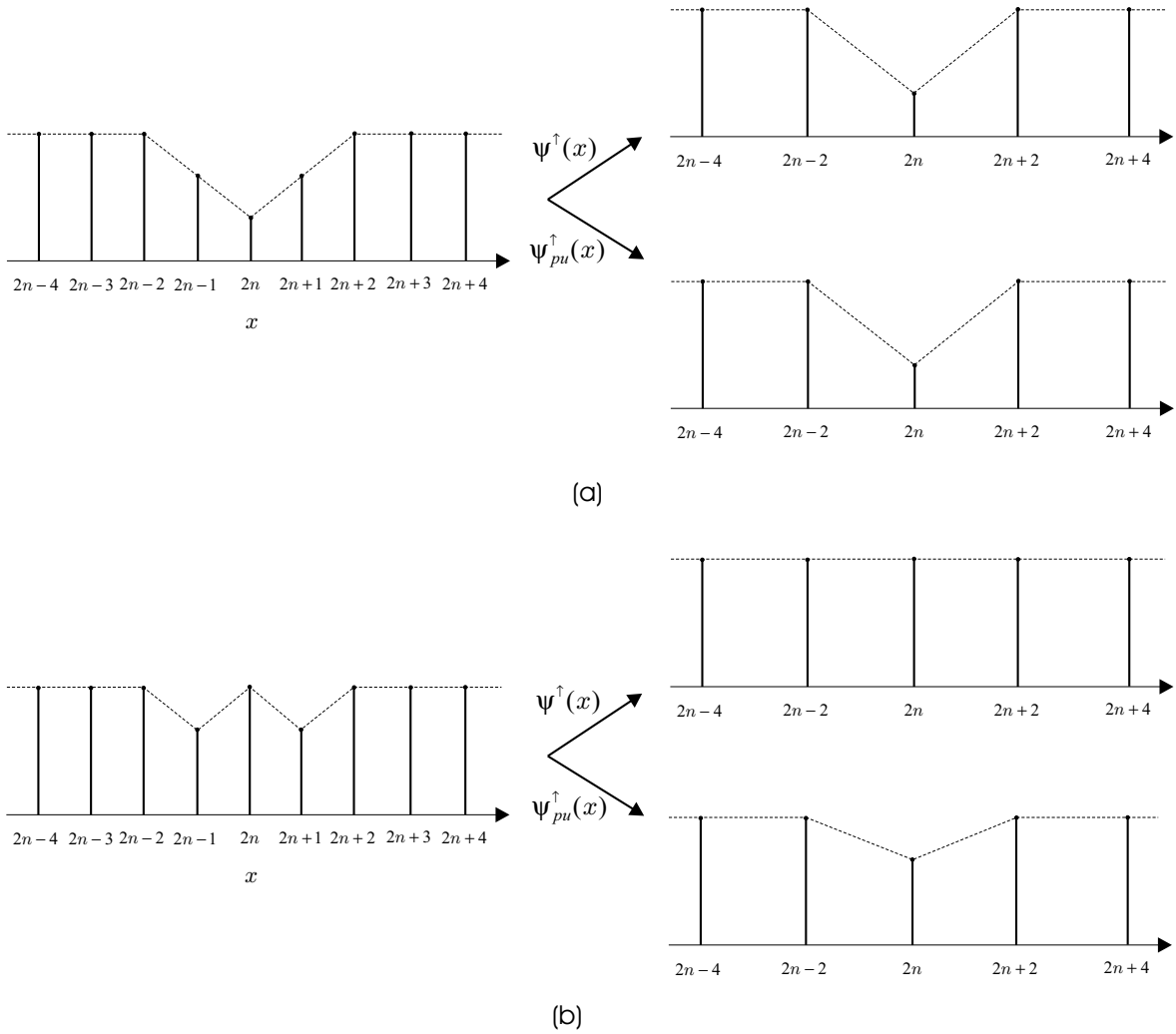


**Fig. 22.** An illustration of update lifting by means of (6.33): (a) Since  $x(2n)$  is a local minimum in  $x$ , (6.33) maps  $x(2n)$  into itself. (b) Since  $x(2n-1) - x(2n-2) = x(2n+1) - x(2n) = -1$ , the value  $x(2n)$  is reduced by one, thus obtaining a scaled signal  $\psi_{pu}^{\uparrow}(x)$  that approximates  $x$  “better” than the scaled signal  $\psi^{\uparrow}(x)$  before prediction-update lifting

Notice that  $\text{median}(0, s, t) = s \wedge t$ , for  $s, t \in \{0, 1\}$ . The analysis and synthesis operators resulting from this lifting scheme can be expressed as:

$$\begin{aligned}\psi_{pu}^{\uparrow}(x)(n) &= a^{\uparrow}(x(2n-2), x(2n-1), x(2n), x(2n+1)) \\ \omega_{pu}^{\uparrow}(x)(n) &= b^{\uparrow}(x(2n-2), x(2n-1), x(2n), x(2n+1)) \\ \Psi_{pu}^{\downarrow}(x, y)(2n) &= a^{\downarrow}(x(n), y(n-1), y(n)) \\ \Psi_{pu}^{\downarrow}(x, y)(2n+1) &= b^{\downarrow}(x(n), y(n-1), y(n)),\end{aligned}$$

where  $a^{\uparrow}, b^{\uparrow}, a^{\downarrow}, b^{\downarrow}$  are Boolean functions given by:

$$\begin{aligned}a^{\uparrow}(u_1, u_2, u_3, u_4) &= u_3 + (u_1 + u_2 - 2u_1u_2)(u_4 - u_3) \\ b^{\uparrow}(u_1, u_2, u_3, u_4) &= u_3 + u_4 - 2u_3u_4 \\ a^{\downarrow}(u_1, u_2, u_3) &= u_1 + (1 - 2u_1)u_2u_3 \\ b^{\downarrow}(u_1, u_2, u_3) &= u_1 + (1 - 2u_1)(1 - u_2)u_3.\end{aligned}$$

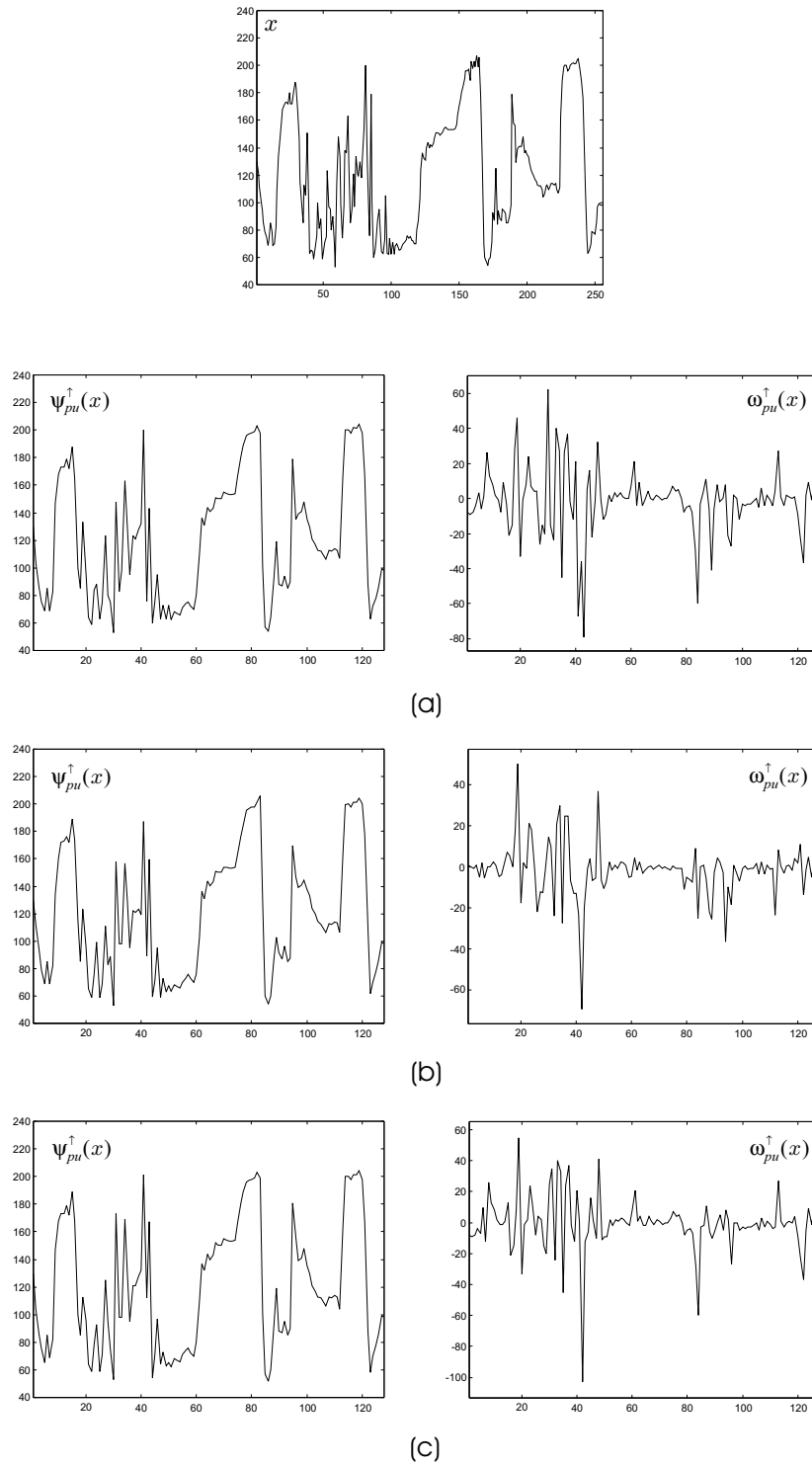


**Fig. 23.** One-stage decomposition of a signal  $x$  by means of prediction-update lifting based on the median operator. Prediction and update operators are given by: (a) (6.31), (6.32), (b) (6.38), (6.32), and (c) (6.39), (6.32). Notice that the detail signal in (b) is small at points where the input signal is linear-like. This is due to the fact that, in (b), the decomposition has two “vanishing moments.”

Clearly, the resulting wavelet decomposition scheme is coupled and *self-dual*, in the sense that

$$\psi_{pu}^\uparrow(\bar{x}) = \overline{\psi_{pu}^\uparrow(x)} \quad \text{and} \quad \omega_{pu}^\uparrow(\bar{x}) = \omega_{pu}^\uparrow(x),$$

where  $\bar{x}(n) = 1 - x(n)$ . An example is illustrated in Figure 24. ■

We now mention the following important consequence of Proposition 6.1 and Proposition 6.4. If the wavelet decomposition used as a starting point for lifting is uncoupled and “linear,” in the sense that the synthesis operators  $\omega^\downarrow$ ,  $\psi^\downarrow$  satisfy (6.6), (6.18), if the binary operators  $\hat{+}$ ,  $\check{+}$  (on  $W_1$  and  $V_1$ ) satisfy (6.2), (6.13), and if the binary operator  $\dot{+}$  on  $V_0$  is associative and commutative, then the resulting scheme after one lifting step (prediction or update) is also uncoupled. However, after a second lifting step (of the opposite type) the scheme will become coupled in general. This implies that the prediction-update and the update-prediction lifting schemes will in general give rise to coupled wavelet decompositions, even if all assumptions associated with Proposition 6.1 and Proposition 6.4 are satisfied. This is illustrated in the following example.

**6.9. Example (Lifting the S-transform).** Let us take  $\hat{-}$ ,  $\check{-}$  to be the standard subtraction,  $\hat{+}$ ,  $\check{+}$ ,  $\dot{+}$  to be the standard addition, and let us limit our interest to integer-valued signals. In Example 6.5 we showed that the S-transform can be obtained by update lifting the wavelet decomposition scheme discussed in Example 6.2. If we further lift the S-transform by means of prediction lifting, with

$$\pi(x)(n) = \left\lfloor \frac{x(n+1) - x(n)}{2} \right\rfloor,$$

we obtain a wavelet decomposition scheme with analysis and synthesis operators given by (recall (6.3)–(6.5) and (6.19)–(6.24)):

$$\begin{aligned} \psi_{up}^\uparrow(x)(n) &= \left\lfloor \frac{x(2n) + x(2n+1)}{2} \right\rfloor \\ \omega_{up}^\uparrow(x)(n) &= \left\lfloor \frac{1}{2} \left\lfloor \frac{5}{2}x(2n+1) - \frac{3}{2}x(2n) \right\rfloor - \frac{1}{2} \left\lfloor \frac{1}{2}x(2n+2) + \frac{1}{2}x(2n+3) \right\rfloor \right\rfloor \\ \Psi_{up}^\downarrow(x, y)(2n) &= - \left\lfloor \frac{1}{2}y(n) + \frac{1}{2} \left\lfloor -\frac{5}{2}x(n) + \frac{1}{2}x(n+1) \right\rfloor \right\rfloor \\ \Psi_{up}^\downarrow(x, y)(2n+1) &= - \left\lfloor -\frac{1}{2}y(n) - \left\lfloor \frac{1}{2}x(n+1) - \frac{1}{2}x(n) \right\rfloor + \frac{1}{2} \left\lfloor -\frac{5}{2}x(n) + \frac{1}{2}x(n+1) \right\rfloor \right\rfloor, \end{aligned}$$

which is clearly coupled. Notice that the resulting scheme has two “vanishing moments,” as compared to the S-transform which has only one. ■

## 7. The Max- and Min-Lifting Schemes

In this section, we discuss a particular example of a wavelet decomposition by means of prediction-update lifting that leads to the so-called *max-lifting* scheme. Its structure is the same as in Figure 21, with  $\hat{-}$ ,  $\check{-}$  being the standard subtraction,  $\hat{+}$ ,  $\check{+}$ ,  $\dot{+}$  being the standard addition, and prediction and update operators given by:

$$\pi(x)(n) = x(n) \vee x(n+1) \quad \text{and} \quad \lambda(y)(n) = -(0 \vee y(n-1) \vee y(n)).$$

In this case,

$$y'_1(n) = y_1(n) - (x_1(n) \vee x_1(n+1)) \quad (\text{prediction}) \quad (7.1)$$

$$x'_1(n) = x_1(n) + (0 \vee y'_1(n-1) \vee y'_1(n)) \quad (\text{update}). \quad (7.2)$$

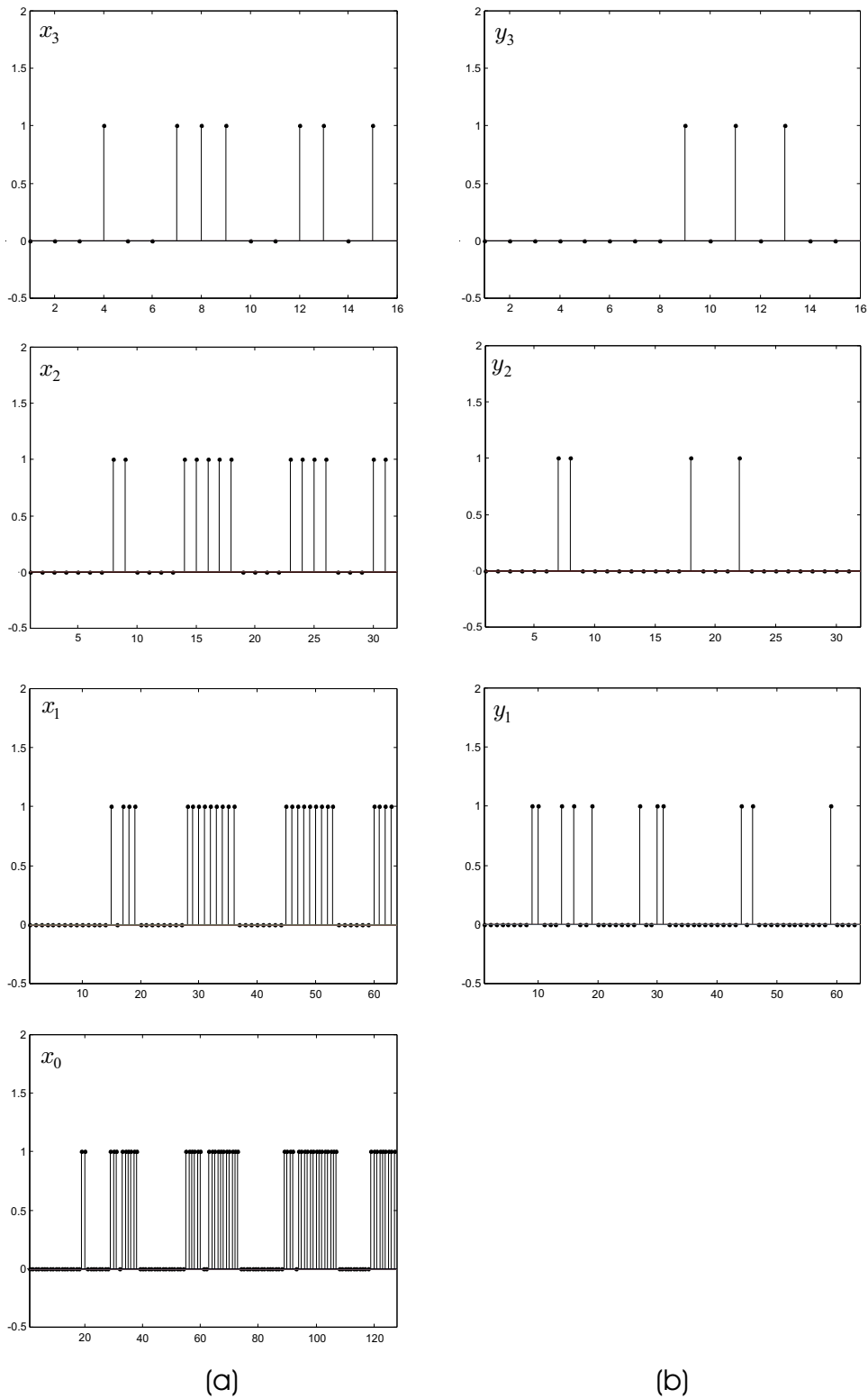


**Fig. 24.** Multiresolution signal decomposition based on the binary wavelet transform of Example 6.8 obtained by means of prediction-update lifting: (a) A binary signal  $x_0$  and its scaled signal decomposition  $\{x_1, x_2, x_3\}$  obtained by means of the analysis operator  $\psi_{pu}^\uparrow$ . (b) The detail signals  $\{y_1, y_2, y_3\}$  obtained from  $\{x_0, x_1, x_2\}$  by means of the analysis operator  $\omega_{pu}^\uparrow$ .

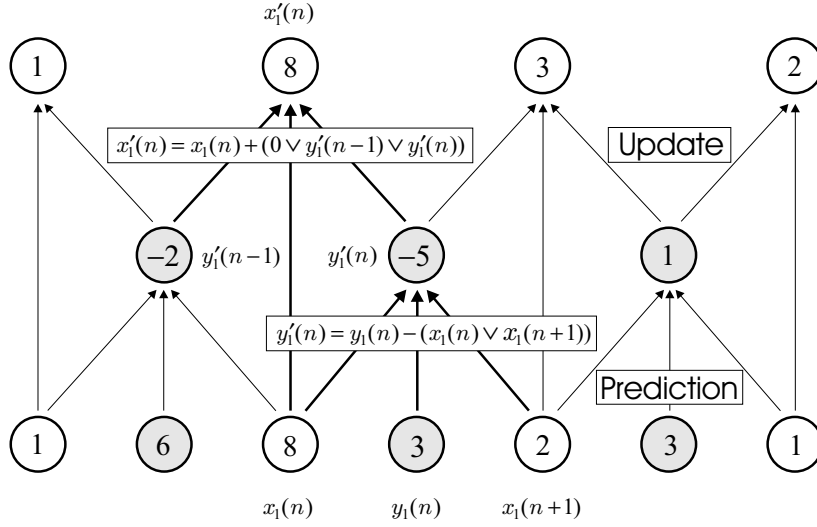


**Fig. 25.** Illustration of one step of the max-lifting scheme. The white and gray nodes correspond to the scaled and detail signals, respectively. Notice that the value 8, which is a local maximum of the input signal  $x_1$ , is directly mapped to the scaled signal  $x'_1$ .

Thus, as a prediction for  $y_1(n)$  we choose the maximum of its two neighbors in  $x_1$ , i.e.,  $x_1(n)$  and  $x_1(n+1)$ . The update step is chosen in such a way that local maxima of the input signal  $x_1$  are mapped to the scaled signal  $x'_1$  (see Proposition 7.1). This is illustrated in Figure 25.

Rather than formulating properties of this one-dimensional scheme, we first explain how this scheme can be generalized to a much larger family of signal spaces, and then prove some results for this more general case. We return to the one-dimensional case in Subsection 7.2.

### 7.1. General max-lifting scheme

Consider a set  $E$  of points, which can be expressed as a disjoint union of two sets  $E_x$  and  $E_y$ , that is  $E = E_x \cup E_y$  and  $E_x \cap E_y = \emptyset$ . Consider a symmetric binary adjacency relation  $\sim$  on  $E$  such that  $p \sim q$  is never satisfied if  $p, q$  lie both in  $E_x$  or  $E_y$ . This relation defines a so-called *bi-graph* with vertex sets  $E_x$  and  $E_y$ ; see Figure 26. If  $p \sim q$ , then we say that  $p$  and  $q$  are neighbors. Neighbors are connected with edges, as depicted in Figure 26.

Throughout this section, we assume that every point has finitely many neighbors. We write  $p \sim \sim r$  if there exists an element  $q$  such that  $p \sim q$  and  $q \sim r$ ; see Figure 26. In particular,  $p \sim \sim p$  if  $p$  has at least one neighbor. Consider the signals mapping  $E$  into  $\mathbb{R}$ . Given an input signal  $x_0$ , define

$$\begin{cases} x_1(p) = x_0(p), & p \in E_x \\ y_1(q) = x_0(q), & q \in E_y. \end{cases} \quad (7.3)$$

The max-lifting scheme can now be defined as follows:

$$y'_1(q) = y_1(q) - \bigvee_{p \sim q} x_1(p), \quad q \in E_y \quad (\text{prediction}) \quad (7.4)$$

$$x'_1(p) = x_1(p) + \left(0 \vee \bigvee_{q \sim p} y'_1(q)\right), \quad p \in E_x \quad (\text{update}). \quad (7.5)$$

Here, the expression  $\bigvee_{p \sim q} x_1(p)$  means the supremum of  $x_1(p)$  over all neighbors  $p$  of  $q$ . Clearly, in this general framework, the prediction and update operators are given by

$$\pi(x)(q) = \bigvee_{p \sim q} x(p), \quad q \in E_y, \quad \text{and} \quad \lambda(y)(p) = -\left(0 \vee \bigvee_{q \sim p} y(q)\right), \quad p \in E_x. \quad (7.6)$$

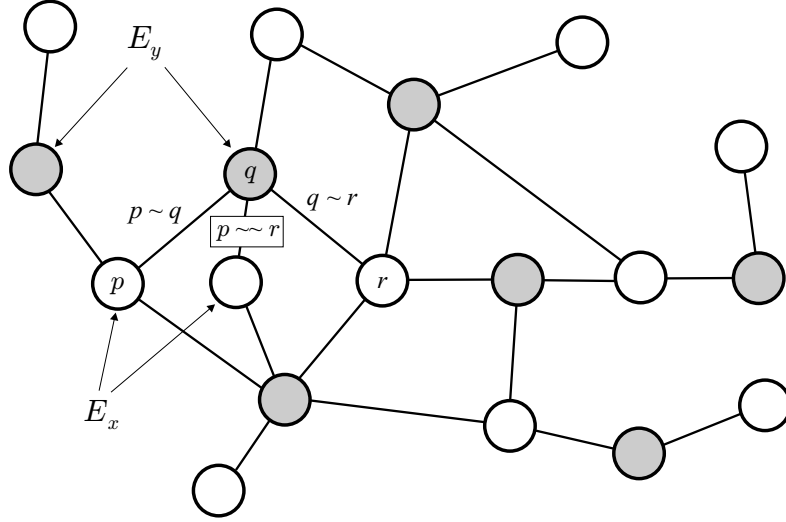


**Fig. 26.** A bi-graph with vertex sets  $E_x$  (white nodes) and  $E_y$  (gray nodes). Neighbors are connected with edges.

We also introduce the following notation: given  $q \in E$ ,  $A(x | q)$  is the set of all neighbors  $p$  of  $q$  such that  $x(p) = \bigvee_{s \sim q} x(s)$ . Note that this set is nonempty, since  $q$  has finitely many neighbors. We now have the following result.

**7.1. Proposition.**

- (a) For  $p \in E_x$ ,  $x_0(p) \leq x'_1(p) \leq \bigvee \{x_0(q) \mid q = p \text{ or } q \sim p\}$ .
- (b) For  $q \in E_y$ ,  $x_0(q) \leq \bigvee_{p \sim q} x'_1(p)$ .
- (c) Assume that  $q \in E_y$  is such that  $x_0(q) \geq x_0(p)$ , for  $q \sim p$  and  $q \sim \sim p$ ; then,  $x'_1(p) = x_0(q)$ , for every  $p \in A(x_0 | q)$ .

PROOF. (a) From (7.3), (7.5), we have that  $x'_1(p) \geq x_1(p) = x_0(p)$ , for  $p \in E_x$ , which shows the first inequality. Furthermore (see (7.5)),

$$x'_1(p) = x_1(p) \vee \bigvee_{q \sim p} (x_1(p) + y'_1(q)), \quad p \in E_x. \quad (7.7)$$

On the other hand, we have that (see (7.4))

$$y'_1(q) = y_1(q) - \bigvee_{r \sim q} x_1(r) \leq y_1(q) - x_1(p), \quad q \sim p, \quad (7.8)$$

since  $p \in E_x$  and  $q \sim p$  implies that  $q \in E_y$ . From (7.3), (7.7), and (7.8), we obtain the second inequality.

(b) Let  $q \in E_y$  and  $p \in A(x_1 | q)$ ; then  $y'_1(q) = y_1(q) - x_1(p)$ , which is a direct consequence of (7.4) and the definition of  $A(x_1 | q)$ . Hence (see (7.3) and (7.5)),

$$\begin{aligned} x_0(q) &= y_1(q) \\ &= y'_1(q) + x_1(p) \\ &= y'_1(q) + x'_1(p) - \left(0 \vee \bigvee_{r \sim p} y'_1(r)\right) \\ &\leq y'_1(q) + x'_1(p) - y'_1(q) = x'_1(p). \end{aligned}$$

This shows that  $x_0(q) \leq \bigvee_{p \sim q} x'_1(p)$ , for every  $q \in E_y$ .

(c) Let  $q \in E_y$  be such that  $x_0(q) \geq x_0(p)$ , for  $q \sim p$  and  $q \sim \sim p$ , and take  $p \in A(x_0 \mid q)$ . We must show that  $x'_1(p) = x_0(q)$ . From (7.5) we know that

$$\begin{aligned} x'_1(p) &= x_1(p) + \left(0 \vee \bigvee_{r \sim p} y'_1(r)\right) \\ &= x_0(p) + \left(0 \vee \bigvee_{r \sim p} y'_1(r)\right), \quad p \in E_x. \end{aligned} \quad (7.9)$$

From (7.4), we get that

$$y'_1(r) = y_1(r) - \bigvee_{s \sim r} x_1(s) = x_0(r) - \bigvee_{s \sim r} x_0(s), \quad r \in E_y. \quad (7.10)$$

If  $r = q$ , then

$$y'_1(q) = x_0(q) - x_0(p) \geq 0,$$

since  $p \in A(x_0 \mid q)$  and  $x_0(q) \geq x_0(p)$  by assumption. If  $r \neq q$ , then

$$\begin{aligned} y'_1(r) &\leq x_0(r) - x_0(p) \leq x_0(q) - x_0(p) \\ &= x_0(q) - \bigvee_{s \sim q} x_0(s) = y'_1(q), \end{aligned}$$

where we have used that  $x_0(r) \leq x_0(q)$ , if  $r \sim p$ , that  $x_0(p) = \bigvee_{s \sim q} x_0(s)$ , since  $p \in A(x_0 \mid q)$ , and (7.10). Substitution in (7.9) yields that

$$x'_1(p) = x_0(p) + y'_1(q) = x_0(p) + x_0(q) - x_0(p) = x_0(q),$$

which was to be shown. ■

From the previous proposition, it is clear that the max-lifting scheme preserves local maxima. The next result states that this scheme does not create new maxima.

**7.2. Proposition.** *Suppose that the scaled signal  $x'_1$  has a local maximum at  $p \in E_x$ ; i.e.,  $x'_1(p) \geq x'_1(r)$ , for  $r \in E_x$ , with  $r \sim \sim p$ . Then,  $x_0$  has a local maximum at some  $s \in E$ , with  $s = p$  or  $s \sim p$ , and  $x_0(s) = x'_1(p)$ .*

PROOF. We distinguish between two cases:

(i)  $x_0(p) \geq x_0(q)$ , for  $q \sim p$ . From (7.4), it is clear that  $y'_1(q) = x_0(q) - \bigvee_{p \sim q} x_0(p) = x_0(q) - x_0(p) \leq 0$ , for  $q \sim p$ . Therefore,  $x'_1(p) = x_0(p)$ , by virtue of (7.5). The assertion holds for  $s = p$ .

(ii)  $x_0(p) < x_0(q)$ , for  $q \in A(x_0 \mid p)$ . By Proposition 7.1(a) we have that  $x'_1(p) \leq x_0(q)$ , and by Proposition 7.1(b) we have that

$$x_0(q) \leq \bigvee_{r \sim q} x'_1(r) = x'_1(p).$$

The equality holds since  $r \sim q$  implies  $r \sim \sim p$  and  $x'_1$  has a local maximum at  $p$ . Thus, we conclude that  $x_0(q) = x'_1(p)$ . We must now show that  $x_0$  has a local maximum at  $q$ ; i.e.,  $x_0(q) \geq x_0(r)$ , for  $r \sim q$ . By Proposition 7.1(a),  $x_0(r) \leq x'_1(r)$ ; hence

$$x_0(q) = x'_1(p) \geq x'_1(r) \geq x_0(r), \quad r \sim q.$$

Here,  $x'_1(p) \geq x'_1(r)$ , since  $x'_1$  has a local maximum at  $p$  and  $p \sim \sim r$ . Therefore, the assertion holds for  $s = q \sim p$ . ■

The max-lifting scheme yields a coupled wavelet decomposition. This is in agreement with the observations of Subsection 6.3, since the max-lifting scheme is constructed by means of two nonlinear lifting steps. It is easy to demonstrate that the resulting wavelet decomposition scheme is both gray-shift and gray-multiplication invariant.

The analysis and synthesis operators associated with the max-lifting scheme are denoted by  $\psi_{\max}^\uparrow, \omega_{\max}^\uparrow$  and  $\Psi_{\max}^\downarrow$ , respectively. That is

$$x'_1 = \psi_{\max}^\uparrow(x_0), \quad y'_1 = \omega_{\max}^\uparrow(x_0), \quad \text{and} \quad x_0 = \Psi_{\max}^\downarrow(x'_1, y'_1).$$

If we replace the supremum in (7.3)–(7.6) with infimum, we obtain the dual scheme, which we refer to as the *min-lifting scheme*. Propositions 7.1 and 7.2 can be modified accordingly, by replacing  $\vee$  with  $\wedge$ ,  $\leq$  with  $\geq$ , and “maximum” with “minimum.”

## 7.2. One-dimensional scheme

The one-dimensional scheme, introduced at the beginning of this section (see (7.1), (7.2)), is a simple example of the previous general framework: take for  $E_x, E_y$  the even and odd samples of  $\mathbb{Z}$ , respectively, and define  $p \sim q$  if  $|p - q| = 1$ . From Proposition 7.1, we deduce that a value  $x_0(2n)$  is mapped to  $x'_1(n)$  provided that  $x_0(2n) \geq x_0(2n \pm 1)$ . A value  $x_0(2n + 1)$  is mapped to  $x'_1(n)$  or  $x'_1(n + 1)$  if it is maximal in a neighborhood of five points; i.e., if  $x_0(2n + 1) \geq x_0(2n + 1 - i)$ , for  $i = -2, -1, 0, 1, 2$ . Depending on which value is the largest,  $x_0(2n)$  or  $x_0(2n + 2)$ ,  $x_0(2n + 1)$  is mapped to  $x'_1(n)$  or  $x'_1(n + 1)$ , respectively. Refer to Figure 27 for an illustration.

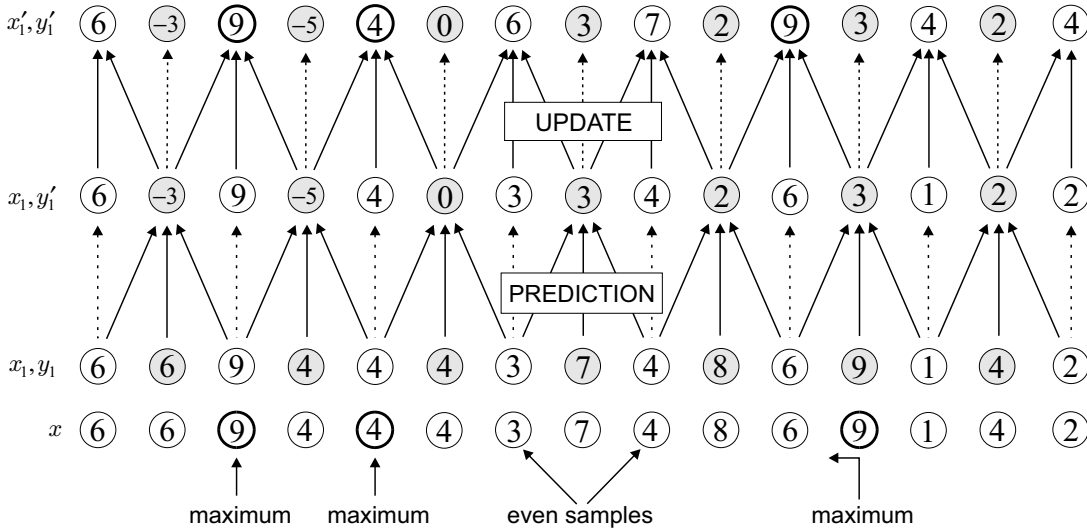


**Fig. 27.** A diagram illustrating the one-dimensional max-lifting scheme. The white nodes contain the scaled signal  $x_1$  (resp.  $x'_1$ ), whereas, the gray nodes contain the detail signal  $y_1$  (resp.  $y'_1$ ). The first lifting step (prediction) modifies the detail signal, whereas the second lifting step (update) modifies the scaled signal such that local maxima are preserved. The initial decomposition  $x \mapsto x_1, y_1$  is done by means of the lazy wavelet.

We can extend the max- and min-lifting schemes to two dimensions by sequentially applying the one-dimensional decomposition on the columns and rows of a two-dimensional image. Figure 28(a) depicts the result of a single level wavelet image decomposition by means of max-lifting,



(a)



(b)

**Fig. 28.** Single-level separable image decomposition by means of: (a) max-lifting, and (b) min-lifting.

whereas, Figure 28(b) depicts the result of a single level image decomposition by means of min-lifting. Notice that each decomposition produces one scaled image and three detail images (a horizontal, vertical, and diagonal detail image). Notice also that the detail signals are zero (or almost zero) at areas of smooth graylevel variation. In the case of max-lifting (Figure 28(a)), sharp graylevel variations are mapped to negative (black) detail signal values, whereas, in the case of min-lifting (Figure 28(b)), sharp graylevel variations are mapped to positive (white values). These results are due to the following observations. In the case of max-lifting, a constant input signal  $x(n) = b$  produces a zero detail signal, whereas, a linear signal  $x(n) = an + b$  produces a constant detail signal with value equal to  $-|a|$ . Moreover, a step signal  $x_0$  with an

upward step between locations  $2n - 1$  and  $2n$  produces a negative spike for the detail signal at location  $n - 1$ . Similarly, a downward step between locations  $2n$  and  $2n + 1$  produces a negative spike for the detail signal at location  $n$ . The amplitude of such spikes equals the strength of the step. On the other hand, if the upward step occurs between locations  $2n$  and  $2n + 1$ , the detail signal will be zero. The same is true for a downward step from  $2n - 1$  to  $2n$ . This is clearly illustrated in Figure 29.

However, keep in mind that the detail signal may contain “positive spikes” as well, which is the case when the scaled signal contains a narrow peak. Similar results for the min-lifting scheme are depicted in Figure 30.

Figure 31 depicts the scaled signals obtained by means of a 3-level linear wavelet decomposition scheme, based on a biorthogonal pair of signal and detail analysis operators (in the first column), a 3-level max-lifting decomposition scheme (in the second column), and a 3-level min-lifting decomposition scheme (in the third column). Notice the sharpness of the scaled signals, generated by means of the max- and min-lifting schemes, as compared to the scaled signals generated by means of the linear decomposition scheme. Notice also that the max-lifting scheme preserves quite well local maxima (e.g., the cornea in the two eyes), as opposed to the min-lifting scheme which preserves very well local minima (e.g., the iris and the lens of the two eyes).

As we said before, the min-lifting scheme preserves local minima over scale. Moreover, it does not generate any new local minima. For these reasons, it may be used for developing a multiscale algorithm for image segmentation. We illustrate this idea in the example depicted in Figure 32.

The bone marrow image, depicted in Figure 32(a), is to be segmented into nonoverlapping regions of interest. One way to do this is to employ an effective tool for image segmentation known as the *watershed algorithm* [2]. A popular version of this algorithm relies on the local minima of the image to be segmented. The subgraph of the image is flooded from below by first piercing it at the location of the local minima, and by then immersing it into water. The water will progressively flood the basins of the subgraph that correspond to the local minima. To prevent water, coming from two adjacent basins, from merging, we erect a dam. The collection of all such dams form the so-called *watershed lines*, which segment the image into desirable regions of interest (see [50] for more details). Figure 32(b) depicts the location of the watershed lines (in white) obtained by applying such an algorithm on the image depicted in Figure 32(a), or more precisely on its inverse  $x_0$ . The local minima, required by the watershed algorithm, have been computed by subtracting  $x_0$  from its morphological closing  $x_0 \bullet B = (x_0 \oplus B) \ominus B$ , with  $B$  being the square structuring element, where  $\oplus$  and  $\ominus$  denote translation invariant flat dilation and flat erosion, respectively [30]. Unfortunately, this technique frequently leads to oversegmentation, as is clear from Figure 32(b). This is primarily due to the fact that  $x_0$  contains a large number of local minima. However, we can reduce oversegmentation by coarsening  $x_0$ . We will do this here by means of the min-lifting scheme. Image  $x_0$  is first decomposed into a sequence of scaled images  $\{x_1, x_2, \dots, x_K\}$ , for some  $K$ , by means of a  $K$ -level min-lifting scheme. At each level  $k$ , we compute the local minima of  $x_k$  by subtracting  $x_k$  from the morphological closing  $x_k \bullet B$ . We then replace  $x_k$  with  $x_k \bullet B - x_k$ , we set all detail signals equal to zero, and we finally reconstruct signal  $z_K$  by means of the inverse min-lifting scheme.  $z_K$  can now be thought of as a coarse version of the local minima marker  $z_0 = x_0 \bullet B - x_0$ . Figure 32(c) to Figure 32(f) depict the watershed lines obtained by applying the watershed algorithm, with marker  $z_K$ , on the image depicted in Figure 32(a), with  $K = 1, 2, 3, 4$ , respectively. Clearly, as  $K$  increases, oversegmentation decreases. Evidently, our modified segmentation algorithm is far from optimal in several respects. But the results in Figure 32 give a strong indication that marker extraction based on the min-lifting scheme may lead to a substantial improvement in the final segmentation.

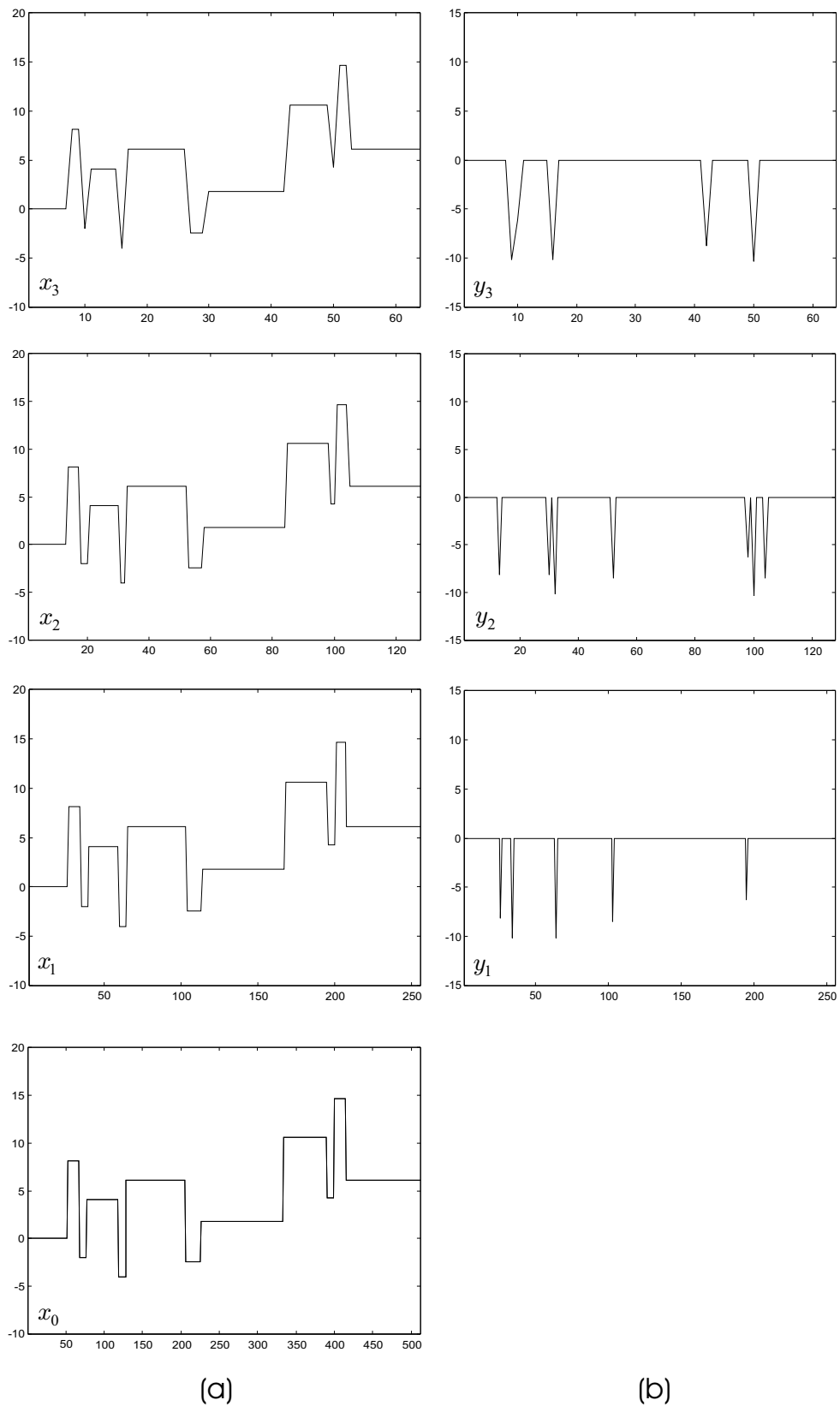


**Fig. 29.** Multiresolution signal decomposition based on max-lifting the lazy wavelet: (a) A signal  $x_0$  and its scaled signal decomposition  $\{x_1, x_2, x_3\}$ . (b) The corresponding detail signals  $\{y_1, y_2, y_3\}$ .

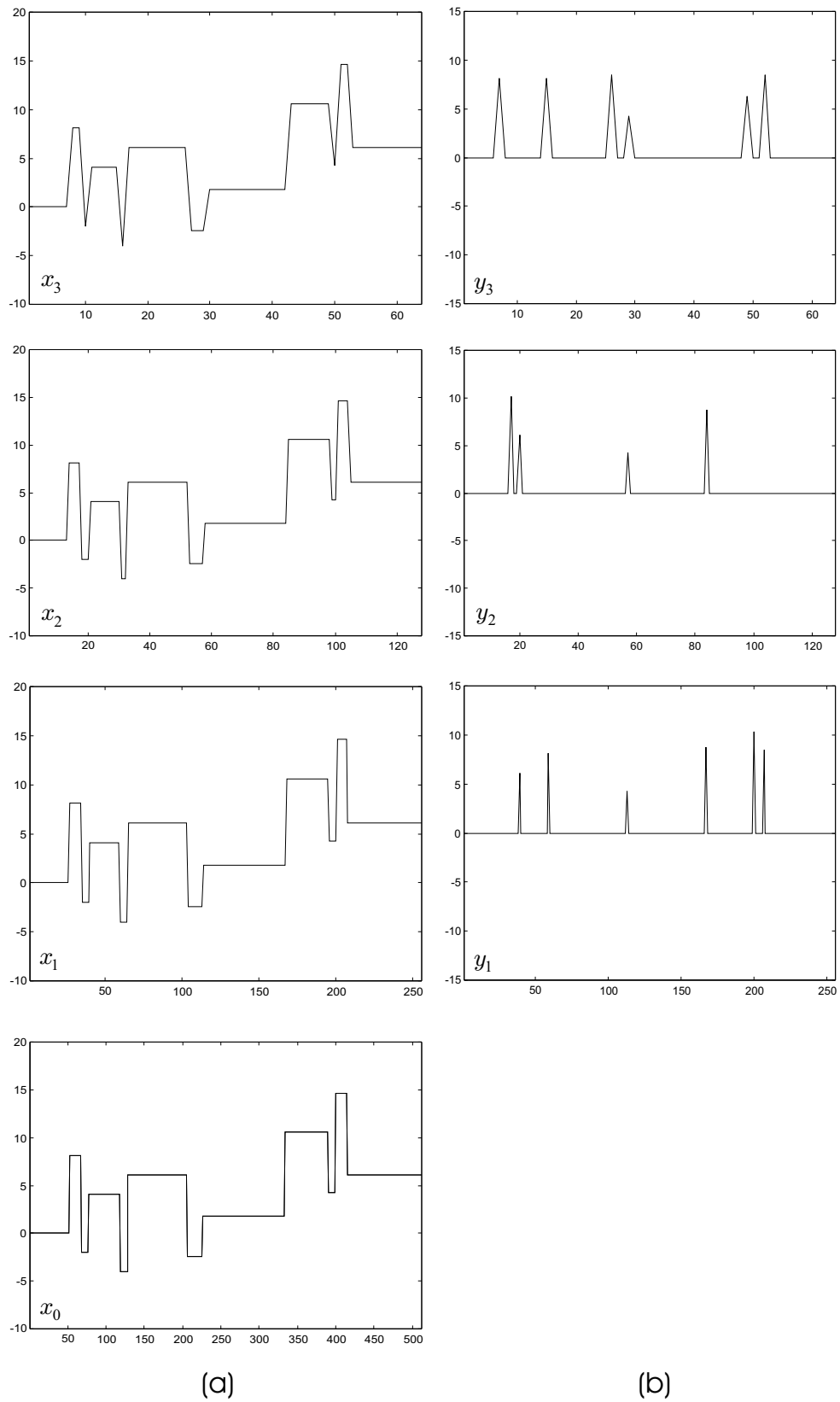


**Fig. 30.** Multiresolution signal decomposition based on min-lifting the lazy wavelet: (a) A signal  $x_0$  and its scaled signal decomposition  $\{x_1, x_2, x_3\}$ . (b) The corresponding detail signals  $\{y_1, y_2, y_3\}$ .



**Fig. 31.** The scaled images obtained by means of: (a) a 3-level linear wavelet decomposition scheme, (b) a 3-level max-lifting scheme, (c) a 3-level min-lifting scheme.

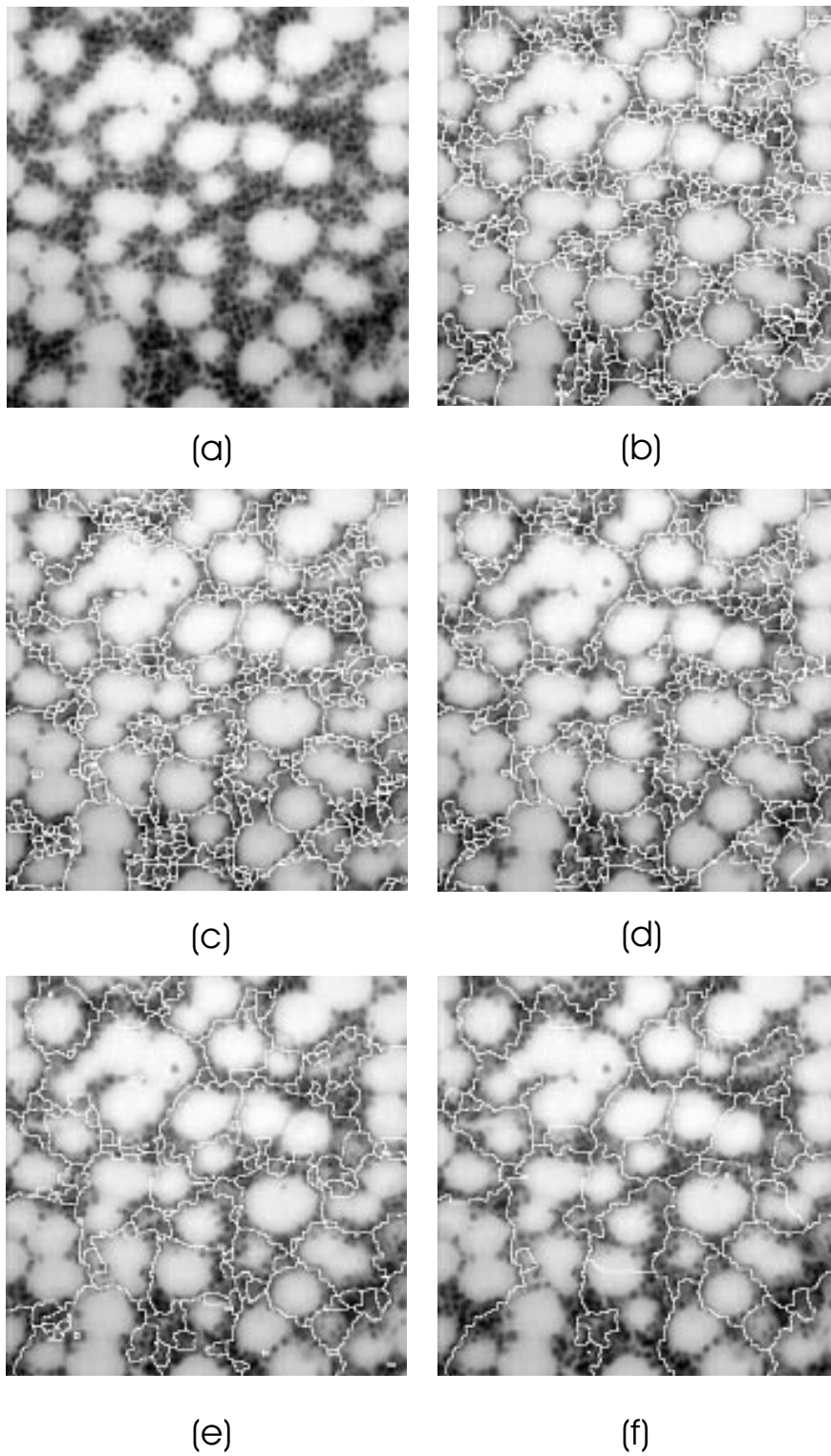


**Fig. 32.** An original bone marrow image that needs to be segmented (in (a)). The watershed lines (in white) obtained by applying the watershed transform on the inverse  $x_0$  of the image in (a) using a marker  $z_0 = x_0 \bullet B - x_0$  (in (b)) and a marker  $z_K$  obtained by means of a  $K$ -level min-lifting scheme with:  $K = 1$  (in (c)),  $K = 2$  (in (d)),  $K = 3$  (in (e)), and  $K = 4$  (in (f)).

### 7.3. Two-dimensional scheme (with quincunx sampling)

A second application of the bi-graph framework is the two-dimensional discrete space  $\mathbb{Z}^2$  with the *quincunx sampling* scheme. The corresponding bi-graph is shown in Figure 33.

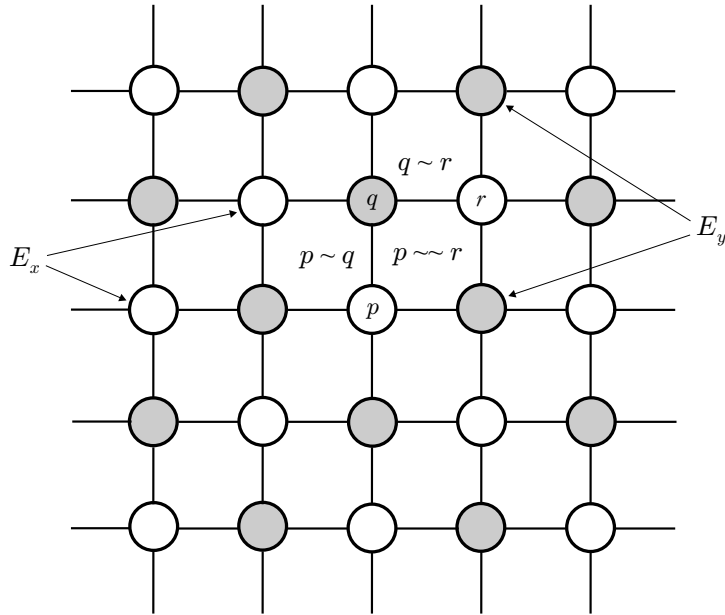


**Fig. 33.** A bi-graph for  $\mathbb{Z}^2$ , with the quincunx sampling scheme, and the vertex sets  $E_x$  (white points) and  $E_y$  (gray points).

Here,  $E_x$  and  $E_y$  comprise of points  $(m, n) \in \mathbb{Z}^2$ , with  $m + n$  even and odd, respectively. Moreover,  $(m_1, n_1) \sim (m_2, n_2)$  if and only if  $|m_1 - m_2| + |n_1 - n_2| = 1$ .

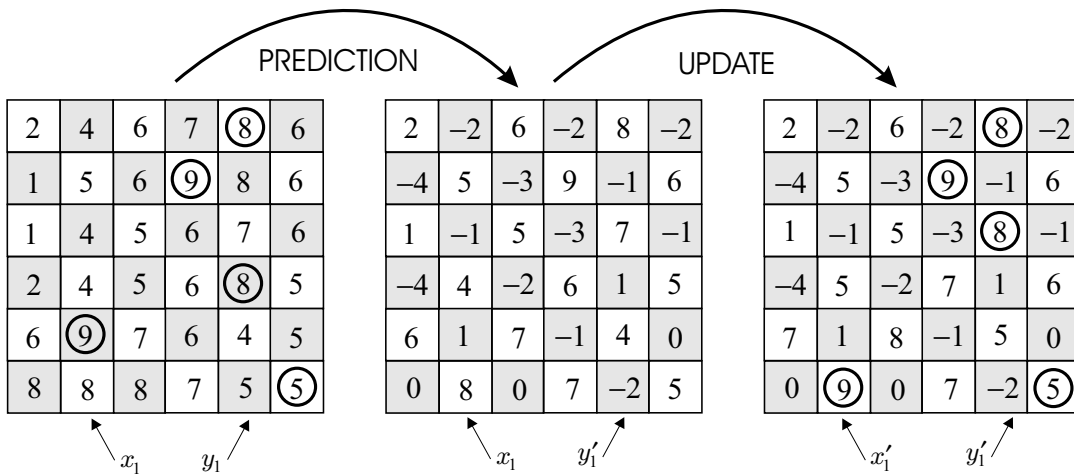


**Fig. 34.** A diagram illustrating the two-dimensional max-lifting scheme. The white nodes contain the scaled signal  $x_1$  (resp.  $x'_1$ ), whereas, the gray nodes contain the detail signal  $y_1$  (resp.  $y'_1$ ). The first lifting step (prediction) modifies the detail signal, whereas the second lifting step (update) modifies the scaled signal such that local maxima (indicated by circles) are preserved.

This leads to pure two-dimensional max- and min-lifting schemes, as opposed to the separable ones discussed in Subsection 7.2.

An important feature of lifting schemes is that they allow in-place calculations. In this case, the original signal values can be replaced by the transformed ones without having to allocate additional memory. This is illustrated in Figure 34, where we apply the two-dimensional max-lifting scheme on the quincunx lattice to a  $6 \times 6$  square matrix. As expected, this scheme preserves the local maxima indicated by circles.

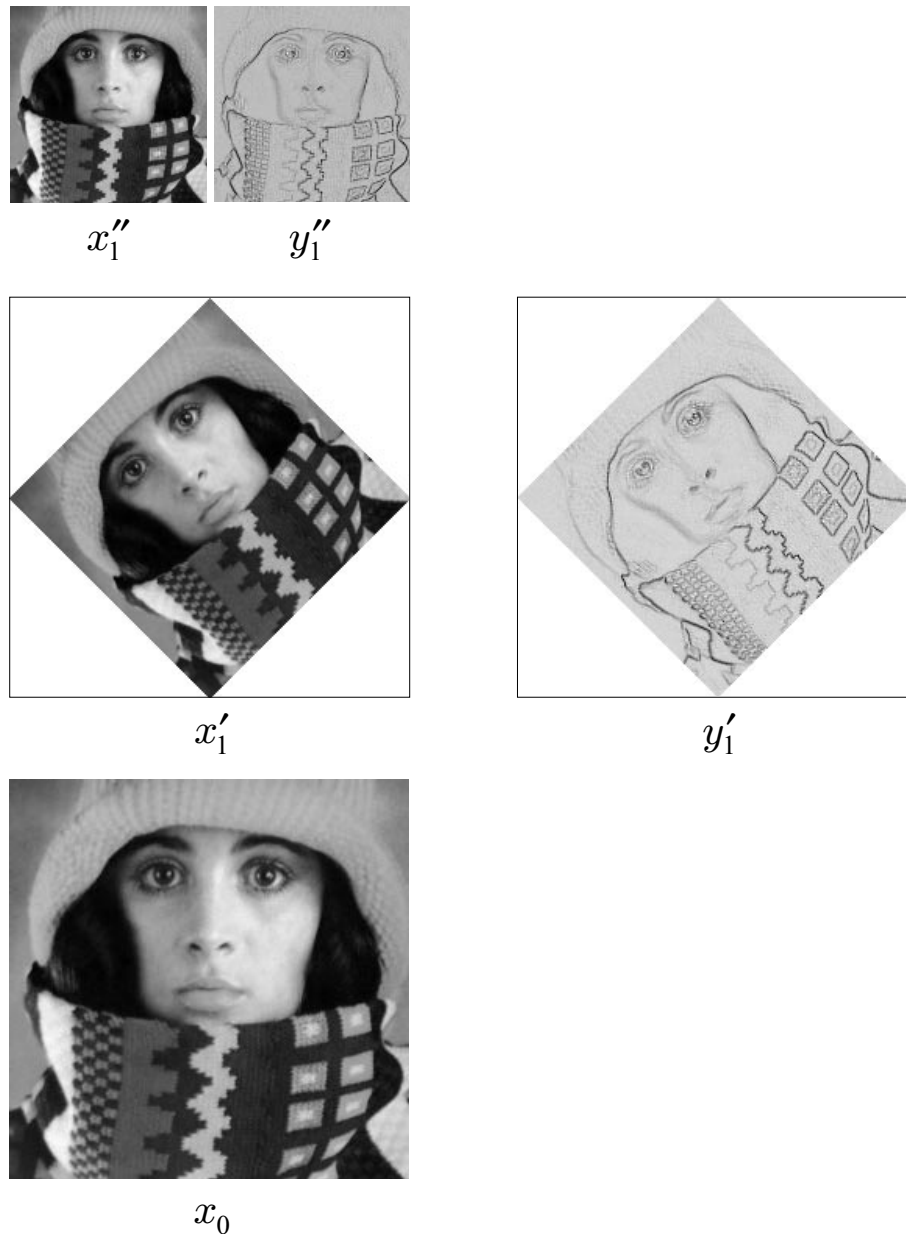


**Fig. 35.** Image decomposition based on the two-dimensional max-lifting scheme with quincunx sampling. Bottom row: original image  $x_0$ . Middle row: wavelet transformed images  $x'_1$  and  $y'_1$  (after  $45^\circ$  counterclockwise rotation). Top row: images  $x''_1$  and  $y''_1$  resulting from the wavelet transform of  $x'_1$ . Notice that the detail image may contain positive (bright) as well as negative (dark) values.

In Figure 35, we apply the two-dimensional max-lifting scheme to a particular image. Here the scaled signal  $x_1$  and the detail signal  $y_1$  are both defined on a quincunx grid. To properly depict these signals, we perform a  $45^\circ$  counterclockwise rotation.

#### 7.4. Filtering

Wavelet decompositions can be used for signal filtering and, more specifically, denoising; for example, see [19]. The basic idea is to compute the wavelet decomposition (up to a given level) and to apply (possibly different) filters to the various parts of the decomposition. Finally, we reconstruct an output signal by applying the inverse wavelet transform to the filtered coefficients. We formalize this method for the simple case when we use one level of the decomposition (see Figure 36).

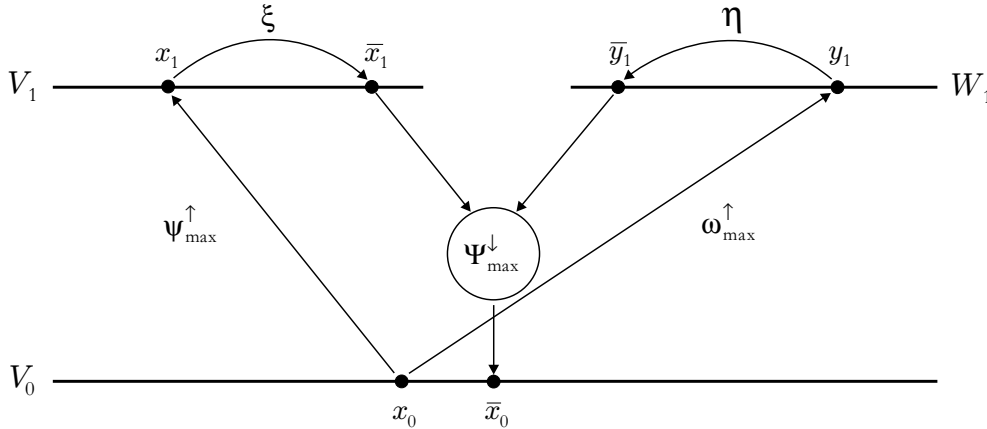


**Fig. 36.** Wavelet filtering scheme. The wavelet transform maps an input signal  $x_0$  to  $(x_1, y_1)$ . The scaled signal is filtered by  $\xi$  yielding  $\bar{x}_1 = \xi(x_1)$  and the detail signal is filtered by  $\eta$  yielding  $\bar{y}_1 = \eta(y_1)$ . By applying the synthesis operator  $\Psi_{\max}^\downarrow$ , we obtain a filtered signal  $\bar{x}_0 = \Psi_{\max}^\downarrow(\bar{x}_1, \bar{y}_1)$ .

Here, the input signal  $x_0$  is mapped to  $(x_1, y_1) \in V_1 \times W_1$  by the max-lifting wavelet scheme; that is,  $x_1 = \psi_{\max}^\uparrow(x_0)$  and  $y_1 = \omega_{\max}^\uparrow(x_0)$ . Notice that we have deleted the accents for convenience. The scaled signal  $x_1 \in V_1$  is “filtered” by an operator  $\xi: V_1 \rightarrow V_1$ , whereas the detail signal  $y_1 \in W_1$  is “filtered” by an operator  $\eta: W_1 \rightarrow W_1$ . Thus, the synthesized signal  $\bar{x}_0$  is given by

$$\bar{x}_0 = \Psi_{\max}^\downarrow(\xi\psi_{\max}^\uparrow(x_0), \eta\omega_{\max}^\uparrow(x_0)) =: \phi_{\xi, \eta}(x_0).$$

We are interested in the (morphological) properties of the operator  $\phi = \phi_{\xi, \eta}: V_0 \rightarrow V_0$  in relation to properties of  $\xi$  and  $\eta$ . Recall that  $V_0 = \mathbb{R}^E$ ,  $V_1 = \mathbb{R}^{E_x}$ , and  $W_1 = \mathbb{R}^{E_y}$ , and as such, these spaces are lattices. We now have the following proposition, whose proof is a direct consequence of (4.2).

**7.3. Proposition.** *If the operators  $\xi, \eta$  are both idempotent, then  $\phi_{\xi, \eta}$  is idempotent as well.*

In the following, we consider three idempotent operators  $\eta$  on  $W_1$ , namely

$$\begin{aligned} \eta_+(y)(q) &= y(q) \vee 0 \\ \eta_-(y)(q) &= y(q) \wedge 0 \\ \eta_0(y)(q) &= 0, \end{aligned}$$

for  $y \in W_1$  and  $q \in E_y$ . Thus,  $\eta_+, \eta_-$  preserve positive and negative detail coefficients, respectively, whereas  $\eta_0$  sets all detail coefficients to zero. Recall that  $\text{id}$  denotes the identity operator. We have the following proposition.

#### 7.4. Proposition.

- (a)  $\phi_{\xi, \eta_+}$  is extensive if  $\xi$  is extensive.
- (b)  $\phi_{\text{id}, \eta_-}$  is extensive.
- (c)  $\phi_{\text{id}, \eta_0}$  is extensive.

PROOF. The transformed signals  $x_1, y_1$  are computed from (cf. (7.3)–(7.5)):

$$y_1(q) = x_0(q) - \bigvee_{p \sim q} x_0(p), \quad q \in E_y \quad (7.11)$$

$$x_1(p) = x_0(p) + (0 \vee \bigvee_{q \sim p} y_1(q)), \quad p \in E_x, \quad (7.12)$$

whereas  $\bar{x}_0 = \phi_{\xi, \eta}(x_0)$  is computed from

$$\bar{x}_0(p) = \bar{x}_1(p) - (0 \vee \bigvee_{q \sim p} \bar{y}_1(q)), \quad p \in E_x \quad (7.13)$$

$$\bar{x}_0(q) = \bar{y}_1(q) + \bigvee_{p \sim q} \bar{x}_0(p), \quad q \in E_y, \quad (7.14)$$

where  $\bar{x}_1 = \xi(x_1)$  and  $\bar{y}_1 = \eta(y_1)$ .

(a) If  $\eta = \eta_+$ , then  $0 \vee \bigvee_{q \sim p} \bar{y}_1(q) = 0 \vee \bigvee_{q \sim p} y_1(q)$ . Since  $\bar{x}_1 = \xi(x_1) \geq x_1$ , we find that  $\bar{x}_0(p) \geq x_0(p)$ , for  $p \in E_x$ . Then, since  $\bar{y}_1(q) \geq y_1(q)$ , we have that  $\bar{x}_0(q) \geq y_1(q) + \bigvee_{p \sim q} x_0(p) = x_0(q)$ . This proves the result.

(b) Assume that  $\xi = \text{id}$  and  $\eta = \eta_-$ . It is obvious that  $0 \vee \bigvee_{q \sim p} \bar{y}_1(q) = 0$ , for every  $p \in E_x$ ; hence  $\bar{x}_0(p) = \bar{x}_1(p) = x_1(p) \geq x_0(p)$ . For  $q \in E_y$ , we have that

$$\bar{x}_0(q) = \bar{y}_1(q) + \bigvee_{p \sim q} \bar{x}_0(p) = \bar{y}_1(q) + \bigvee_{p \sim q} x_1(p).$$

We distinguish between two cases:

(i)  $y_1(q) < 0$ : then  $\bar{y}_1(q) = y_1(q)$  and

$$\bar{x}_0(q) = y_1(q) + \bigvee_{p \sim q} x_1(p) \geq y_1(q) + \bigvee_{p \sim q} x_0(p) = x_0(q).$$

(ii)  $y_1(q) \geq 0$ : then  $\bar{y}_1(q) = 0$  and

$$\bar{x}_0(q) = \bigvee_{p \sim q} x_1(p) = \bigvee_{p \sim q} \left[ x_0(p) + (0 \vee \bigvee_{r \sim p} y_1(r)) \right].$$

Choose  $p \in A(x_0 \mid q)$ . Then, by using (7.11), we obtain

$$\begin{aligned} \bar{x}_0(q) &\geq x_0(p) + (0 \vee \bigvee_{r \sim p} y_1(r)) \\ &\geq x_0(p) + (0 \vee y_1(q)) = x_0(p) + y_1(q) \\ &= x_0(p) + (x_0(q) - x_0(p)) = x_0(q). \end{aligned}$$

This concludes the proof of (b).

(c) Assume that  $\xi = \text{id}$  and  $\eta = \eta_0$ . Then,  $\bar{x}_1(p) = x_1(p)$  and  $\bar{y}_1(q) = 0$ . From (7.13), we have that

$$\bar{x}_0(p) = \bar{x}_1(p) = x_1(p) \geq x_0(p),$$

and from (7.14), we have that

$$\bar{x}_0(q) = \bigvee_{p \sim q} \bar{x}_0(p) = \bigvee_{p \sim q} x_1(p) \geq x_0(q),$$

where we have used Proposition 7.1(b) to obtain the last inequality. ■

We now consider the operator  $\phi_{\text{id},\eta_+}$  in more detail. The output signal  $\bar{x}_0 = \phi_{\text{id},\eta_+}(x_0)$  is obtained by synthesis of the scaled signal  $x_1$  and the thresholded detail signal  $\bar{y}_1 = \eta_+(y_1)$ . This yields

$$\bar{x}_0(p) = x_1(p) - (0 \vee \bigvee_{q \sim p} \bar{y}_1(q)) = x_1(p) - (0 \vee \bigvee_{q \sim p} y_1(q)) = x_0(p), \quad p \in E_x.$$

For  $q \in E_y$ , we have that

$$\begin{aligned} \bar{x}_0(q) &= \bar{y}_1(q) + \bigvee_{p \sim q} \bar{x}_0(p) \\ &= (y_1(q) \vee 0) + \bigvee_{p \sim q} x_0(p) \\ &= \left[ (x_0(q) - \bigvee_{p \sim q} x_0(p)) \vee 0 \right] + \bigvee_{p \sim q} x_0(p) \\ &= x_0(q) \vee \bigvee_{p \sim q} x_0(p). \end{aligned}$$

From these expressions for  $\bar{x}_0$ , it follows immediately that  $\phi_{\text{id},\eta_+}$  is increasing. Combining this result with the results in Proposition 7.3 and Proposition 7.4(a) we arrive at the following corollary.

**7.5. Corollary.** *The operator  $\phi_{\text{id},\eta_+}$  is a closing.*

In fact, this result follows easily if one uses the explicit expressions for  $\bar{x}_0$  given above. Dual results hold for the min-lifting scheme. The operators  $\phi_{\text{id},\eta_-}$  and  $\phi_{\text{id},\eta_0}$ , however, are not increasing.

**7.6. Example (One-dimensional signal segmentation).** In this example, we illustrate the one-dimensional max-lifting and min-lifting schemes, applied on a signal  $x_0(n)$  of 512 samples, and demonstrate the potential of these schemes for signal segmentation. Signal segmentation is the problem of partitioning a given signal into nonoverlapping regions of stationary signal behavior. We may assume that a signal  $x_0(n)$  consists of noise, representing signal variation within a region, superimposed on a piecewise constant signal  $s_0(n)$ , representing regions of stationary signal behavior. The problem of signal segmentation is to obtain an approximation  $\hat{s}_0$  of  $s$  from given data  $x_0$ .

Figure 29(a) depicts a piecewise constant signal and the resulting scaled signals produced by a 3-level max-lifting scheme. The corresponding detail signals are depicted in Figure 29(b). A very important observation here is that the max-lifting scheme preserves the number and shapes of flat regions in a piecewise constant signal. This is a direct consequence of the fact that this scheme preserves local maxima and, moreover, it does not create new ones. It is therefore expected that max-lifting will preserve, over a range of scales, the number and shapes of regions of constant signal value, and it may therefore be used for signal segmentation. Similar results for the min-lifting scheme are depicted in Figure 30.

Figure 37 depicts the results of seven segmentation experiments based on a 3-level linear wavelet decomposition scheme, a 4-level max-lifting scheme, and a 4-level min-lifting scheme. Our computations consist of three steps: (i) signal analysis  $x_0 \mapsto \{x_k, y_k, y_{k-1}, \dots, y_1\}$ , (ii) filtering  $y_j \mapsto \bar{y}_j = \eta(y_j)$ , for  $j = 1, 2, \dots, k$ , and (iii) signal synthesis  $\{x_k, \bar{y}_k, \bar{y}_{k-1}, \dots, \bar{y}_1\} \mapsto \bar{x}_0 = \hat{s}_0$ . Figure 37(a) depicts a signal  $x_0$  to be segmented into regions of stationary signal behavior, depicted by the signal  $s_0(n)$  plotted with a thick line. Figure 37(b) depicts the signal  $\hat{s}_0$  (plotted with a thick line), obtained by means of a 3-level linear denoising scheme (the use of

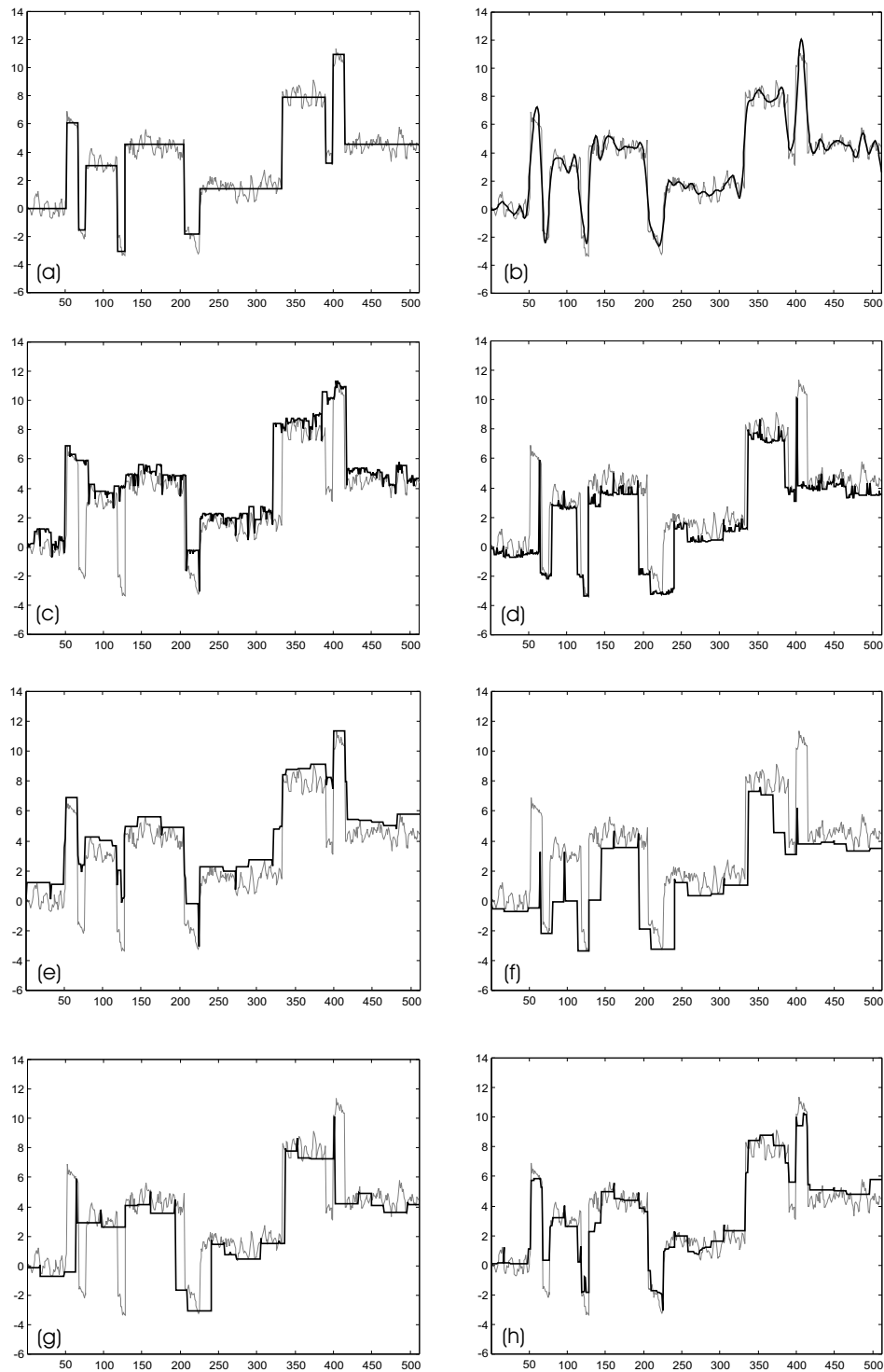


**Fig. 37.** (a) A signal  $x_0$  to be segmented into regions of stationary signal behavior (plotted with a thick line). The result of applying on  $x_0$  a denoising scheme based on: (b) the Symmlet-8 wavelet with soft thresholding, (c) max-lifting with max-thresholding, (d) min-lifting with min-thresholding, (e) max-lifting with soft thresholding, (f) min-lifting with soft thresholding, (g) max-lifting with max-thresholding followed by min-lifting with min-thresholding, (h) max-lifting with soft thresholding followed by min-lifting with soft thresholding.

a denoising scheme for signal segmentation is justified here by considering  $s_0(n)$  as the noise-free signal to be recovered by means of denoising, and the signal variation within a particular signal region as noise to be removed by denoising). This scheme performs a 3-level signal analysis by using the *Symmlet-8* wavelet [35], filters the detail signals by means of the *soft thresholding* operator  $\eta(y)(n) = \text{sign}(y(n))(|y(n)| - t)$ , if  $|y(n)| > t$ , and  $\eta(y)(n) = 0$ , if  $|y(n)| \leq t$ , where  $t = \gamma\sqrt{2} * \ln N$  [19], and produces signal  $\hat{s}_0$  by means of signal synthesis based on the filtered detail signals. We set  $\gamma = 1$ . It is worthwhile noticing that, although signal variation has been substantially reduced, the reconstructed signal  $\hat{s}_0$  fails to capture the staircase structure of signal  $s_0$ . This is mainly due to the linear nature of the wavelet decomposition scheme used. The signal  $\hat{s}_0$  depicted in Figure 37(c) has been obtained by using the max-lifting scheme with  $\eta = \eta_+$ , whereas, Figure 37(d) depicts the signal  $\hat{s}_0$  obtained by using the min-lifting scheme with  $\eta = \eta_-$ . By taking  $\eta = \eta_+$ , we preserve positive detail signal information, whereas we discard negative information (i.e., we apply *max-thresholding*). By taking  $\eta = \eta_-$ , we preserve negative detail signal information, whereas we discard positive information (i.e., we apply *min-thresholding*). Notice that the signal  $\hat{s}_0$  depicted in Figure 37(c) is larger than the original signal  $x_0(n)$  (i.e.,  $\hat{s}_0$  is like an “upper envelope” for  $x_0(n)$ ), which is in correspondence with the fact that  $\phi_{\text{id},\eta_+}$  is a closing (Corollary 7.5), whereas the signal  $\hat{s}_0$  depicted in Figure 37(d) is smaller than signal  $x_0(n)$  (i.e.,  $\hat{s}_0$  is like a “lower envelope” for  $x_0(n)$ ). On the other hand, Figure 37(e) depicts the signal  $\hat{s}_0$  obtained by using the max-lifting scheme with soft thresholding (with  $\gamma = 1$ ), whereas the signal  $\hat{s}_0$  depicted in Figure 37(f) has been obtained by means of the min-lifting scheme with soft thresholding (with  $\gamma = 1$ ). Figure 37(g) depicts the signal  $\hat{s}_0$  obtained by means of applying max-lifting on  $x_0$  with max-thresholding, followed by min-lifting with min-thresholding. On the other hand, Figure 37(h) depicts the signal  $\hat{s}_0$  obtained by means of applying max-lifting on  $x_0$ , followed by min-lifting. Denoising is obtained by applying soft thresholding on the detail signals (with  $\gamma = 0.4$ ), in the same manner as in Figure 37(e), (f). Notice that, in both cases, signal variation has been substantially reduced, whereas the resulting signal successfully captures the staircase nature of signal  $s_0$ . ■

## 8. Conclusions and Final Remarks

The literature on nonlinear wavelet decompositions, or *critically decimated nonlinear filter banks* as they are sometimes called, is not very extensive. In 1991, Pei and Chen [38, 39] were among the first authors to propose a non-redundant (in the sense that it preserves the number of pixels in the original image) nonlinear subband decomposition scheme based on mathematical morphology. Their approach however does not guarantee perfect reconstruction. In 1994, Egger and Li [20] proposed a nonlinear decomposition scheme with perfect reconstruction (see also [21]). Rephrased in the terminology introduced in this paper, it comprises a lazy wavelet decomposition followed by one nonlinear prediction lifting step. In this case, prediction is implemented by means of a median-type operator. Independently, Florêncio and Schafer [23] have presented a similar filter bank decomposition based on a median-type operator; see also [22, Chapter 7]. In particular, the “Type I” structure proposed in Section 5.3 of [22] (and in [24]) comprises a lazy wavelet decomposition followed by a nonlinear prediction lifting step. More recently, Queiroz, Florêncio and Schafer [18] proposed a nonlinear wavelet decomposition for low-complexity image coding; see also [22, Chapter 8]. This scheme consists of a lazy wavelet decomposition, corresponding to the quincunx sampling grid, followed by a prediction lifting step using a median type of operator. In his thesis [22], Florêncio discusses nonlinear perfect reconstruction filter banks in more detail, and attempts to give a better understanding of these issues by relating them to the so-called *critical morphological sampling theorem*. In [8], Cha and Chaparro constructed a

nonlinear wavelet decomposition scheme with the scaled signal being a subsampled version of the original signal and the detail signal calculated by means of a morphological opening applied on the scaled signal. The resulting signal decomposition scheme guarantees perfect reconstruction. Using the terminology of this report, the Cha and Chaparro scheme consists of a lazy wavelet decomposition followed by prediction lifting. In this case, the prediction lifting operator is a morphological opening.

It is important to point out here that the aforementioned authors did not have at their disposal the lifting scheme, which was developed during the same period [45, 46, 47]. The same remark applies to the work of Hampson and Pesquet [27, 28, 29] who developed nonlinear perfect reconstruction filter banks by considering a triangular form of the polyphase representation of a filter bank. The resulting approach is more or less identical to the lifting scheme.

In four recent papers [10, 11, 12, 13], Claypoole and co-workers also use the lifting scheme to build nonlinear wavelet transforms. In the first paper [10], they use a set of linear predictors which are chosen adaptively using a nonlinear selection criterion. In the other three papers [11, 12, 13], they use combinations of linear and nonlinear lifting steps (based on a median operator), and discuss applications in compression and denoising.

Many of the schemes proposed in the previously mentioned papers are special cases of the general schemes discussed in this report. Therefore, the theory presented here provides a rather general framework for constructing nonlinear filter banks with perfect reconstruction. It is worth noticing however that the proposed theory depends on three conditions, namely the condition of perfect reconstruction (4.1) (or (4.8), for the uncoupled case) and the two conditions of non-redundancy (4.2) (or (4.9) and (4.10), for the uncoupled case). These conditions are required in order for the proposed multiresolution schemes to guarantee perfect reconstruction and be non-redundant (in the sense that repeated applications of these schemes produce the same result). Moreover, these conditions lead to the concept of nonlinear biorthogonal-like multiresolution analysis, discussed in Subsection 4.4, which is a natural extension of the concept of biorthogonal multiresolution analysis associated with linear wavelet decompositions.

The main objective of the work presented in this report was to provide a rigorous theoretical approach to the problem of nonlinear wavelet decomposition and develop tools that can be effectively used for building nonlinear multiresolution signal decomposition schemes that are non-redundant and guarantee perfect reconstruction. The nonlinear schemes discussed as examples in this report enjoy some useful and attractive properties:

- (a) Implementation can be done extremely fast by means of simple operations (e.g., addition, subtraction, max, min, median, etc.). This is partially due to the fact that only integer arithmetic is used in calculations and that use of prediction/update steps in the decomposition produces computationally efficient implementations.
- (b) If the input to the proposed schemes is integer-valued, the output will be integer-valued as well. Clearly, these schemes can avoid quantization, an attractive property for lossless data compression.
- (c) The proposed schemes can be easily adopted to the case of binary images. This is of particular interest to document image processing, analysis, and compression applications (and other industrial applications) and is important on its own right (e.g., see [44] for a recent work on constructing wavelet decomposition schemes for binary images).
- (d) Due to the nonlinear nature of the proposed signal analysis operators, important geometric information (e.g., edges) is well preserved at lower resolutions. In the case of the max-(min-) lifting schemes, for example, local maxima (minima) are well preserved at lower resolutions. This property may turn out to be particularly useful in wavelet-based pattern recognition approaches as, for example, wavelet-based face recognition schemes [9], as is clear from the results depicted in Figure 31.

Despite all these attractive properties, a number of open theoretical and practical questions need to be addressed before such tools become useful in signal processing and analysis applications. For example, we need to better understand how to design prediction and update operators that lead to nonlinear wavelet decompositions that satisfy properties key to a given application at hand; e.g., see the max-lifting scheme discussed in Section 7. Another problem of interest is to investigate the relationship between the discrete nonlinear approach presented in this report and another nonlinear multiresolution approach to signal analysis known as nonlinear (morphological) scale spaces [1, 3, 34, 48, 51]. In fact, due to the popularity of nonlinear scale spaces in signal analysis, it may be attractive to investigate the design of nonlinear filter banks by means of discretizing continuous morphological scale spaces. Towards this direction, Pouye et. al. [40] have recently proposed a nonlinear filter bank that is built by discretizing nonlinear *partial differential equations* (PDEs) used in scale-space theory. This is a very interesting approach for constructing nonlinear filter banks that may be compatible with current multiscale signal analysis techniques based on nonlinear PDEs.

## Acknowledgments

The authors want to thank Jean-Christophe Pesquet for interesting and stimulating discussions and suggestions, as well as Ulisses Braga-Neto for suggesting the watershed-based segmentation result depicted in Figure 32.

## References

- [1] ALVAREZ, L., AND MOREL, J. Formalization and computational aspects of image analysis. *Acta Numerica* (1994), 1–59.
- [2] BEUCHER, S., AND MEYER, F. The morphological approach to segmentation: the watershed transformation. In *Mathematical Morphology in Image Processing*, E. R. Dougherty, Ed. Marcel Dekker, New York, 1993, ch. 12, pp. 433–481.
- [3] BROCKETT, R., AND MARAGOS, P. Evolution equations for continuous-scale morphological filtering. *IEEE Transactions on Signal Processing* 42, 12 (1994), 3377–3386.
- [4] BRUEKERS, F. A. M. L., AND VAN DEN ENDEN, A. W. M. New networks for perfect inversion and perfect reconstruction. *IEEE Journal on Selected Areas in Communications* 10 (1992), 130–137.
- [5] BURKE HUBBARD, B. *The World According to Wavelets: The Story of a Mathematical Technique in the Making*, 2nd ed. A. K. Peters, Wellesley, Massachusetts, 1998.
- [6] BURT, P. J., AND ADELSON, E. H. The Laplacian pyramid as a compact image code. *IEEE Transactions on Communications* 31 (1983), 532–540.
- [7] CALDERBANK, A. R., DAUBECHIES, I., SWELDENS, W., AND YEO, B.-L. Wavelet transforms that map integers to integers. *Applied and Computational Harmonic Analysis* 5 (1998), 332–369.
- [8] CHA, H., AND CHAPARRO, L. F. Adaptive morphological representation of signals: Polynomial and wavelet methods. *Multidimensional Systems and Signal Processing* 8 (1997), 249–271.
- [9] CHELLAPPA, R., WILSON, C. L., AND SIROHEY, S. Human and machine recognition of faces: A survey. *Proceedings of the IEEE* 83 (1995), 705–740.

- [10] CLAYPOOLE, R., DAVIS, G., SWELDENS, W., AND BARANIUK, R. Nonlinear wavelet transforms for image coding. In *Proceedings of the 31st Asilomar Conference on Signals, Systems, and Computers, Volume 1* (1997), pp. 662–667.
- [11] CLAYPOOLE, R. L., BARANIUK, R. G., AND NOWAK, R. D. Adaptive wavelet transforms via lifting. In *Proceedings of the IEEE International Conference on Acoustics, Speech, and Signal Processing* (Seattle, Washington, May 12-15, 1998).
- [12] CLAYPOOLE, R. L., BARANIUK, R. G., AND NOWAK, R. D. Lifting construction of nonlinear wavelet transforms. In *Proceedings of the IEEE-SP International Symposium on Time-Frequency and Time-Scale Analysis* (Pittsburgh, Pennsylvania, October 6-9, 1998), pp. 49–52.
- [13] CLAYPOOLE, R. L., BARANIUK, R. G., AND NOWAK, R. D. Adaptive wavelet transforms via lifting. Technical Report 9304, Department of Electrical and Computer Engineering, Rice University, Houston, Texas, April 1999.
- [14] COHEN, A., DAUBECHIES, I., AND FEAUVEAU, J. C. Biorthogonal bases of compactly supported wavelets. *Communications on Pure and Applied Mathematics* 45 (1992), 485–500.
- [15] COMBETTES, P. L., AND PESQUET, J.-C. Convex multiresolution analysis. *IEEE Transactions on Pattern Analysis and Machine Intelligence* 20 (1998), 1308–1318.
- [16] DAUBECHIES, I. *Ten Lectures on Wavelets*. Society for Industrial and Applied Mathematics, Philadelphia, Pennsylvania, 1992.
- [17] DAUBECHIES, I., AND SWELDENS, W. Factoring wavelet transforms into lifting steps. *Journal of Fourier Analysis and Applications* 4 (1998), 245–267.
- [18] DE QUEIROZ, R. L., FLORÊNCIO, D. A. F., AND SCHAFER, R. W. Nonexpansive pyramid for image coding using a nonlinear filterbank. *IEEE Transactions on Image Processing* 7 (1998), 246–252.
- [19] DONOHO, D. L. De-noising by soft-thresholding. *IEEE Transactions on Information Theory* 41 (1995), 613–627.
- [20] EGGER, O., AND LI, W. Very low bit rate image coding using morphological operators and adaptive decompositions. In *Proceedings of the IEEE International Conference on Image Processing* (Austin, Texas, 1994), pp. 326–330.
- [21] EGGER, O., LI, W., AND KUNT, M. High compression image coding using an adaptive morphological subband decomposition. *Proceedings of the IEEE* 83 (1995), 272–287.
- [22] FLORÊNCIO, D. A. F. *A New Sampling Theory and a Framework for Nonlinear Filter Banks*. PhD thesis, School of Electrical Engineering, Georgia Institute of Technology, Atlanta, Georgia, 1996.
- [23] FLORÊNCIO, D. A. F., AND SCHAFER, R. W. A non-expansive pyramidal morphological image coder. In *Proceedings of the IEEE International Conference on Image Processing* (Austin, Texas, 1994), pp. 331–335.
- [24] FLORÊNCIO, D. A. F., AND SCHAFER, R. W. Perfect reconstructing nonlinear filter banks. In *Proceedings of the IEEE International Conference on Acoustics, Speech, and Signal Processing* (Atlanta, Georgia, 1996), pp. 1815–1818.

- [25] GOUTSIAS, J., AND HEIJMANS, H. J. A. M. An axiomatic approach to multiresolution signal decomposition. In *Proceedings of the IEEE International Conference on Image Processing* (Chicago, Illinois, October 4-7, 1998).
- [26] GOUTSIAS, J., AND HEIJMANS, H. J. A. M. Multiresolution signal decomposition schemes. Part 1: Linear and morphological pyramids. Technical Report PNA-R9810, CWI, Amsterdam, The Netherlands, October 1998.
- [27] HAMPSON, F. J. *Méthodes Non Linéaires en Codage d'Images et Estimation de Mouvement*. PhD thesis, l'Université Paris XI Orsay, Paris, France, 1997.
- [28] HAMPSON, F. J., AND PESQUET, J.-C. A nonlinear subband decomposition with perfect reconstruction. In *Proceedings of the IEEE International Conference on Acoustics, Speech, and Signal Processing* (Atlanta, Georgia, May 7-10, 1996), pp. 1523–1526.
- [29] HAMPSON, F. J., AND PESQUET, J.-C.  $M$ -band nonlinear subband decompositions with perfect reconstruction. *IEEE Transactions on Image Processing* 7 (1998), 1547–1560.
- [30] HEIJMANS, H. J. A. M. *Morphological Image Operators*. Academic Press, Boston, 1994.
- [31] HEIJMANS, H. J. A. M., AND GOUTSIAS, J. Morphology-based perfect reconstruction filter banks. In *Proceedings of the IEEE-SP International Symposium on Time-Frequency and Time-Scale Analysis* (Pittsburgh, Pennsylvania, October 6-9, 1998), pp. 353–356.
- [32] HEIJMANS, H. J. A. M., AND GOUTSIAS, J. Some thoughts on morphological pyramids and wavelets. In *Signal Processing IX: Theories and Applications* (EUSIPCO, Island of Rhodes, Greece, September 8-11, 1998), S. Theodoridis, I. Pitas, A. Stouraitis, and N. Kaloupsidis, Eds., pp. 133–136.
- [33] HEIJMANS, H. J. A. M., AND GOUTSIAS, J. Constructing morphological wavelets with the lifting scheme. In *Pattern Recognition and Information Processing, Proceedings of the Fifth International Conference on Pattern Recognition and Information Processing (PRIP'99)* (Minsk, Belarus, May 18-20, 1999), pp. 65–72.
- [34] JACKWAY, P. T., AND DERICHE, M. Scale-space properties of the multiscale morphological dilation-erosion. *IEEE Transactions on Pattern Analysis and Machine Intelligence* 18, 1 (1996), 38–51.
- [35] MALLAT, S. *A Wavelet Tour of Signal Processing*. Academic Press, San Diego, California, 1998.
- [36] MALLAT, S. G. A theory for multiresolution signal decomposition: The wavelet representation. *IEEE Transactions on Pattern Analysis and Machine Intelligence* 11 (1989), 674–693.
- [37] MARAGOS, P. Morphological skeleton representation and coding of binary images. *IEEE Transactions on Acoustics, Speech and Signal Processing* 34 (1986), 1228–1244.
- [38] PEI, S.-C., AND CHEN, F.-C. Subband decomposition of monochrome and color images by mathematical morphology. *Optical Engineering* 30 (1991), 921–933.
- [39] PEI, S.-C., AND CHEN, F.-C. Hierarchical image representation by mathematical morphology subband decomposition. *Pattern Recognition Letters* 16 (1995), 183–192.
- [40] POUYE, B., BENAZZA-BENYAHIA, A., POLLAK, I., PESQUET, J.-C., AND KRIM, H. Nonlinear frame-like decompositions. In *Signal Processing IX: Theories and Applications*

- (EUSIPCO, Island of Rhodes, Greece, September 8-11, 1998), S. Theodoridis, I. Pitas, A. Stouraitis, and N. Kaloupsidis, Eds., pp. 1393–1396.
- [41] RĀNGANATH, S., AND BLUME, H. Hierarchical image decomposition and filtering using the S-transform. In *Proceedings of the SPIE Workshop on Medical Imaging II, Vol. 914* (1988), pp. 799–814.
- [42] RIOUL, O. A discrete-time multiresolution theory. *IEEE Transactions on Signal Processing* 41 (1993), 2591–2606.
- [43] SAID, A., AND PEARLMAN, W. A. An image multiresolution representation for lossless and lossy compression. *IEEE Transactions on Image Processing* 5 (1996), 1303–1310.
- [44] SWANSON, M. D., AND TEWFIK, A. H. A binary wavelet decomposition of binary images. *IEEE Transactions on Image Processing* 5 (1996), 1637–1650.
- [45] SWELDENS, W. The lifting scheme: A new philosophy in biorthogonal wavelet constructions. In *Wavelet Applications in Signal and Image Processing III* (1995), A. F. Lain and M. Unser, Eds., Proceedings of SPIE, vol. 2569, pp. 68–79.
- [46] SWELDENS, W. The lifting scheme: A custom-design construction of biorthogonal wavelets. *Applied and Computational Harmonic Analysis* 3 (1996), 186–200.
- [47] SWELDENS, W. The lifting scheme: A construction of second generation wavelets. *SIAM Journal of Mathematical Analysis* 29 (1998), 511–546.
- [48] VAN DEN BOOMGAARD, R., AND SMEULDERS, A. The morphological structure of images: the differential equations of morphological scale space. *IEEE Transactions on Pattern Analysis and Machine Intelligence* 16 (1994), 1101–1113.
- [49] VETTERLI, M., AND KOVAČEVIĆ, J. *Wavelets and Subband Coding*. Prentice Hall, Englewood Cliffs, New Jersey, 1995.
- [50] VINCENT, L., AND SOILLE, P. Watersheds in digital spaces: an efficient algorithm based on immersion simulations. *IEEE Transactions on Pattern Analysis and Machine Intelligence* 13 (1991), 583–598.
- [51] WEICKERT, J. *Anisotropic Diffusion in Image Processing*. Teubner-Verlag, Stuttgart, Germany, 1998.